EXPLICIT NONLINEAR ANALYSIS FOR QUASI-STATIC BEHAVIOR OF FRAME STRUCTURES WITH PID CONTROL AND MASS SCALING

A THESIS SUBMITTED TO
THE GRADUATE SCHOOL OF NATURAL AND APPLIED SCIENCES
OF
MIDDLE EAST TECHNICAL UNIVERSITY

BY

KORHAN KOCAMAZ

IN PARTIAL FULFILLMENT OF THE REQUIREMENTS
FOR
THE DEGREE OF MASTER OF SCIENCE
IN
CIVIL ENGINEERING

AUGUST 2018

Approval of the thesis:

EXPLICIT NONLINEAR ANALYSIS FOR QUASI-STATIC BEHAVIOR OF FRAME STRUCTURES WITH PID CONTROL AND MASS SCALING

submitted by **KORHAN KOCAMAZ** in partial fulfillment of the requirements for the degree of **Master of Science in Civil Engineering Department, Middle East Technical University** by,

Prof. Dr. Halil Kalıpçılar _____
Dean, Graduate School of **Natural and Applied Sciences**

Prof. Dr. İsmail Özgür Yaman _____
Head of Department, **Civil Engineering**

Prof. Dr. Kağan Tuncay _____
Supervisor, **Civil Engineering Dept., METU**

Examining Committee Members:

Prof. Dr. Barış Binici _____
Civil Engineering Dept., METU

Prof. Dr. Kağan Tuncay _____
Civil Engineering Dept., METU

Prof. Dr. Tolga Akış _____
Civil Engineering Dept., Atılım University

Assoc. Prof. Dr. Yalın Arıcı _____
Civil Engineering Dept., METU

Assoc. Prof. Dr. Ozan Cem Çelik _____
Civil Engineering Dept., METU

Date: August 15, 2018

I hereby declare that all information in this document has been obtained and presented in accordance with academic rules and ethical conduct. I also declare that, as required by these rules and conduct, I have fully cited and referenced all material and results that are not original to this work.

Name, Last name: Korhan Kocamaz

Signature :

ABSTRACT

EXPLICIT NONLINEAR ANALYSIS FOR QUASI-STATIC BEHAVIOR OF FRAME STRUCTURES WITH PID CONTROL AND MASS SCALING

Kocamaz, Korhan

M.S., Department of Civil Engineering

Supervisor: Prof. Dr. Kağan Tuncay

August 2018, 88 pages

Performance-based seismic design of reinforced concrete frame systems requires time history analysis of the structural model under earthquake loads and estimation of damage in the members. Time history analysis of these structures is usually performed using implicit time integration methods. For the implicit integration methods, divergence of the solution is typically treated as the onset of collapse of modelled system.

In this study, a nonlinear analysis platform that enables the analysis of the effect of earthquake loads and estimation of damage by using explicit time integration was developed. In the time history analysis, mass scaling is utilized to increase the stable time step size without changing the overall dynamics.

Explicit time integration methods are convenient for dynamic analysis and the determination of the collapse behavior. However, for quasi-static loading as well as

relatively faster pseudo-dynamic experiments, dynamic effects should be minimized for a fast solution with analysis time comparable to implicit solutions. For this purpose, a control algorithm was implemented that mimics load control in displacement-controlled experiments. The method is tested with an experiment as well as a recently conducted pseudo-dynamic experiment.

Keywords: PID Control, Reinforced Concrete, Explicit Integration, Mass Scaling

ÖZ

ÇERÇEVELİ YAPILARIN PID KONTOL VE KÜTLE ÖLÇEKLENDİRME İLE DOĞRUSAL OLMAYAN AÇIK İNTEGRASYON ANALİZİ

Kocamaz, Korhan
Yüksek Lisans, İnşaat Mühendisliği Bölümü
Tez Yöneticisi: Prof. Dr. Kağan Tuncay

Ağustos 2018, 88 sayfa

Betonarme çerçeve sistemlerinin performansa dayalı tasarımı, yapısal modelin deprem yükleri altında zaman tarihinin analizini ve yapısal elemanlardaki hasar tahminlerini gerektirmektedir. Bu yapıların zaman tanım alanındaki analizi genellikle kapalı zaman entegrasyon yöntemleri kullanılarak gerçekleştirilir. Kapalı entegrasyon yöntemleri için, çözümün ıraksaması genellikle modellenmiş sistemin çöküşünün başlangıcı olarak ele alınır.

Bu çalışmada, deprem yüklerinin etkisinin analizini ve hasar tahminlerini sağlayan, açık zaman entegrasyonu kullanan doğrusal olmayan bir analiz platformu geliştirilmiştir. Zaman tanım alanında analiz yönteminde, kütle ölçeklendirmeden faydalanılarak, kararlı zaman adımı genel dinamikleri değiştirmeden yükseltilmiştir.

Açık zaman entegrasyon yöntemleri dinamik analiz ve çöküş davranışının belirlenmesi için elverişlidir. Ancak, statik yüklemeler ve görece olarak daha hızlı yapılan sözde dinamik deneyler için, dinamik etkiler hızlı bir çözüm ve kapalı integrasyona göre

karşılaştırılabilir bir analiz süresi için en aza indirilmelidir. Bu amaçla, yer değiştirme kontrollü deneylerde kullanılan yük kontrolünü taklit eden bir kontrol algoritması tatbik edilmiştir. Yöntem, yakın zamanda gerçekleştirilen bir sözde dinamik deney ile birlikte bir dizi sentetik deneyle test edilmiştir.

Keywords: PID Kontrol, Betonarme, Açık Entegrasyon, Kütle Ölçeklendirme

To My Family

ACKNOWLEDGMENT

I want to express my profound gratitude to my advisor Prof. Dr. Kağan Tuncay whose knowledge, criticism, patience and support enabled me to develop the ideas behind this dissertation. The door to his office was always open whenever I ran into a trouble spot or had a question about my research or writing. I will always admire his attitude towards his students and carry the honor of working with him all my life.

I would also like to thank Prof. Dr. Barış Binici and Assoc. Prof. Dr. Yalın Arıcı for their willingness to help, and comments.

I wish to thank all those people whose friendly assistance and wise guidance supported me throughout the duration of this research.

TABLE OF CONTENTS

LIST OF TABLES

LIST OF FIGURES

CHAPTER 1

INTRODUCTION

1.1 General

Simulating the collapse mechanism and behavior under dynamic loads is quite important for the performance-based seismic design of reinforced concrete frame structures. In this regard, nonlinear pushover analysis and nonlinear time history analysis have been developed and extensively used in the last thirty years. Nonlinear pushover analysis attempts to solve static problems by incrementally increasing the force. Predefined force pattern is applied until the formation of collapse mechanism of modelled structure and the lateral force-roof displacement relationship, i.e., the capacity curve, is determined for the structures. On the other hand, nonlinear time history analysis attempts to solve the dynamic equations of motion of the modelled structure under the prescribed dynamic force or ground motion. Direct integration method is used in nonlinear time history analysis; hence, dynamic equilibrium equation is solved at each time point and the time-dependent response of the modelled structure is obtained. Therefore, nonlinear time history analysis provides more information about the structure when compared to nonlinear pushover analysis and it is a relatively open field for further studies.

Displacement-based fiber frame elements with implicit integration methods became the state of the art for the dynamic analysis of reinforced concrete structures in recent years (Mazzoni et al. 2010). Despite their established formulation, this approach usually suffers from convergence issues especially for systems approaching collapse. A similar problem is also encountered during inelastic static analysis, i.e., pushover analysis, of buildings at large deformation demands. A better alternative to overcome these limitations is the use of explicit time integration which is non-iterative and can be easily coded. Explicit methods also allow for the parallelization in a rather straight

forward manner. The most important benefit of explicit integration for dynamic analysis of buildings is its ability to capture damage without any divergence issues.

In this study, a dynamic analysis computer program that uses an explicit time integration scheme and employs displacement-based fiber frame elements was developed for the two-dimensional dynamic analysis of reinforced concrete buildings. A Proportional Integral Derivative (PID) Control algorithm was employed to extend the capability of explicit dynamic analysis methodology to the static inelastic analysis of buildings PID algorithm is usually employed for accurate control of hydraulic actuators in dynamic testing. In this study, it is employed for dynamic simulations of static loading. The developed computer program was validated by using the results of a number of numerical experiments and a pseudo-dynamic (PsD) test conducted at the Middle East Technical University in 2012.

1.2 Motivation

Most research efforts focusing on structures have used implicit time integration techniques. In this work, the explicit time integration scheme was adopted conducting static analysis with explicit time integration is notoriously difficult, therefore, in order to use this simulation technique on quasi-static problems, a PID algorithm was implemented simulating load control similar to displacement-controlled tests. A major problem in the explicit solvers is the computation time of the simulation. To overcome this issue, a novel mass scaling technique was developed.

1.3 Organization of Thesis

This chapter has presented an overview of the state of the art and the motivation of this study.

Chapter 2 presents literature review of the related topics are presented. The development of the finite element method, and lumped and distributed plasticity models are reviewed. Then, definitions for the plastic hinge length are provided. Implicit and explicit time integration methods are investigated. Next, the mass scaling technique is described and reviewed. Then, the PID controller is introduced and its

application to structural engineering problems is discussed. Tuning methods for the control parameters of the PID controller are also reviewed.

Chapter 3 describes the modelling technique and analysis methods which are used in this study. First, the formulation of the displacement-based fiber element is presented. Second, the constitutive models used for confined concrete, unconfined concrete and the reinforcing steel are provided. Then, the application of the PID control and the mass scaling technique on the developed computer program are described. Finally, the explicit integration method used in the analyses is given.

Chapter 4 presents the verification studies for the developed program. First, the element formulation and the time integration scheme are validated with the derived analytical solution. Second, the PID controller algorithm verification is presented. Third, the mass scaling is described and the application of mass scaling is verified by using the experimental data. Finally, ground motion is applied to the modelled structure and results of the developed program is compared with the experimental results.

Chapter 5 presents a summary of the thesis and conclusions.

CHAPTER 2

LITERATURE REVIEW

2.1 Finite Element Method

The two methods used in structural analysis for frame structures are the displacement- and forced-based methods. They are also called as the stiffness and flexibility methods, respectively. The displacement method uses the principle of minimum potential energy or virtual displacements in the formulation. Therefore, the displacement field is adopted for the element and the compatibility is satisfied with the adjacent elements and within the element itself. The force method, on the other hand, utilizes the minimum complimentary energy principle and virtual forces. Hence, a stress (force) field is accepted for the element domain. Consequently, force continuity with the adjacent elements and force equilibrium along the element is satisfied. In the force method, the equilibrium is satisfied by the virtue of its formulation and unknown displacements are calculated based on the compatibility conditions. On the other hand, in the displacement method, the compatibility condition is satisfied exactly, and the equilibrium equations are used for the calculation of the unknown primary variable.

The pioneering work in this area are by Argyris (1954) and Argyris and Kelsey (1957). Argyris and Kelsey (1957) used energy principles and derived both displacement- and forced-based matrix formulations. Turner et al. (1956) formulated the stiffness matrices for the truss and beam elements. They conducted a study on two dimensional triangular and rectangular elements under plane stress condition and derived the element stiffness matrices. They also showed a procedure to assemble the global stiffness matrix of structure (which is also known as the direct stiffness approach). The "Finite Element Method (FEM)" phrase in his paper on structural analysis method was introduced by Clough (1960). This work is generally considered as the starting point of FEM (Zienkiewicz 1996).

Przemieniecki (1967) studied the derivation of flexibility and stiffness matrices of a beam element in detail by using the complementary and the virtual work principles. He also investigated the nonlinear structural analysis of bar and beam elements.

Cook (1981), Bathe (1982) and Zienkiewicz and Taylor (1989) obtained the displacement-based elements based on the assumption of a continuous displacement field expressed as a function of nodal displacements over the element domain. Stiffness matrix of a displacement-based finite element was obtained by using the minimum potential energy principle.

The first force-based finite element which is based on the force equilibrium principle was proposed by Ciampi and Carlesimo (1986). This element was improved by Spacone (1994), Spacone et al. (1996a) and Spacone et al. (1996b) considering the material nonlinearity (distributed plasticity approach). An iterative procedure within the element to ensure satisfaction of the compatibility conditions for the force-based finite elements was proposed.

The localization problem of the displacement-based finite element was pointed out by Bažant and Oh (1983) based on the fracture energy of concrete. Due to the softening behavior of concrete, the deformation was shown to take place only in one of the elements in the crack band (Bažant and Oh, 1983).

Coleman and Spacone (2001) introduced the localization issue in force-based elements and stated that localization occurs at only one integration point, i.e., Gaussian point or monitoring section in the element depending on the constitutive law of the material. By using constant fracture energy concept, a normalization of the constitutive law was proposed depending on the post-peak behavior (Coleman and Spacone 2001). Since the localization occurs at only one integration point, Scott and Fenves (2006) modified the integration scheme for force-based analysis.

2.2 Plasticity Models

Chronologically, the lumped plasticity models were introduced first, followed by the distributed nonlinearity models. The distributed nonlinearity models, which divide the

cross-section of the member into fibers, are described in further detail as implemented in this study.

2.2.1 Lumped Plasticity Models

Under dynamic loads, the demand on the reinforced concrete systems generally exceeds the elastic limit leading to inelastic behavior. Commonly, the inelastic behavior is localized at the ends of columns and beams. Therefore, the simplest approach to modeling of this behavior is putting zero-length nonlinear springs at the ends of the structural members. These springs might be linked in parallel or in series. Clough and Johnston (1966) proposed parallel connected spring elements with a bilinear moment-rotation behavior. The element, which is shown in Figure 2.1(a), is composed of two elements; one stands for yielding, the other represents strain-hardening. In this approach, the two components have a bilinear moment-rotation behavior and the summation of the two gives the stiffness of the element. The model was improved by Takizawa (1976) extending to multilinear behavior including degradation by considering the influence of the cracking of the reinforced concrete members.

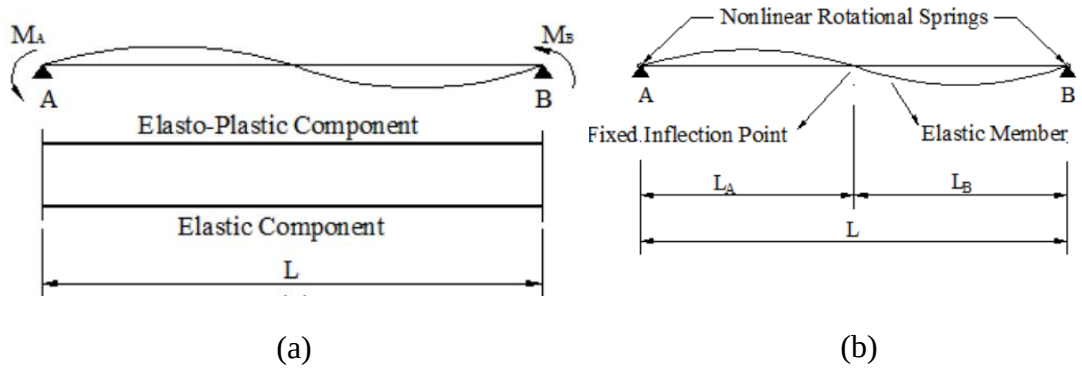

Figure 2.1. Lumped plasticity elements: (a) parallel model (Clough and Johnston 1966); (b) series model (Giberson 1967) (Figure adopted from Taucer et al. (1991))

In the same year the parallel element was introduced, Giberson (1967) proposed the first serially connected spring element in his Ph.D. dissertation which is shown in Figure 2.1(b). The model contains one elastic member which has the actual member length and two zero-length nonlinear rotational springs located at the ends of the elastic portion. Elastic displacements occur in the zero-length springs and the model has fixed

inflection point (i.e. zero curvature point) at the midpoint of the elastic component. Main advantage of this model over the parallel counterpart is that any moment-rotation behavior can be assigned to the zero-length springs. However, the model cannot accurately simulate a reinforced concrete members with the two identical zero-length springs due to the fact that different nonlinear curvature profiles can occur as shown in Figure 2.2. The model is based on the assumption that the inflection point is located at the mid-span. By using this assumption, the stiffness of the zero-length rotational spring can be calculated. Nonetheless, the curvature profile and the location of the inflection point can vary, especially after the yielding occurs. Therefore, the assumption of a fixed inflection point is not always valid. However, for the sake of simplicity, it can be used for low-rise structures as inflection points are typically near the mid-span (Otani 1980).

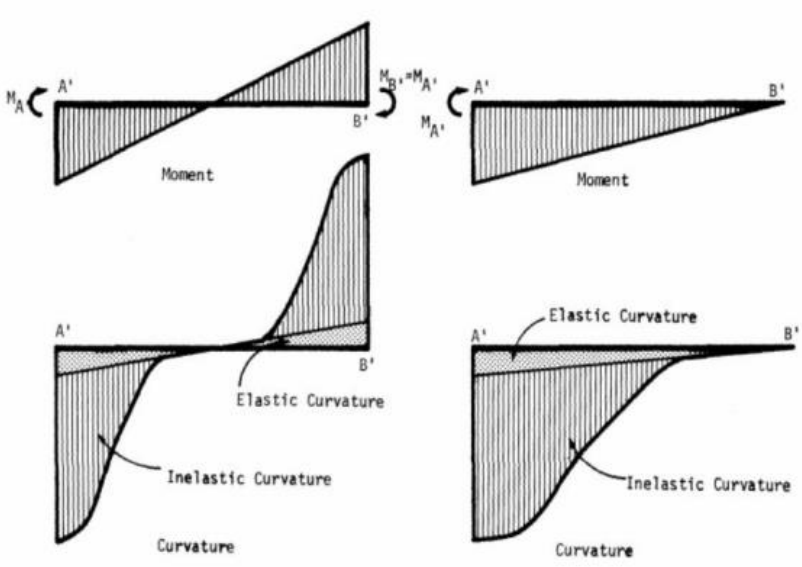

Figure 2.2 Moment and curvature variations for two cases (Otani 1980)

Lai et al. (1984) introduced a fiber model that contains a linear elastic element having the length of the modelled reinforced concrete member and two inelastic elements at the ends of the linear element as shown in the Figure 2.3. Inelastic elements consist of a spring which is only active in compression at the center point on the cross-section and four springs at the corners of the cross-section that stand for the longitudinal reinforcing steel bars. The main difference between Lai et al. (1984) model and the previously proposed models is that Lai's model accounts for the axial force-bending moment interaction.

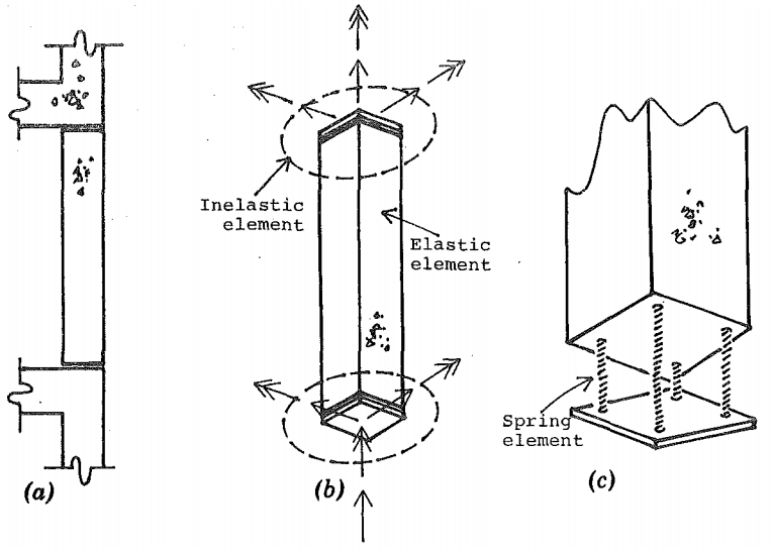

Figure 2.3 Degrading inelastic element for RC beam/columns Lai et al. (1984)
(a) member in frame; (b) member model; (c) inelastic element

Lumped models oversimplify the spread of inelastic region in the member. This drawback was noticed in various studies, especially those investigating flexural behavior of reinforced elements (Charney and Bertero 1982; Bertero et al. 1984). Another drawback is the requirement to set the zero-length spring properties before the structural analysis. Anagnostopoulos (1981) showed that there was a substantial dependency between inelastic deformation level and model parameters in his study where lumped plasticity modelling technique was used.

2.2.2 Distributed Plasticity Models

Research on the distributed nonlinearity modelling of reinforced concrete frames has started in 1970s. A model which contains two cantilever beams that are linked at the fixed inflection point of the member by proposed by Otani (1974). Due to the non-symmetrical stiffness matrix, it is assumed that the inelastic deformations occurs only in the zero-length springs located at the ends of the elements by Otani. In the proposed model the formulation of the model is derived by taking integration of curvatures along the entire element length. Takayanagi and Schnobrich (1979) introduced a new model that splits the element to a number of elements. Divided segments were transformed to the nonlinear springs whose behavior depend on moment segment carries, and behavior was assumed to be constant along the segment. Therefore, inelastic

deformations occurred over the whole element. Filippou and Issa (1988) proposed a new model for distributed plasticity. They divided the element into segments (i.e., sections as Takayanagi and Schnobrich (1979)) but in this model, sections were also divided into sub-elements, i.e., fibers (Figure 2.4). In contrast to the distributed plasticity models, this approach allows the use of a constitutive model for each fiber, and displacement field functions are used to derive the stiffness matrix similar to the displacement-based finite element approaches. Filippou and Issa (1988) assumed that fibers are only axially loaded.

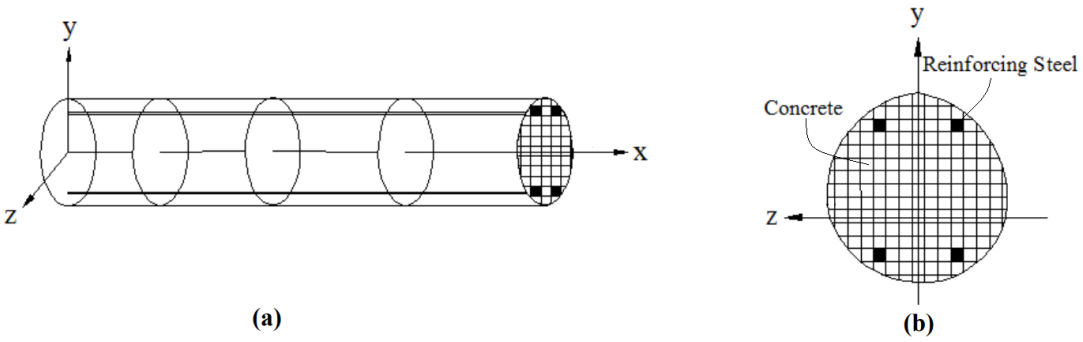

Figure 2.4 Fiber element: (a) distribution of sections; (b) fibers in the section (Taucer et al. 1991)

2.3 Plastic Hinge

For accurate simulations of the inelastic response of reinforced concrete elements, without going into detail of the spreading nature of the plasticity on the element, researchers have simplified the plastic region with a constant length, L_p, which was called the plastic hinge length (Park and Paulay 1975). This approach reduces the moment-curvature behavior to two regions: plastic and elastic regions as shown in Figure 2.5.

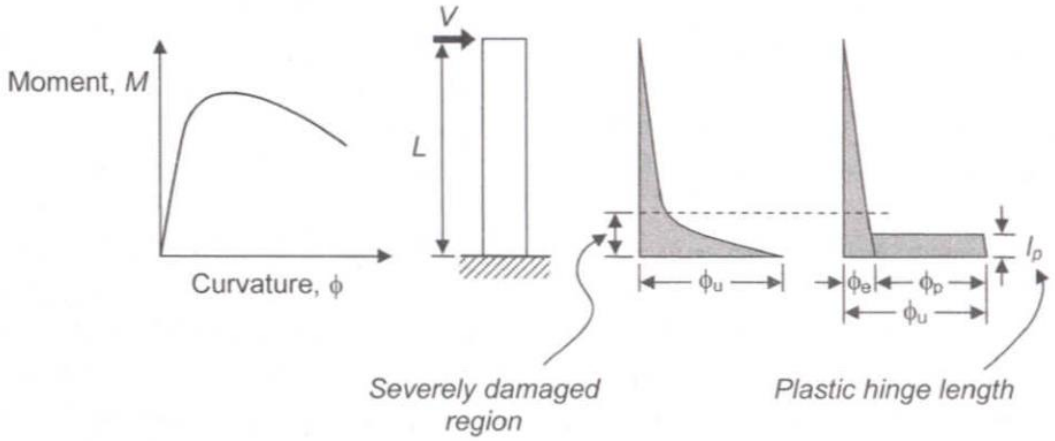

Figure 2.5 Definition of plastic hinge length (Park and Paulay 1975)

2.3.1 Plastic Hinge Length Models

Since the late 1950s, plastic hinge models have been used extensively to determine the equivalent length of these hinges in the reinforced concrete elements. General opinion is that plastic hinge length L_p depends on the length of the member and the steel reinforcement ratio. In the context of the performance based-design approach, various researchers have proposed different plastic hinge lengths in the light of the experimental data.

In 1959, European Committee for Concrete (CEB) tested 94 columns and beams with varying yield strength of reinforcing steel, concrete strength and ratio of the reinforcement steel. Single point or two-point loads were applied on the test members along with the axial load. The following expression was suggested for the plastic hinge length by Baker and Amarakone (1965) based on the test results.

$$L_p = k_1 k_2 k_3 \left(\frac{z}{d}\right)^{0.25} d \qquad (2.1)$$

where k_1 is 0.9 for cold formed steel or 0.7 for hot rolled steel, and

$k_2 = \left(1+0.5\frac{P}{P_u}\right)$, where P_u is the ultimate axial load without bending and P is the ultimate axial load when bending is present. k_3 is 0.6 for concrete strength of 6000 psi (41 MPa), 0.9 for concrete strength of 2000 psi (14 MPa). For other concrete strength values, k_3 can be obtained by interpolation, z is the length between the critical section

and the contraflexure point, and d is the distance from outermost compression concrete fiber to the tension reinforcement.

Corley (1966) was among the first researchers to study the plastic hinge zone. He conducted experiments with 40 simply supported concrete beams with varying confinement levels and beam lengths. It was concluded that the beam size had minor influence on the plastic hinge zone and that geometry of a concrete beam significantly affected the plastic hinge zone length. A simple equation for determining the plastic hinge length was proposed, where D is the diameter of the column cross-section (Corley 1966).

$$L_p=0.5D+0.2\frac{z}{\sqrt{d}} \tag{2.2}$$

Park et al. (1982) conducted full scale experiments with reinforced concrete columns whose length to depth ratio was 2. In the experiments, axial loads on the members were varied between $0.2f_c^{'}A_g$ to $0.6f_c^{'}A_g$. The plastic hinge length was determined to be independent of the axial load. A mean value of 0.42h was determined where h is the height of the cross section in the bending direction. Improvement to this approach came from Priestley and Park (1987) using a similar approach. They proposed Equation (2.3) for L_p calculation for the reinforced concrete columns. The expression in Equation (2.3) is dependent on L, the length of the member, and d_b, is the longitudinal reinforcing steel bar diameter. The first part was explained with bending while the other part accounted for the strain penetration into the adjacent member or into the foundation. Further revision was made by Paulay and Priestley (1992) taking different kinds of reinforcing steel into consideration to yield the expression shown in Equation (2.4)

$$L_p= 0.08L+6d_b \tag{2.3}$$

$$L_p= 0.08L+0.022d_bf_y \text{ (MPa)} \tag{2.4}$$

where f_y is the reinforcing steel yield strength.

Lehman et al. (2004) investigated the parameters that have noticeable impact on the length of the plastic hinge region by carrying out experiments on reinforced concrete column members. The longitudinal reinforcement ratio, the axial road ratio, the aspect ratio, the spiral reinforcement ratio, and the size of confined zone contiguous to the

expected plastic hinge zone were varied. Based on Lehman et al. findings and the evaluation of the 37 reinforced concrete column members from the database of Pacific Earthquake Engineering Research ((PEER 2011), Berry et al. (2008) suggested an approximate plastic hinge length expression shown in Equation (2.5) using statistical analysis. In a similar fashion to the Priestley and Park (1987) proposal, the Berry et al. (2008) prediction equation consists of the strain penetration and the moment gradient terms.

$$L_p = 0.0375L + 0.01 f_y \frac{d_b}{\sqrt{f'_c}} \text{ (ksi)} \tag{2.5}$$

Bae and Bayrak (2008) reviewed the previous proposals for approximating the plastic hinge length and introduced a new expression almost the same time with Berry et al. (2008) by conducting a series of experiments focusing on rectangular columns. The main difference between this study and earlier studies was that their expression depended on the axial load (P) on the reinforced concrete member. Along with the member's geometric and the reinforcement characteristics, axial load on the member also was also proposed to effect plastic hinge zone length. Based on this idea, in order to estimate the tip displacement of a reinforced concrete column under varying axial loads following Equation (2.6) for plastic hinge length was proposed.

$$L_p = L\left(0.3\frac{P}{P_0} + 3\frac{A_s}{A_g} - 0.1\right) + 0.25h \geq 0.25h \tag{2.6}$$

where $P_0 = 0.85f'_c(A_g - A_s) + f_y A_s$. In this equation, h is the section depth, f'_c represents concrete compressive strength, f_y is the reinforcing steel yield strength, A_g is the gross area of the cross section and A_s is the steel area. This equation indicates that plastic hinge regions extend to at least 0.25h depth independently of length of the member.

2.3.2 Time Integration Methods

Most physical and chemical processes are modelled mathematically using partial differential equations with the appropriate boundary and initial conditions. First, the partial differential equations are discretized in the spatial domain using finite elements, finite difference or a similar method. After the spatial discretization, the partial differential equations are reduced to a set of ordinary differential equations which only

depend on time with the initial conditions. To generate numerical solutions for the spatially discretized ordinary differential equations, time integration methods are employed.

Time integration methods are classified into the implicit and explicit methods. In implicit methods, solution of a linear/nonlinear set of equations is unavoidable. Therefore, these methods need a much higher computational time per time step compared to the explicit time integration methods. Implicit time integration procedures are generally unconditionally stable and, hence, maximum time step is governed by the desired solution accuracy. However, unconditional stability in a linear problem does not guarantee unconditional stability in a nonlinear problem. Solution of a set of algebraic equations may not be required for the explicit time integration methods, leading to straight forward vector computations when a diagonal mass matrix is used. For this reason, explicit time integration methods have much less computational cost and storage requirement per time step than implicit methods. Moreover, the utilization of the explicit time integration methods in a computer program is relatively simple. Since explicit time integration schemes are generally conditionally stable, they have limits on the time step value to assure the stability of numerical solution. This deficiency restricts the effectiveness of the method especially for dynamic problems requiring a large number of time steps, leading to significant solution times due to very small time steps.

For linear or nonlinear structural dynamic problems, the equation of motion is

$$m\ddot{u}+c\dot{u}+ku = f^{ext} \tag{2.7}$$

where m is the mass matrix, c is the damping matrix, k is the stiffness matrix, u is the displacement, $\dot{u}$ is the velocity, $\ddot{u}$ is the acceleration, and f^{ext} is the external force.

The central difference method is commonly employed in structural dynamic simulations. According to Krieg (1973), the central difference method has the maximum stability limit and the highest accuracy for any explicit integration method. The formulation of central difference method is based on the central finite difference approximation. According to Abramowitz and Stegun (1972), the estimations for $\ddot{u}_i$ and $\dot{u}_i$ are given as

$$\dot{u}_i=\frac{u_{i+1}-u_{i-1}}{2\Delta t} \tag{2.8}$$

$$\ddot{u}_i=\frac{u_{i+1}-2u_i+u_{i-1}}{(\Delta t)^2} \tag{2.9}$$

when Equation (2.8) and (2.9), approximate expressions for first and second time derivatives of displacement, are substituted in Equation (2.7) which is the equation of motion for a linearly elastic system, the following expression is obtained,

$$m\frac{u_{i+1}-2u_i+u_{i-1}}{(\Delta t)^2}+c\frac{u_{i+1}-u_{i-1}}{2\Delta t}+ku_i=p_i \tag{2.10}$$

As u_i and u_{i-1} are known at time step i, we can write,

$$\left[\frac{m}{(\Delta t)^2}+\frac{c}{2\Delta t}\right]u_{i+1}=p_i-\left[\frac{m}{(\Delta t)^2}-\frac{c}{2\Delta t}\right]u_{i-1}-\left[k-\frac{2m}{(\Delta t)^2}\right]u_i \tag{2.11}$$

The value of u_{i+1} can be calculated from

$$u_{i+1}=\left\{\frac{m}{(\Delta t)^2}+\frac{c}{2\Delta t}\right\}^{-1}\left\{p_i-\left[\frac{m}{(\Delta t)^2}-\frac{c}{2\Delta t}\right]u_{i-1}-\left[k-\frac{2m}{(\Delta t)^2}\right]u_i\right\} \tag{2.12}$$

Equation (2.12) implies that if a damping matrix with off-diagonal elements is used, matrix factorization is needed for linear structural dynamic problems. In the case of non-linear problems, iteration within a time step is needed to satisfy equilibrium (Krieg 1973). To tackle this problem, Warburton (1985) proposed an altered type of the central difference which uses backward difference approximation for velocity rather than central difference approximation. Instead of Equation (2.8), Warburton's method uses the velocity formulation as,

$$\dot{u}_i=\frac{u_i-u_{i-1}}{\Delta t} \tag{2.13}$$

Owing to the use of the backward difference approximation for the velocity, unknown values of u_{i+1} can be computed without matrix factorization from Equation (2.14) when a diagonal mass matrix is used.

$$u_{i+1}=\{m\}^{-1}\{(\Delta t)^2(p_i-ku_i)-\Delta tc[u_i-u_{i-1}]\}+2u_i-u_{i-1} \tag{2.14}$$

Hahn (1991) proposed a modified Euler method which is identical to the Warburton's modified central difference method. Although they have the same base formulation, Hahn's method involves a multi-step procedure for unknown variable computation

where the other one has one step procedure. Nonetheless, both methods have only first order accuracy where the central difference method is second-order accurate in time.

Tamma and Namburu (1990) proposed a second order accurate explicit time integration scheme that integrates the equation without the computation of accelerations. The scheme has a self-starting feature and a velocity based algorithm.

Hilber et al. (1977) proposed a time integration scheme known as HHT-α method which is implicit and unconditionally stable. In this method, the main objective is to conserve low frequency response with high frequency dissipation. With the same approach and taking HHT-α method as basis, Wood et al. (1980) introduced a method generally known as WBZ-α method. Both HHT-α and WBZ-α methods have a tuning parameter α to control the rate of dissipation. Chung and Hulbert (1993) introduced a time integration scheme which is second order accurate in time that can dissipate high-frequency components while preventing low frequency dissipation. The algorithm is the combination of HHT-α method (Hilber, Hughes and Taylor 1977) and WBZ-α method (Wood, Bossak and Zienkiewiez 1980) schemes and it involves two additional parameters which are α_f and α_m. The algorithm evaluates stiffness and damping terms at time $t_{k+1-\alpha_f}$ and inertia term at time $t_{k+1-\alpha_m}$.

Chung and Lee (1994) presented a single step explicit time integration scheme with a tuning parameter β to control the high frequency dissipation. The method is second order accurate in time. When diagonal mass matrix is used, there is no matrix factorization even with the non-diagonal damping matrix. Therefore, this method is quite efficient for non-linear analyses.

Generally, for the static or quasi-static analyses implicit method is preferred whereas, for dynamic analyses such as collapse and impact simulations explicit time integration scheme is chosen. Explicit time integration allows problems of significant size to be solved for dynamic loading, however the static solutions also had to be conducted in time domain usually applying the initial static loads very slowly. This process leads to a considerable time loss, especially when the dynamic loads are usually very short

duration. The PID algorithm in this work was developed to alleviate this difficulty (Section 4.3).

2.3.3 Mass Scaling

For highly nonlinear, time dependent problems, explicit integration schemes have been extensively used. Dynamic simulations with explicit time integration suffer from considerable decrease of the critical time step as the mesh size decreases, i.e., mesh detail increases which consequently increases the highest natural frequency. Typically, the critical time step is in the same order of magnitude as the smallest period of the system. The maximum stable time step is usually small, gets smaller for larger models, and a large number of time steps are needed for the solution procedure.

To tackle this problem, the mass scaling technique was proposed (Belytschko et al. 2000). For a model that has a very stiff part or small elements, mass scaling can be used by adding non-physical mass to those small or stiff elements to increase the critical time step. However, it should be noted that applying extreme classical mass scaling can inevitably introduce undesirable, non-physical inertial effects as the dominant dynamical modes of the system will also be affected.

For most dynamic simulations such as ground motion simulations and sheet metal forming simulations, most of the kinetic energy is commonly trapped in low frequency modes while remaining small part of the kinetic energy resides in the high frequency modes. Considering this, the straightforward classical mass scaling technique might be modified with a more accurate selective mass scaling technique. In this type of problems, time steps greater than the critical time step can be used to accurately simulate the low frequency behavior without considering the high frequency modes. The multiscale explicit dynamics method proposed by Spencer et al. (2008) is aimed to overcome this problem. In this method, the objective is to decompose the dynamics of the model into high frequency and low frequency responses by spatial discretization, i.e., coarse and fine spaces. Thereafter, mass scaling is implemented only for the high frequency portion to increase the critical time step. Assuming that the low frequency modes control the global response, decomposing the global response into high and low frequency modes and then selectively applying mass scaling only to high frequency

modes gives more accurate results than the classical mass scaling method. However, a major deficiency of this method is that it requires assembly of the fine and coarse meshes for high frequency and low frequency responses, respectively. Arranging finite element mesh for this method to split low and high frequency modes responses in advance of analysis is quite difficult to achieve.

Instead of the multiscale explicit dynamic method, Olovsson et al. (2005) proposed two methods for more precise mass scaling. The main idea for both methods is adding mass to the mass matrix so that higher frequencies are lowered while low frequencies are left almost unchanged. For both methods, global mass matrix is modified by Equation (2.15)

$$\bar{\mathbf{m}}=\mathbf{m}+\boldsymbol{\lambda} \tag{2.15}$$

where m is the original global mass matrix of the system, λ is the artificially added mass matrix, and $\bar{\mathrm{m}}$ is the modified mass matrix. In this method, the objective is to find λ so that system's frequencies become lower while translational rigid body behavior is not affected. For the first method, Olovsson et al. (2005) suggested λ to be taken proportional the stiffness matrix. They proposed Equations (2.16) and (2.17) for calculating modified angular frequencies after the application of the method where ω is frequency of any mode of the system and $\bar{\omega}$ is the frequency of same mode after the application of mass scaling

$$\boldsymbol{\lambda}=\alpha\mathbf{k}, \qquad \alpha \geq 0 \tag{2.16}$$

$$\bar{\omega}=\omega^2/(1+\alpha\omega^2) \tag{2.17}$$

Based on Equation (2.17), Figure 2.6 was generated by Olovsson et al. to demonstrate the effect of added mass on the system's frequency spectra with varying α value. As can be seen from Figure 2.6, higher frequencies can be lowered by increasing α without affecting the lower frequencies.

In the second method proposed by Olovsson et al. (2005), they defined λ as an altered type of element mass matrix depending on the finite element type, i.e., truss, beam, solid elements. For an eight-noded, tri-linear, solid element in 3D space, element 24x24 lumped mass matrix is

$$\mathbf{m}_e = \frac{m^e}{8}\begin{bmatrix} 1 & 0 & \dots & 0 \\ 0 & 1 & & \\ \vdots & & \ddots & \\ 0 & & & 1 \end{bmatrix} \tag{2.18}$$

where m^e is total element mass. For this type of element, λ is proposed such that

$$\lambda = \begin{bmatrix} \lambda_{8x8} & 0 & 0 \\ 0 & \lambda_{8x8} & 0 \\ 0 & 0 & \lambda_{8x8} \end{bmatrix} \tag{2.19}$$

where

$$\lambda_{8x8} = \frac{\beta m^e}{56}\begin{bmatrix} 7 & -1 & \dots & -1 \\ -1 & 7 & & \\ \vdots & & \ddots & \\ -1 & & & 7 \end{bmatrix} \quad \beta \geq 0 \tag{2.20}$$

They applied the second method to a numerical model with solid elements. The ratio of eigenfrequencies for different β is shown in Figure 2.7. Figure 2.7 shows that a sudden change occurs even at low frequencies which is not desired situation as they dominate the global response.

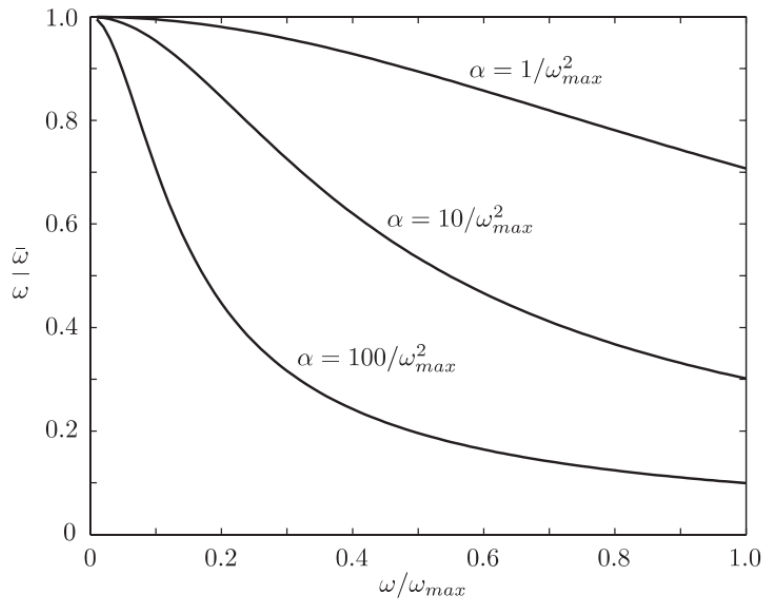

Figure 2.6 Ratio of modified and original frequencies of system with varying α for method I (Olovsson et al. 2005)

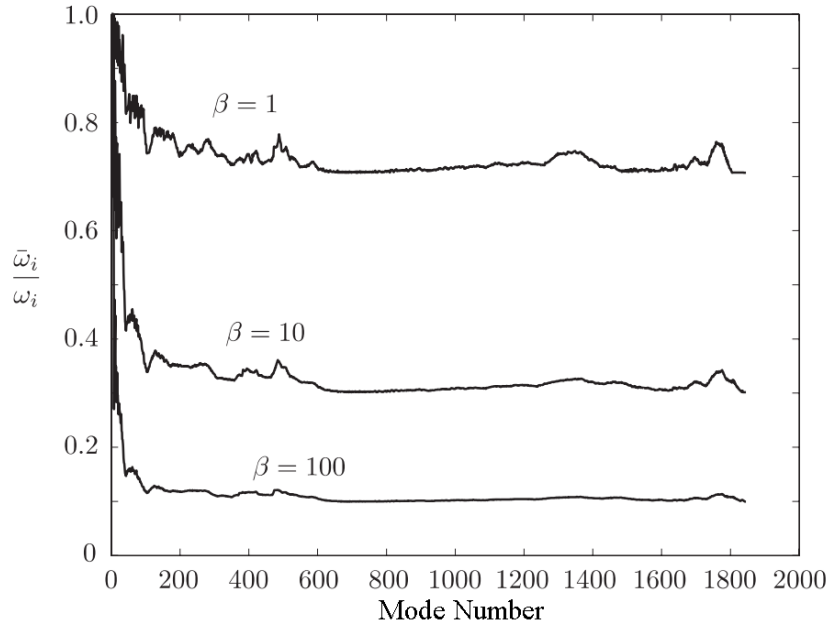

Figure 2.7 Ratio of modified and original frequencies of system with varying β for method II (Olovsson et al. 2005)

Due to the fact that in their earlier studies proposed to add matrices which contains non-diagonal terms to the original mass matrix, he suggested factorization of the modified mass matrix at every time step. Taking this as a basis, Olovsson and Simonsson (2006) proposed an iterative solution technique for selective mass scaling. For iterative solution, they suggested to use the conjugate gradient method and presented a new convergence criterion.

In order to increase the maximum stable time step of the analysis that uses explicit time integration, Cocchetti et al. (2013) introduced a mass scaling technique for a specific type of finite element (eight-node solid shell element) without affecting the dynamic response of the system. The method builds on the idea of a linear transformation of the degrees of freedom and application of mass scaling straightforwardly to the transformed degrees of freedom.

2.3.4 PID Control and Tuning Parameters

In spite of the development of more novel controlling techniques, PID controllers are effective and still very widely used in control systems. Although this controlling

approach is simple, it is capable of operating in a wide variety of conditions. The PID controlling algorithm is generally used by electrical engineers for circuit design. In this study, it will be used in the context of load control in structural analysis (Section 4.3).

The main idea of the PID algorithm is to calculate the error between the desired input and the output of the system by summing the proportional, integral and derivative errors. Then the algorithm decreases the error in time by intelligently controlling the input. Before going on the PID theory, closed loop and open loop control systems need to be defined and distinguished.

In open loop systems, input is not effected by output and it is prescribed for the process before the initiation. On the other hand, closed loop systems have feedbacks, and unlike open loop systems, the output of the system can effect and adjust the prospective input. Figure 2.8 shows block diagram representations for the open loop and closed loop systems. It can be said that most of the structural engineering simulations have open loop control system due to the fact that they have no feedback during the simulation.

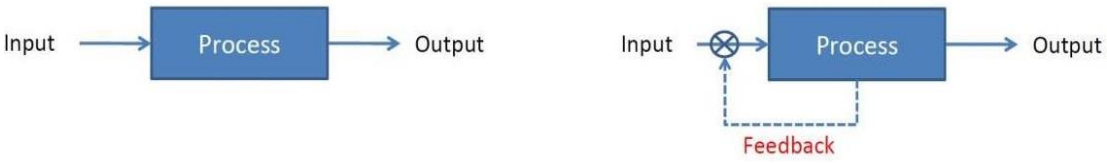

(a) Open Loop System (b) Closed Loop System

Figure 2.8. Block diagram representation of the open loop and closed loop systems.

Before starting the process, controller effect on the system should be checked whether it meets the performance requirements which are defined prior to the simulation. This can be achieved by applying a test function, which is generally a step function, for the set point which is the desired value of the selected variable and evaluating the response of the same variable. Response of the system is characterized by its transient and steady state differences with respect to the applied test function in order to decide if the controlled system fulfills the requirements. As Figure 2.9 shows, the attributes of

the response are the steady-state error, percent overshoot, settling time and the rise time. The steady-state error is the variation between the desired value and the response value after the transient vibration. Rise time is the amount of time required to reach 90% of the desired value of the variable from 10%. Percent overshoot is the percent error between the maximum value of the response and the desired value. The settling time is the time elapsed for the response variable to reach stability with the specified tolerance quantity (typically 5% which is located close to the end of the transient response).

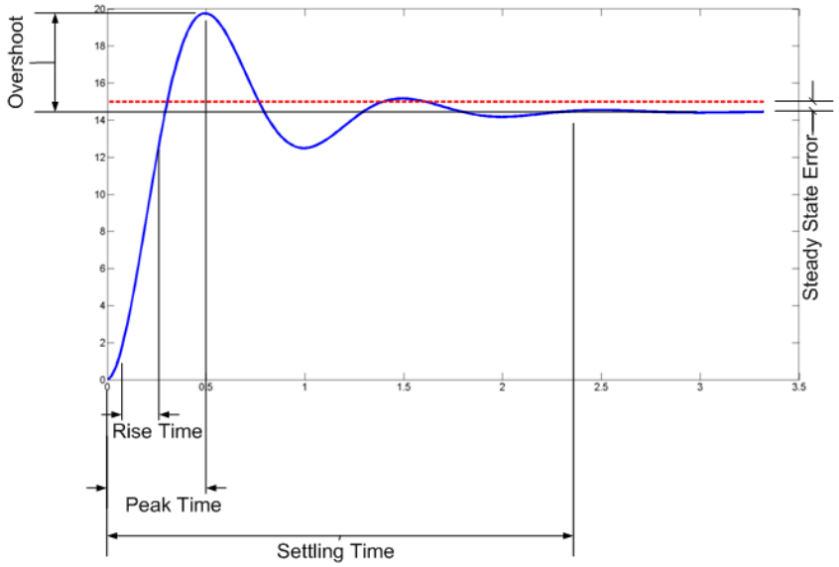

Figure 2.9. An ordinary response of the system under step point defined as step function. (Tehrani and Mpanda, 2012)

The integro-differential equations of a PID controller are given below

$$co(t)=K_p e(t)+K_i \int e(t)dt+K_d \frac{de}{dt} \tag{2.21}$$

$$e(t)=r(t)-y(t) \tag{2.22}$$

$$co(t)=K_p \left(e(t)+\frac{1}{T_i}\int e(t)dt+T_d \frac{de}{dt}\right) \tag{2.23}$$

where co(t) is the controller output, e(t) is the tracking error, K_p is the proportional gain coefficient, K_i is the integral gain coefficient and K_d is the derivative gain coefficients. Tracking error is the difference between desired value of the controlling variable i.e. set point, r(t), and process measurement of the same variable, y(t), as in the Equation (2.22). In this expression, the proportional term can be considered as

current error, the integral term as the cumulative error from the initial to the present, and the third term which is derivative term can be regarded as forecast of the prospective error. The effects of coefficients of these terms can be seen in Table 2.2. Rather than Equation (2.21), the controller equation can also be expressed as Equation (2.23) where T_i is the integral time and T_d is the derivative time. PID controller can be adopted to the numerical analysis, after the implementation a representative control block diagram of the numerical analysis can be seen in Figure 2.10.

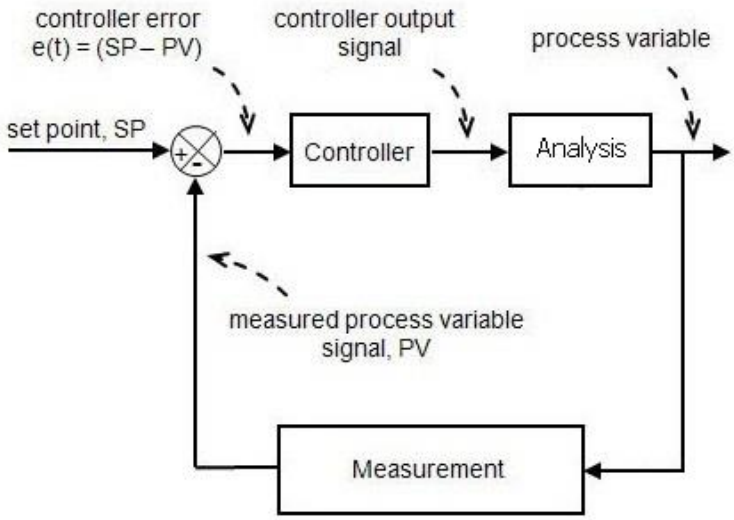

Figure 2.10. A representative block diagram of the numerical analysis (Tehrani and Mpanda, 2012)

The most challenging part for a PID controller is the determination of its parameters. One of the classical tuning method is the Ziegler and Nichols (1942) step response method which is widely used although it was proposed in 1942. This method uses the unit step function response of the system as the base for tuning process. The response of the system to the unit step function is described by α and L as shown in Figure 2.11. These parameters are the intercept values on the time & displacement axes when a tangent is drawn from the inflection point of the response. Ziegler and Nichols (1942) proposed controller parameter values as shown in the Table 2.1.

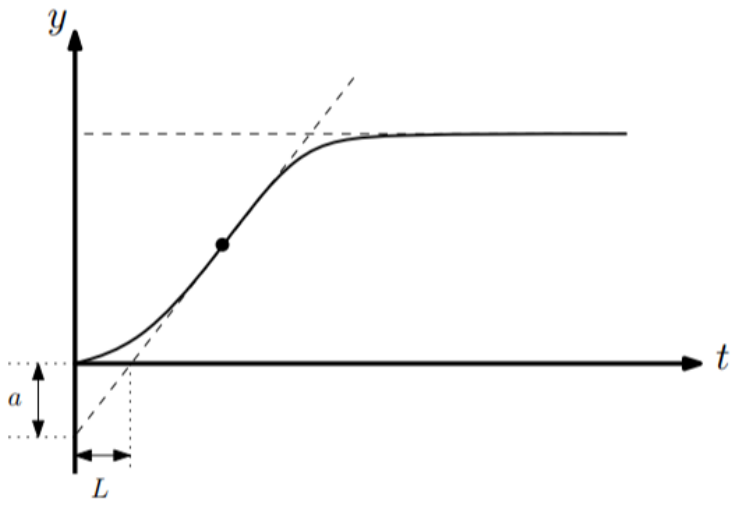

Figure 2.11. Characterization of a step-response in Zeigler-Nichols method (Hang et al. 1991)

Table 2.1. Parameters of a PID controller estimated by the Ziegler-Nichols method

K_p	T_i	T_d
1.2/α	2L	L/2

Table 2.2. Effects of the coefficients on the response (Tehrani and Mpanda 2012)

	Rise Time	Overshoot	Settling Time	Steady-State Error
Increasing K_p	Decrease	Increase	Small Increase	Decrease
Increasing K_i	Small Decrease	Increase	Increase	Large Decrease
Increasing K_d	Small Decrease	Decrease	Decrease	Minor Change

In the view of structural analysis, controlling variable can be chosen as the rate of change of any quantity to control the external force. To be more descriptive, as can be seen from the Figure 2.12, the rate of change of the relative displacement between point A and B, time derivative of displacement in the x-direction at points A, the rate of change of the crack width at point C or the rate of change of stress or strain at point D can be chosen as the controlling variable to control the time derivate of the external force. After the estimation of the coefficients K_p, K_i, K_d, external force is solved using

the integro-differential equation (Equation 2.21) whose application yields the desired output time history.

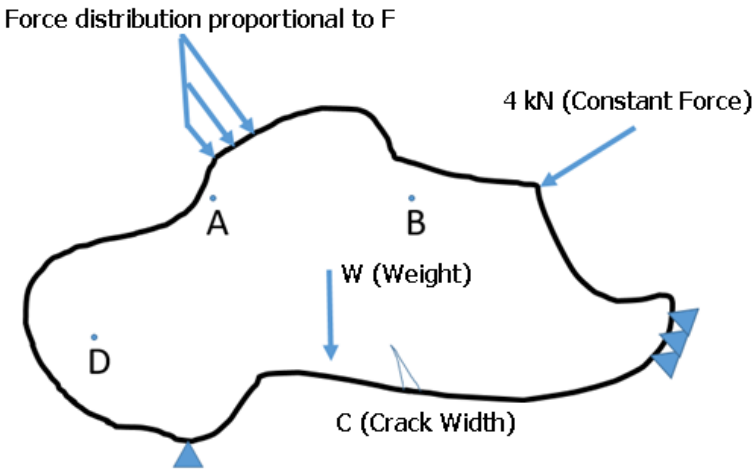

Figure 2.12. A representative structural body under loads

2.3.5 Numerical Integration

In the formulation of the displacement-based fiber elements, an integration scheme is required within the finite element framework (Section 2.2). In this study, integrals that arise in the displacement-based fiber element formulation are computed by using a numerical integration technique. Therefore, a brief literature review for the numerical integration technique is presented in here.

The definition of integral is given as

$$I(f)=\int_a^b f(x)dx \tag{2.24}$$

which is the area under the f(x) from a to b. Instead of analytical integration, approximation techniques are used when the integrand is a complicated function. These numerical techniques are generally called quadrature formulas and they are expressed in the following form

$$I_{n+1}(f)=\sum_{i=0}^{n} f(x_i)w_i + E_{n+1} \tag{2.25}$$

where

w_i is the weight factor (independent of f(x)),

$f(x_i)$ is the sampled value of the function at the integration point x_i,
E_{n+1} is the error due to the use of numerical integration.

In this chapter, the two quadrature formulations commonly used are reviewed: Newton-Cotes and Gaussian quadratures.

2.3.5.1 Newton-Cotes formulas

There are two Newton-Cotes formulas: open and closed Newton-Cotes. In the closed Newton-Cotes formulation, in order to integrate f(x) over the interval of [a, b], domain is divided into n equal parts and Lagrange interpolating polynomials are used in between each node and the corresponding function values are calculated at these integration points. The Lagrange polynomial P_n used for this purpose is given below.

$$P_n(x)=\sum_{i=0}^{n} f(x_i)\prod_{\substack{j=0\\ j\neq i}}^{n}\frac{(x-x_j)}{(x_i-x_j)} \tag{2.26}$$

The Lagrange polynomial is integrated over the domain [a, b] in order to obtain the closed Newton-Cotes formulation

$$I_{n+1}(f)=\int_a^b P_n(x)dx=\int_a^b [\sum_{i=0}^{n} f(x_i)\prod_{\substack{j=0\\ j\neq i}}^{n}\frac{(x-x_j)}{(x_i-x_j)}]dx=\sum_{i=0}^{n} f(x_i)w_i \tag{2.27}$$

where

$$w_i=\int_a^b \prod_{\substack{j=0\\ j\neq i}}^{n}\frac{(x-x_j)}{(x_i-x_j)}dx=\sum_{i=0}^{n} f(x_i)w_i \tag{2.28}$$

It should be noted that weights do not depend on f(x) according to Equation (2.28). For instance, for n = 1 (linear interpolation case), x_1=a, x_2=b and h=b-a, Lagrange polynomial takes the form

$$P_1(x)=\frac{(x-x_2)}{(x_1-x_2)}f(x_1)+\frac{(x-x_1)}{(x_2-x_1)}f(x_2) \tag{2.29}$$

$$P_1(x)=\frac{(x-x_1-h)}{-h}f(x_1)+\frac{(x-x_1)}{h}f(x_2) \tag{2.30}$$

$$P_1(x)=\frac{x}{h}(f(x_2)-f(x_1))+(f(x_1)+\frac{x_1}{h}f(x_1)-\frac{x_1}{h}f(x_2)) \tag{2.31}$$

Substitution of Equation (2.31) into the Equation (2.26) gives

$$\int_{x_1}^{x_2} f(x)dx \approx \int_{x_1}^{x_2} P_1(x)dx \tag{2.32}$$

$$\int_{x_1}^{x_2} f(x)dx \approx \frac{1}{2h}(f(x_2)-f(x_1))[x^2]_{x_1}^{x_2}+(f(x_1)+\frac{x_1}{h}f(x_1)-\frac{x_1}{h}f(x_2))[x]_{x_1}^{x_2} \tag{2.33}$$

$$\int_{x_1}^{x_2} f(x)dx \approx \frac{1}{2h}(f(x_2)-f(x_1))(x_2+x_1)(x_2-x_1)+(x_2-x_1)(f(x_1)+\frac{x_1}{h}f(x_1)-\frac{x_1}{h}f(x_2)) \tag{2.34}$$

$$\int_{x_1}^{x_2} f(x)dx \approx \frac{1}{2}(f(x_2)-f(x_1))(2x_1+h)+f(x_1)h+x_1(f(x_1)-f(x_2)) \tag{2.35}$$

$$\int_{x_1}^{x_2} f(x)dx \approx x_1(f(x_2)-f(x_1))+\frac{1}{2}h(f(x_2)-f(x_1))+hf(x_1)-x_1(f(x_2)-f(x_1)) \tag{2.36}$$

$$\int_{x_1}^{x_2} f(x)dx \approx \frac{1}{2}h(f(x_1)+f(x_2)) \tag{2.37}$$

Equation (2.37) is the trapezoidal rule (Ueberhuber, 1997). Error terms for the Newton-Cotes approach is derived by Steffensen (1950) as if n is an even integer and integrand, f(x), is differentiable (n+2) times in the domain of [a, b] then there exist a number ξ in the interval of [a, b] for which

$$E_{n+1}(f)=\frac{h^{n+3}f^{n+2}(\xi)}{(n+2)!}\int_0^n t^2(t-1)\dots(t-n)dt \tag{2.38}$$

If n is odd and integrand, f(x), is differentiable (n+1) times on [a, b], then

$$E_{n+1}(f)=\frac{h^{n+2}f^{n+1}(\xi)}{(n+1)!}\int_0^n t(t-1)\dots(t-n)dt \tag{2.39}$$

For trapezoidal rule (n=1), substituting n into the Equation (2.39), error term becomes

$$E_2(f)=\frac{h^3}{12}f^2(\xi) \tag{2.40}$$

For closed Newton-Cotes formulas, other than trapezoidal rule, n=2 case is commonly referred as Simpson's rule, n=3 is referred as Simpson's three-eighths rule.

In the open Newton-Cotes formulation, instead of dividing domain [a, b] as x_i where $x_i = x_0$+ih for i=0,1,2…n by setting x_0=a, x_n=b and h=(b-a)/n the domain is divided as $x_j=x_0$+jh for each j=0,1,2…n where h=(b-a)/(n+2) and x_0=a+h. Difference in the discretization can be seen in Figure 2.13. Rest of the procedure is the same as the procedure presented for the closed Newton-Cotes formulation.

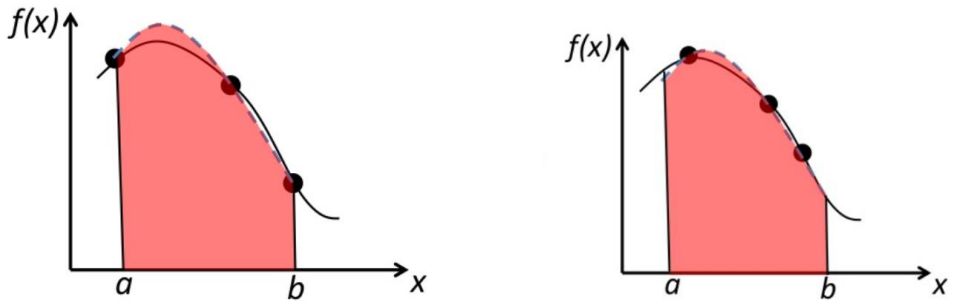

(a) (b)

Figure 2.13. Difference in between open and closed Newton-Cotes Formulas
(a) Closed (b) Open

2.3.5.2 Gauss Quadrature

Newton-Cotes formulas requires that the function is sampled uniformly. In the Gauss quadrature, these integration points are determined according to the number of integration points. This method approximates the integral as follows

$$\int_a^b f(x)dx \approx \sum_{i=0}^{m} f(x_i)w_i \tag{2.41}$$

with the sampling points x_i and the corresponding weights w_i.

Gauss quadrature formulation is based on following theory. $Q_0(x)$, $Q_1(x)$, …, $Q_m(x)$ be a series of orthogonal polynomials on [a, b] with respect to the scalar inner product

$$<f,g> = \int_a^b f(x)g(x)c(x)dx \tag{2.42}$$

where c(x) is a weighting function. Then for k<m, the polynomial $Q_k(x)$ has exactly k roots in [a, b].

Therefore, Gauss quadrature formula has a form of

$$\int_a^b f(x)c(x)dx = \sum_{i=0}^{m} f(x_i)w_i + E_m(f) \tag{2.43}$$

where w_i do not depend on $f(x_i)$. The weights w_i can be written as follows

$$w_i = \frac{<Q_{m-1}(x), Q_m'(x)>}{mQ_{m-1}(x)Q_m'(x)} = \frac{\int_a^b Q_{m-1}(x)Q_m'(x)\,c(x)dx}{mQ_{m-1}(x)Q_m'(x)} \tag{2.44}$$

Error in this method is

$$E_m(f)=\frac{f^{2m}(\xi)}{(2m)!}<Q_m(x),Q_m(x)> \quad (2.45)$$

From the error term definition, it is obvious that in this method using m polynomials exactly integrates (2m-1) degree of polynomials. Orthogonal polynomials must be chosen to apply this method, i.e., Hermite, Jacobi, Legendre, Chebtshev. Legendre polynomials are the commonly utilized polynomials bases. All of the polynomial families are orthogonal with c(x)=1 over the [-1, 1]. The first four Legendre polynomials are

$$Q_0(x)=1 \quad (2.46)$$

$$Q_1(x)=x \quad (2.47)$$

$$Q_2(x)=x^2-\frac{1}{3} \quad (2.48)$$

$$Q_3(x)=x^3-\frac{3}{5}x \quad (2.49)$$

In case of domain is not [-1, 1], linear transformation (Equation (2.50)) is needed for using Gauss-Legendre method.

$$\int_a^b f(x)dx=\int_{-1}^{1} f\left(\frac{(b-a)\xi+(a+b)}{2}\right)\left(\frac{b-a}{2}\right)d\xi \quad (2.50)$$

Another Gauss quadrature formula is the so called Gauss-Lobatto quadrature. In this method, two integration points are fixed at the ends of the interval, i. e., -1 and 1. This method exactly integrates 2m-3 degree of polynomials which is two orders lower than the Gauss-Legendre formula (Hildebrand 1974). Gauss-Lobatto quadrature is generally implemented in force-based elements since the element ends have largest bending moment when they are not subjected to axial loads (Scott and Fenves 2006).

CHAPTER 3

MODELING AND ANALYSIS

3.1 General

In this Chapter, the modeling technique and analysis methods which are used in this study are presented. The formulation of the displacement-based fiber elements are shown. Constitutive laws for the materials used in the simulations are discussed. PID control, the utilized mass scaling and solution procedures to the nonlinear equation are also presented.

3.2 Displacement-Based Fiber Element

For a displacement-based fiber element, the forces, **p**, and the corresponding deformations, **u**, are illustrated at the element level in Figure 3.1(a), that they the following forms

$$\mathbf{p} = [p_1, p_2, p_3, p_4, p_5, p_6]^T \tag{3.1}$$

$$\mathbf{u} = [u_1, u_2, u_3, u_4, u_5, u_6]^T \tag{3.2}$$

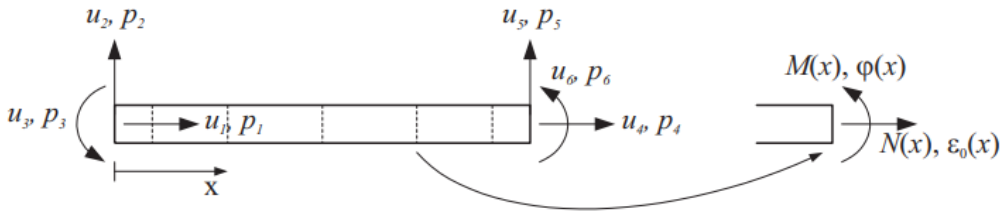

(a) Element (b) Section

Figure 3.1. Force and deformation variables at the element and section levels (Lee and Mosalam, 2006)

Beside element level variebles, the section deformation, $v_s(x)$, and force vector, q(x), are given in the Equations(3.3) and (3.4), and they are shown in Figure 3.1(b) where N is the normal force, M is the bending moment, ε_0 is the axial strain at the reference axis, φ is the curvature with respect to section position x. The section deformation vector and the force vector have the following form for all sections within an element

$$\mathbf{q}(x) = [N(x), M(x)]^T \tag{3.3}$$

$$\mathbf{v_s}(x) = [\varepsilon_0(x), \varphi(x)]^T \tag{3.4}$$

Increment of the strain in the i^{th} fiber is

$$d\varepsilon_i = d\varepsilon_0(x) - y_i d\varphi(x) \tag{3.5}$$

$$d\varepsilon_i = \mathbf{a_s}(y) d\mathbf{v_s}(x) \tag{3.6}$$

where y_i is the distance between the reference axis and the i^{th} fiber. The definition of $\mathbf{a_s}(y)$ and $\mathbf{v_s}(x)$ vectors are given in Equations (3.7) and (3.8) where $\mathbf{B}(x)$ is the transformation matrix from strain to displacement by using first and second derivatives of the displacement field functions which are derived for small deformations

$$\mathbf{v}_s(x) = \mathbf{B}(x)\mathbf{u}_{n+1} \tag{3.7}$$

$$\mathbf{a}_s(y) = [1, -y_i] \tag{3.8}$$

Formulation of matrix B is given in Equation (3.9) (Lee & Mosalam 2006)

$$\mathbf{B}(x) = \begin{bmatrix} \frac{-1}{L} & 0 & 0 & \frac{1}{L} & 0 & 0 \\ 0 & -\frac{6}{L^2}+\frac{12x}{L^3} & \frac{-4}{L}+\frac{6x}{L^2} & 0 & \frac{6}{L^2}-\frac{12x}{L^3} & \frac{-2}{L}+\frac{6x}{L^2} \end{bmatrix} \tag{3.9}$$

where L is the element length and u_{n+1} is the element deformation matrix at the time step n+1.

For the i^{th} fiber, the stress σ_i and the secant modulus E_{si} which are used in the computation are calculated from the strain ε_i using the constitutive model. By using the principle of virtual work, section force matrix and the section stiffness matrix are obtained and the resulting expressions are given in Equation (3.10) and (3.11).

$$\mathbf{k}_s(x) = \int_{A(x)} a_s{}^T(y)\, E_s(x,y) a_s(y) dA \tag{3.10}$$

$$\mathbf{r}_s(x) = \int_{A(x)} a_s{}^T(y)\, E_s(x,y) dA \tag{3.11}$$

The section stiffness and restoring force integrals are calculated numerically for n fibers in the section by using the midpoint rule. Therefore, equations take the following form

$$\mathbf{k}_s(x) = \sum_{i=1}^{n} a_{si}{}^T E_{si} a_{si} a_i \tag{3.12}$$

$$\mathbf{r}_s(x) = \sum_{i=1}^{n} a_{si}{}^T E_{si} a_i \tag{3.13}$$

where A(x) is the cross sectional area and equals to $\sum_{i=1}^{n} a_i$.

After the section deformation $v_s(x)$ is calculated, the resisting forces $r_s(x)$ and the section stiffness $k_s(x)$ are determined. By using the virtual work principle, the element resisting forces r_e and the element stiffness k_e are obtained as follows

$$\mathbf{k}_e = \int_L \mathbf{B}^T(x)\, \mathbf{k}_s(x) \mathbf{B}(x) dx \tag{3.14}$$

$$\mathbf{r}_e = \int_L \mathbf{B}^T(x)\, \mathbf{r}_s(x) dx \tag{3.15}$$

To evaluate these integrals, Gauss-Lobatto numerical integration technique is adopted in this study. In the computer program developed within the scope of this thesis study, the integration points to be used in the elements are determined by the user. By using the element end forces, the global restoring force vector is assembled and transferred to the time explicit integration algorithm.

3.3 Material Models

In order to calculate the secant modulus of elasticity, material models are needed for concrete and reinforcing steel. For concrete, Mander et al. (1988a) material model is used whereas for the reinforcing steel one dimensional plasticity with linear kinematic hardening is adopted.

3.3.1 Constitutive Model for Confined Concrete

Mander et al. (1988b) tested full scale columns that have square, rectangular, and circular cross sections to examine the effect of different transverse reinforcing steel patterns on the general behavior of columns and on the effectiveness of confinement.

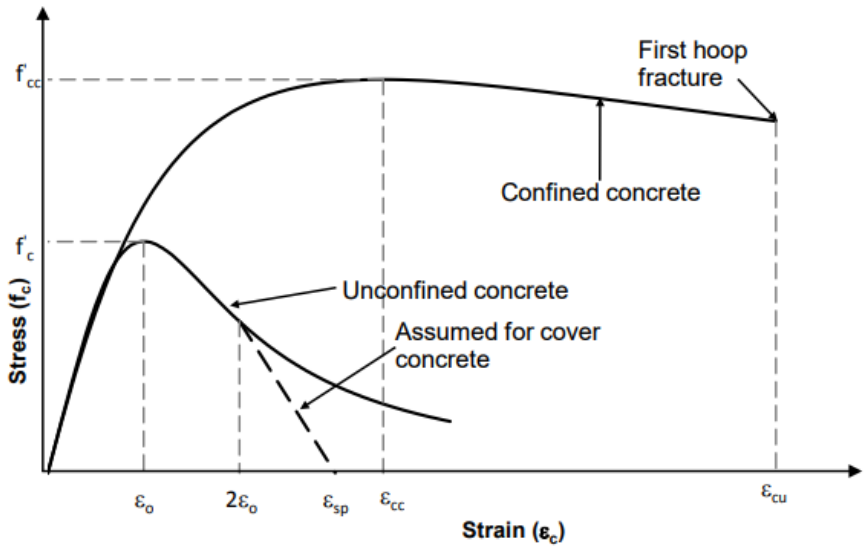

Figure 3.2. Stress-strain relation of unconfined and confined concrete (Mander et al. 1988b)

Thereafter, Mander et al. (1988b) proposed a generalized stress-strain model for confined concrete whose envelope curve is shown in Figure 3.2. The envelope curve of the proposed model in the figure can be calculated using the following expressions

$$f_c = \frac{f'_{cc} x r}{r-1+x^r} \tag{3.16}$$

$$x = \frac{\varepsilon_c}{\varepsilon_{cc}} \tag{3.17}$$

$$\varepsilon_{cc} = \varepsilon_{co}\left[1+5\left(\frac{f'_{cc}}{f'_{co}}-1\right)\right] \tag{3.18}$$

$$r = \frac{E_c}{E_c - E_{sec}} \tag{3.19}$$

$$E_c = 5000\sqrt{f'_{co}} \tag{3.20}$$

$$E_{sec} = \frac{f'_{cc}}{\varepsilon_{cc}} \tag{3.21}$$

where f_c is the compressive concrete stress, ε_c is the compressive strain of concrete, f'_{cc} is the peak compressive stress of confined concrete, ε_{cc} is the concrete strain at peak stress, f'_{co} is the peak compressive stress of unconfined concrete, ε_{co} is the strain at peak stress of unconfined concrete, E_c is the modulus of elasticity of concrete, and E_{sec} is the secant modulus of confined concrete at peak stress.

For columns with circular hoops or circular spirals, the peak compressive stress of confined concrete, f'_{cc}, is given as

$$f'_{cc} = f'_{co}\left[-1.254+2.254\sqrt{1+\frac{7.94f'_l}{f'_{co}}}-2\frac{f'_l}{f'_{co}}\right] \quad (3.22)$$

where f'_l is calculated from

$$f'_l = \frac{1}{2}k_e\rho_s f_{yh} \quad (3.23)$$

Here ρ_s is the ratio of area of longitudinal reinforcement to the gross area of the column, f_{yh} is the yield strength of transverse reinforcement, and k_e is the confinement effectiveness coefficient.

The confinement coefficient can be calculated for different confinement types and cross sections as follows for circular hoops,

$$k_e = \frac{\left(1-\frac{s'}{2d_s}\right)^2}{1-\rho_{ss}} \quad (3.24)$$

for circular spirals,

$$k_e = \frac{1-\frac{s'}{2d_s}}{1-\rho_{ss}} \quad (3.25)$$

where ρ_{ss} is the ratio of area of longitudinal reinforcement to the core area of the section, and s' is the clear spacing between spiral or hoop bars, and d_s is the diameter of spiral.

For rectangular columns, $$k_e = \left(1-\sum_{i=1}^{n}\frac{(w_i')^2}{6b_cd_c}\right)\left(1-\frac{s'}{2b_c}\right)\left(1-\frac{s'}{2d_c}\right)\Big/(1-\rho_{ss}) \quad (3.26)$$

where w_i' is the i^{th} clear transverse spacing between adjacent longitudinal bars, b_c is the concrete core dimension to center line of perimeter hoop in x direction and d_c is the same dimension in y direction.

It is very common for rectangular columns to have different amounts of transverse steel in the x- and y-directions. For these cases effective lateral confining stresses can be computed from Equation (3.27) and (3.28) in the x- and y-directions as follows

$$f'_{lx} = k_e \frac{A_{sx}}{sd_c} f_{yh} \tag{3.27}$$

$$f'_{ly} = k_e \frac{A_{sy}}{sb_c} f_{yh} \tag{3.28}$$

For the computation of the peak compressive stress of confined concrete, f'_{cc}, the chart given in Figure 3.3 is utilized.

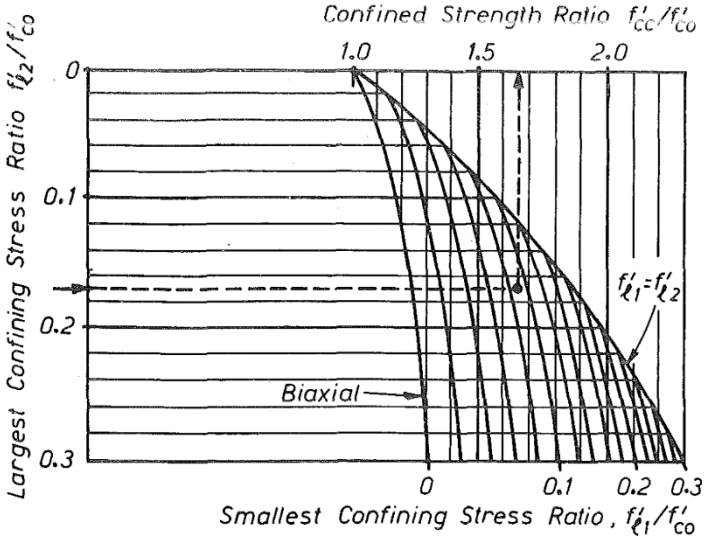

Figure 3.3. Confined peak stress determination from lateral confining stresses for rectangular sections (Mander et al. 1988b)

For tension behavior up to the tensile strength, f'_t, linear stress-strain relation with the slope of E_{sec} is used.

There are two unloading cases: the compressive unloading and the tensile unloading. For the compressive unloading case, nonlinear behavior is modelled as shown in Figure 3.4.

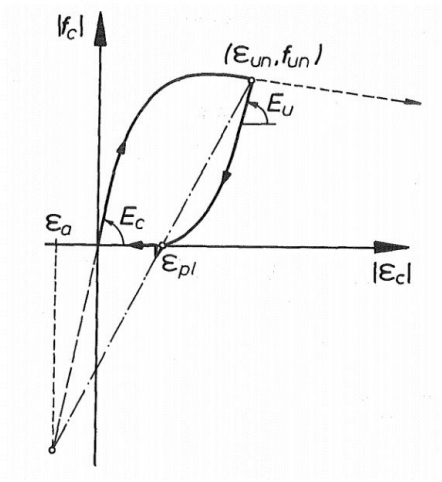

Figure 3.4. Stress-strain curves for unloading case
(Mander et al. 1988b)

The auxiliary strain variable, ε_a, proposed to compute plastic strain, ε_{pl}, are expressed as

$$\varepsilon_a = a\sqrt{\varepsilon_{un}\varepsilon_{cc}} \tag{3.29}$$

$$a = \max\left(\frac{\varepsilon_{cc}}{\varepsilon_{cc}+\varepsilon_{un}}, \frac{0.09\varepsilon_{un}}{\varepsilon_{cc}}\right) \tag{3.30}$$

$$\varepsilon_{pl} = \varepsilon_{un} - \left((\varepsilon_{un}+\varepsilon_a)f_{un}\right) / (f_{un}+E_c\varepsilon_a) \tag{3.31}$$

For the unloading curve shown in Figure 3.4, Equation (3.32) is introduced which is the altered form of envelope curve equation

$$f_c = f_{un} - \frac{f_{un}xr}{r-1+x^r} \tag{3.32}$$

where

$$x = \frac{\varepsilon_c - \varepsilon_{un}}{\varepsilon_{pl} - \varepsilon_{un}} \tag{3.33}$$

$$r = \frac{bcE_c}{bcE_c - (f_{un} / (\varepsilon_{un}-\varepsilon_{pl}))} \tag{3.34}$$

$$b = \frac{f_{un}}{f'_{co}} \geq 1 \tag{3.35}$$

$$c = \left(\frac{\varepsilon_{cc}}{\varepsilon_{un}}\right)^{0.5} \geq 1 \tag{3.36}$$

The effect of unloading from compression to tension was examined by Morita and Kaku (1975) and based on their findings Mander et al. (1988b) idealized the

deterioration in the tension behavior because of earlier compression behavior as shown in Figure 3.5.

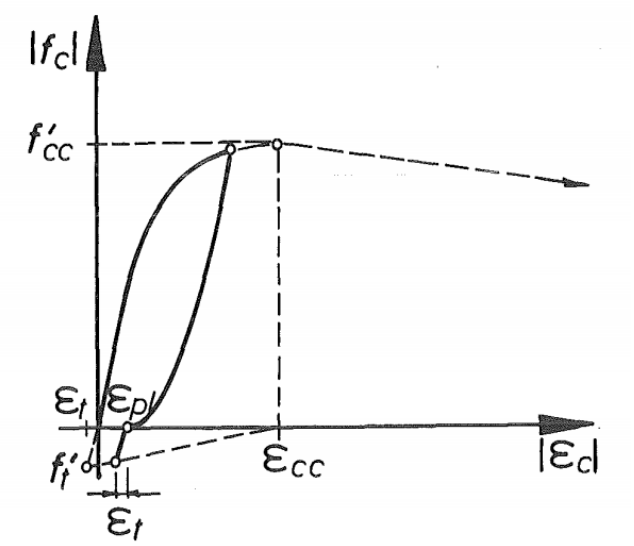

Figure 3.5. Assumed deterioration in tensile strength of concrete due to prior compression loading (Mander et al. 1988b)

When concrete makes the transition from compression to tension, the tensile strength is given by

$$f_t^{'} = f_t^{'}\left(1-\frac{\varepsilon_{pl}}{\varepsilon_{cc}}\right) \tag{3.37}$$

where $f_t^{'}$ is the tensile strength of concrete. The stress-strain relation is given by

$$f_t = E_t\left(\varepsilon_c-\varepsilon_{pl}\right) \tag{3.38}$$

$$E_t=\frac{f_t}{\varepsilon_t} \tag{3.39}$$

$$\varepsilon_t=\frac{f_t^{'}}{E_c} \tag{3.40}$$

If the strain on concrete exceeds the tensile strain, tensile strength of the concrete becomes zero for future loadings. The proposed reloading behavior can be seen in Figure 3.6 which also shows unloading branches.

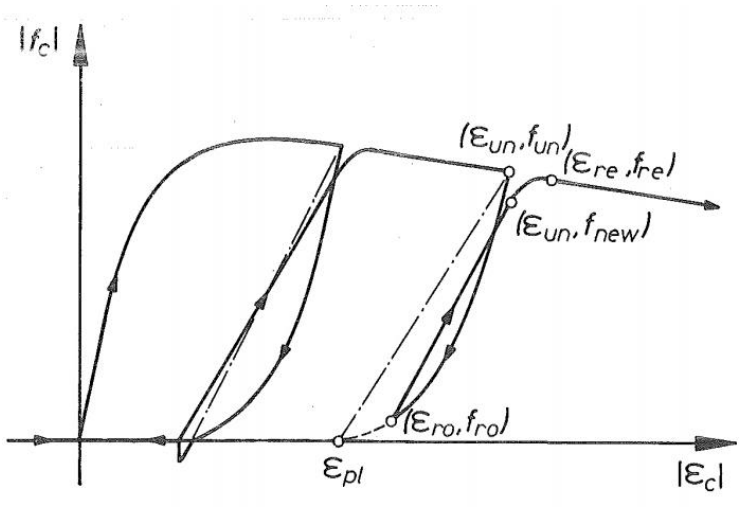

Figure 3.6. Assumed stress-strain curves for reloading branch
Mander et al. (1988b)

To model the reloading behavior, an auxiliary variable f_{new} was defined. For the following equations ε_{ro} and f_{ro} denote the strain and stress at the reloading point. Between ε_{ro} and ε_{un}, a linear relationship was proposed for the stress strain behavior as shown in Equation (3.41). In order to take account of the cyclic degradation, slope of the line decreases due to the loading-unloading cycles.

$$f_c = f_{ro} + E_r(\varepsilon_c - \varepsilon_{ro}) \tag{3.41}$$

$$E_r = (f_{ro} - f_{new})/(\varepsilon_{ro} - \varepsilon_{un}) \tag{3.42}$$

$$f_{new} = 0.92 f_{un} + 0.08 f_{ro} \tag{3.43}$$

A second order polynomial curve i.e. Equation (3.44) is proposed between (ε_{un} , f_{new}) and (ε_{re} , f_{re}) where the second point is the strain and stress at the return part on the monotonic stress strain curve, and E_r is the tangent modulus of the returning point on the envelope curve.

$$\varepsilon_{re} = \varepsilon_{un} + (f_{un} - f_{new}) / \left(E_r \left(2 + \frac{f'_{cc}}{f'_{co}} \right) \right) \tag{3.44}$$

$$f_c = f_{re} + E_r(\varepsilon_c - \varepsilon_{re}) + A(\varepsilon_c - \varepsilon_{re})^2 \tag{3.45}$$

$$A = \frac{E_r - E_{re}}{-4[(f_{new} - f_{re}) - E_r(\varepsilon_{un} - \varepsilon_{re})} \tag{3.46}$$

3.3.2 Constitutive Model for Unconfined Concrete

For unconfined concrete, Hognestad (1951) model is adopted. Material model is shown in Figure 3.7. It has a parabolic curve for strains smaller than ε_{co} and a linear line for greater strains. The constitutive model is expressed as

$$\sigma = f_c \left(\frac{2\varepsilon_c}{\varepsilon_{co}} - \left(\frac{\varepsilon_c}{\varepsilon_{co}} \right)^2 \right) \text{ for } \varepsilon_c \leq \varepsilon_{co} \tag{3.47}$$

$$\sigma = f_c \left(1 - 0.15 \left(\frac{\varepsilon_c - \varepsilon_{co}}{\varepsilon_{cu} - \varepsilon_{co}} \right) \right) \text{ for } \varepsilon_{co} \leq \varepsilon_c \leq \varepsilon_{cu} \tag{3.48}$$

where

$$\varepsilon_{co} = \frac{2f_c}{E_c} \tag{3.49}$$

$$E_c = 12680 + 460 f_c \tag{3.50}$$

and ε_{cu} is taken as 0.0038 as proposed by Hognestad. Although Hognestad (1951) proposed an envelope curve for unconfined concrete, for the cyclic loading, linear loading-unloading line with a slope of E_c is assumed.

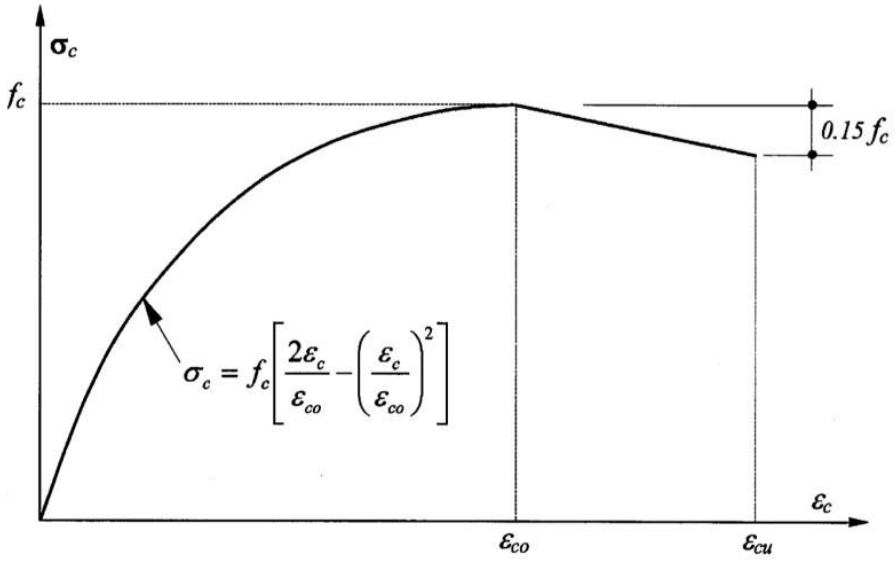

Figure 3.7. Proposed constitutive model for unconfined concrete model (Hognestad 1951)

3.3.3 Constitutive Model for Steel Reinforcement

In this study, elastoplasticity with kinematic hardening material model was assumed for the reinforcement steel. In this model, yield surface, i.e., elastic domain moves

rigidly in the direction of plastic flow as shown in Figure 3.8. If the amount of shift of the elastic domain is denoted by β, the shifted yield surface can be expressed as

$$\varphi(\sigma, \beta) = |\sigma - \beta| - y_o \leq 0 \tag{3.51}$$

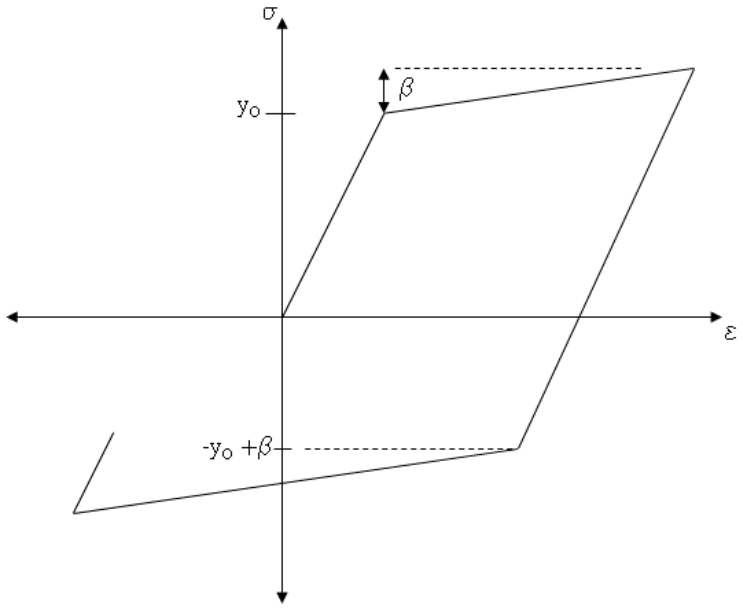

Figure 3.8. The stress-strain relation for elastoplasticity with kinematic hardening

The state of the material is a function of the total strain ε, plastic strain ε^p and the plastic arc length variable, α, for kinematic hardening. The stored energy (Green and Naghdi 1977) as given in Equation (3.52) can be decomposed into elastic and plastic parts where ρ is the mass density, Ψ is the free energy function, ε^e is the elastic strain , H is the kinematic hardening modulus and E is the Young's modulus

$$\rho\Psi = \frac{1}{2}E(\varepsilon^e)^2 + \frac{1}{2}H\alpha^2 \tag{3.52}$$

To be thermodynamically consistent, the principle of maximum dissipation is satisfied by using the method of Lagrangian multiplier on the dissipation inequality derived from Equation (3.52) by using the Clausius-Planck inequality (Green and Naghdi 1977)

$$\sigma\dot{\varepsilon}^p - \beta\dot{\alpha} \geq 0 \tag{3.53}$$

Return mapping algorithm is used for the implementation of this material model. Algorithm has two parts which are the elastic predictor step and the plastic corrector step if needed. The algorithm consists of two cases which are plastic corrector case and elastic case. These cases can be visualized graphically as Figure 3.9.

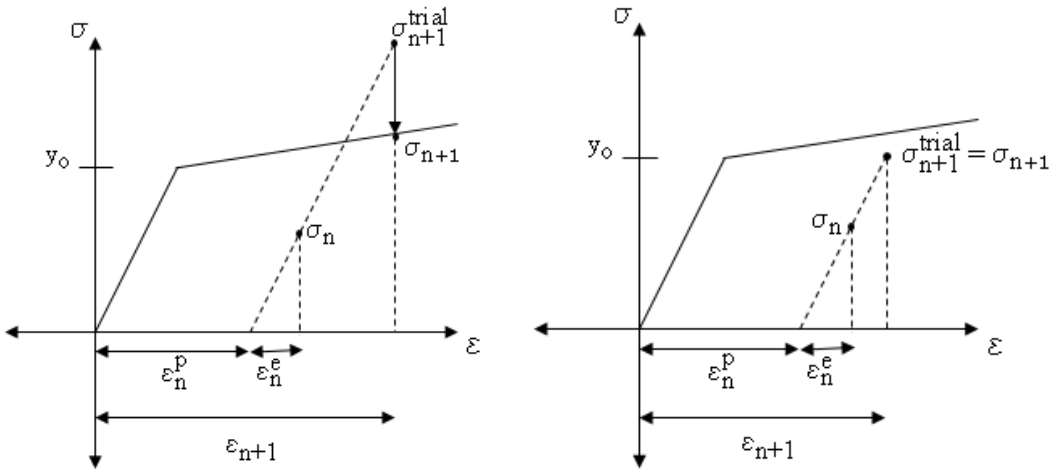

(a) Plastic corrector case (b) Elastic case

Figure 3.9. Return mapping algorithm and its cases

The algorithm consists of the following steps:

From the previous time step plastic strain ε^p_n, plastic arc length α_n are known as well as total strain ε_{n+1} in the present time step.

Elastic predictor step:

$$\sigma^{*,trial}_{n+1}=\sigma^{trial}_{n+1}-\sigma^{trial}_{n}=E\left(\varepsilon_{n+1}-\varepsilon^p_n\right)-H\alpha_n \tag{3.54}$$

$$\varphi^{trial}_{n+1}=|\sigma^{*,trial}_{n+1}|-y_o \tag{3.55}$$

If $\varphi^{trial}_{n+1} \le 0$ (Elastic step)

$$\varepsilon^p_{n+1}=\varepsilon^p_n \tag{3.56}$$

$$\alpha_{n+1}=\alpha_n \tag{3.57}$$

$$\sigma_{n+1}=\sigma^{trial}_{n+1} \tag{3.58}$$

$$\beta_{n+1}=\beta^{trial}_{n+1} \tag{3.59}$$

else (Plastic corrector step)

$$\sigma_{n+1}=\sigma^{trial}_{n+1}-E\frac{\varphi^{trial}_{n+1}}{E+H}\frac{\sigma^{*,trial}_{n+1}}{|\sigma^{*,trial}_{n+1}|} \tag{3.60}$$

$$\beta_{n+1}=\beta^{trial}_{n+1}+H\frac{\varphi^{trial}_{n+1}}{E+H}\frac{\sigma^{*,trial}_{n+1}}{|\sigma^{*,trial}_{n+1}|} \tag{3.61}$$

$$\varepsilon^p_{n+1}=\varepsilon_{n+1}-\frac{\sigma_{n+1}}{E} \tag{3.62}$$

3.4 PID Control

Before starting the analysis, coefficients of the PID control algorithm must be determined. For this purpose, the Ziegler-Nichols method was adopted; several simulations were computed to test whether the control algorithm is working in a tolerable range. Prior to a simulation, the time series values for the control parameter must be provided to the PID algorithm. For example; if the results of the simulation are to be compared with those obtained in a quasi-static experiment, values of the control parameter should be determined so as to keep acceleration values sufficiently small.

3.5 Mass Scaling

In the scope of this thesis, a new mass scaling approach is proposed. In this approach, a frequency is selected from the frequency spectrum of the system and modes having higher frequency values than the selected frequency are filtered out. Formulation of this mass scaling technique is as follows. The original eigenvalue problem can be written as

$$\underline{k}\underline{\phi}=\underline{m}\underline{\phi}\underline{\Omega}^2 \tag{3.63}$$

Our objective is to change $\underline{m}$ by $\Delta\underline{m}$ such that $\underline{\Omega}^2=\underline{\Omega}^2_{mod}$ and $\underline{\phi}=\underline{\phi}^*$ where

$$\underline{\Omega}^2=\begin{bmatrix}\omega_1^2 & & \\ & \ddots & \\ & & \omega_n^2\end{bmatrix} \tag{3.64}$$

$$\underline{\Omega}^2_{mod}=\begin{bmatrix}\omega_1^2 & & & \\ & \omega_a^2 & & \\ & & \ddots & \\ & & & \omega_a^2\end{bmatrix}=\begin{bmatrix}\omega_1^2 & & & \\ & \omega_a^2 & & \\ & & \ddots & \\ & & & \omega_n^2\end{bmatrix}+\begin{bmatrix}0 & & & \\ & 0 & & \\ & & \omega_a^2-\omega_{n-1}^2 & \\ & & & \omega_a^2-\omega_n^2\end{bmatrix} \tag{3.65}$$

$$\underline{\Omega}^2_{mod}=\underline{\Omega}^2+\Delta\underline{\Omega}^2 \tag{3.66}$$

Equation becomes

$$\underline{k}\underline{\phi}^*=(\underline{m}+\Delta\underline{m})\underline{\phi}^*\underline{\Omega}^2_{mod} \tag{3.67}$$

$$\underline{k}(\underline{\phi}+\Delta\underline{\phi})=(\underline{m}+\Delta\underline{m})(\underline{\phi}+\Delta\underline{\phi})(\underline{\Omega}^2+\Delta\underline{\Omega}^2) \tag{3.68}$$

$$\underline{k}\underline{\phi}+\underline{k}\Delta\underline{\phi}=\underline{m}\underline{\phi}\underline{\Omega}^2+\underline{m}\Delta\underline{\phi}\underline{\Omega}^2+\Delta\underline{m}\underline{\phi}\underline{\Omega}^2+\Delta\underline{m}\Delta\underline{\phi}\underline{\Omega}^2+\underline{m}\underline{\phi}\Delta\underline{\Omega}^2+\underline{m}\Delta\underline{\phi}\Delta\underline{\Omega}^2+\Delta\underline{m}\underline{\phi}\Delta\underline{\Omega}^2+\Delta\underline{m}\Delta\underline{\phi}\Delta\underline{\Omega}^2 \tag{3.69}$$

In the above equation, first terms of both side of the equality cancel each other out due to Equation (3.63). Equilibrium is satisfied if and only if $\underline{k}\Delta\underline{\phi} = \underline{m}\Delta\underline{\phi}\underline{\Omega}^2$. Then the equation given below must be solved.

$$\Delta\underline{m}\underline{\phi}\underline{\Omega}^2+\Delta\underline{m}\Delta\underline{\phi}\underline{\Omega}^2+\Delta\underline{m}\underline{\phi}\Delta\underline{\Omega}^2+\Delta\underline{m}\Delta\underline{\phi}\Delta\underline{\Omega}^2 = -\underline{m}\underline{\phi}\Delta\underline{\Omega}^2 - \underline{m}\Delta\underline{\phi}\Delta\underline{\Omega}^2 \quad (3.70)$$

$$\Delta\underline{m}(\underline{\phi}\underline{\Omega}^2+\Delta\underline{\phi}\underline{\Omega}^2+\underline{\phi}\Delta\underline{\Omega}^2+\Delta\underline{\phi}\Delta\underline{\Omega}^2) = -\underline{m}(\underline{\phi}\Delta\underline{\Omega}^2 + \Delta\underline{\phi}\Delta\underline{\Omega}^2) \quad (3.71)$$

$$\Delta\underline{m}((\underline{\phi} + \Delta\underline{\phi})\underline{\Omega}^2+(\underline{\phi} + \Delta\underline{\phi})\Delta\underline{\Omega}^2) = -\underline{m}(\underline{\phi} + \Delta\underline{\phi})\Delta\underline{\Omega}^2 \quad (3.72)$$

$$\Delta\underline{m}(\underline{\phi} + \Delta\underline{\phi})(\underline{\Omega}^2+\Delta\underline{\Omega}^2) = -\underline{m}(\underline{\phi} + \Delta\underline{\phi})\Delta\underline{\Omega}^2 \quad (3.73)$$

$$\Delta\underline{m}(\underline{\phi} + \Delta\underline{\phi}) = -\underline{m}(\underline{\phi} + \Delta\underline{\phi})\Delta\underline{\Omega}^2(\underline{\Omega}^2_{\text{mod}})^{-1} \quad (3.74)$$

$$\Delta\underline{m}\underline{\phi}^* = -\underline{m}\underline{\phi}^* D \quad (3.75)$$

$$\Delta\underline{m} = -\underline{m}\underline{\phi}^* D(\underline{\phi}^{*-1}) \quad (3.76)$$

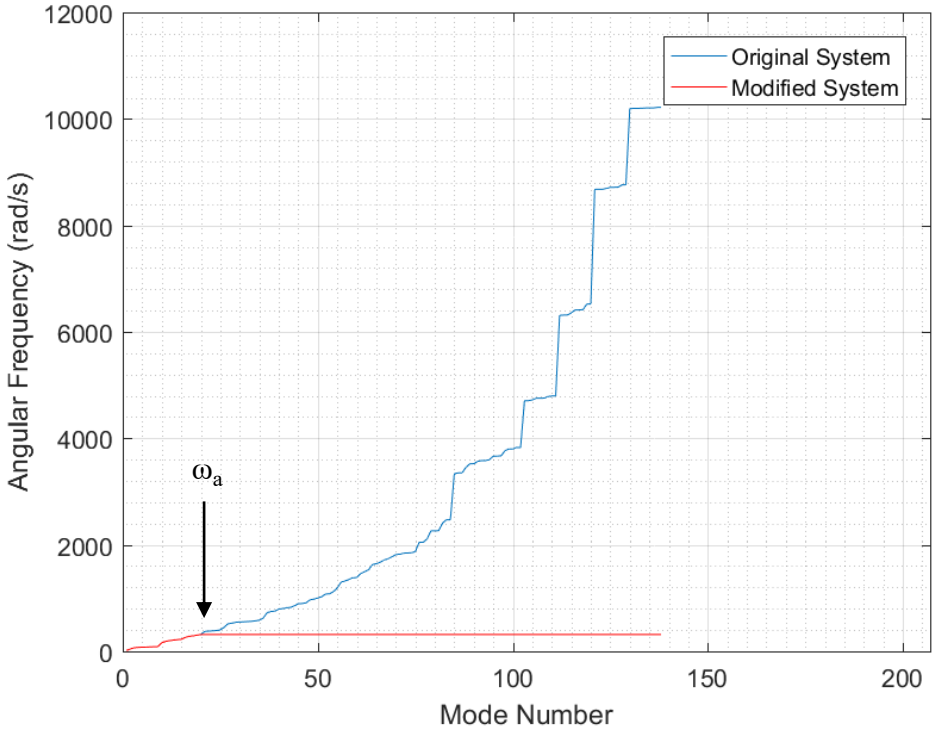

Figure 3.10. Angular frequencies before and after the application of selective mass scaling technique to a system

Equation (3.76) where D is the diagonal matrix can be used in the calculation of $\Delta\underline{m}$ in order to utilize this mass scaling approach. For simplicity, an alternative $\Delta\underline{m}$ formulation can be used which is given below. Modal mass is written as

$$\underline{m}^*=\underline{\phi}^T\underline{m}\underline{\phi} \tag{3.77}$$

$$\underline{m}^*\underline{\phi}^{-1}=\underline{\phi}^T\underline{m} \tag{3.78}$$

$$\underline{\phi}^{-1}=(\underline{m}^*)^{-1}\underline{\phi}^T\underline{m} \tag{3.79}$$

Substitution of Equation (3.79) into Equation (3.76) yields

$$\Delta\underline{m}=-\underline{m}\underline{\phi}^*D(\underline{m}^*)^{-1}\underline{\phi}^{*T}\underline{m} \tag{3.80}$$

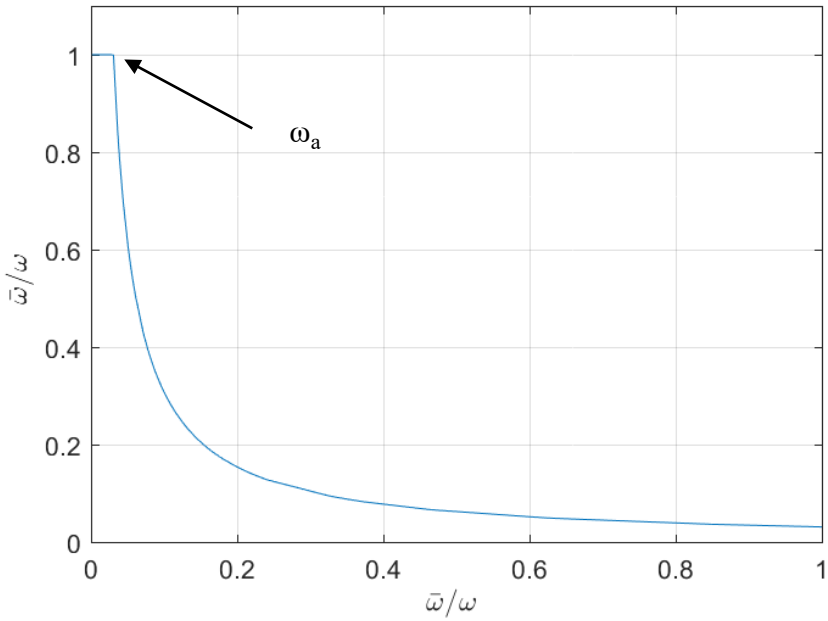

Figure 3.11. Ratio of modified and original frequencies of system

When this approach is applied to a sample system with a selected corner frequency ω_a, the effect on the frequency spectrum of the system can be seen in Figure 3.10, Figure 3.11 and Figure 3.12. It should be noted that frequency values and eigenmode matrices of the modes that have lower frequency value than the selected corner frequency do not change.

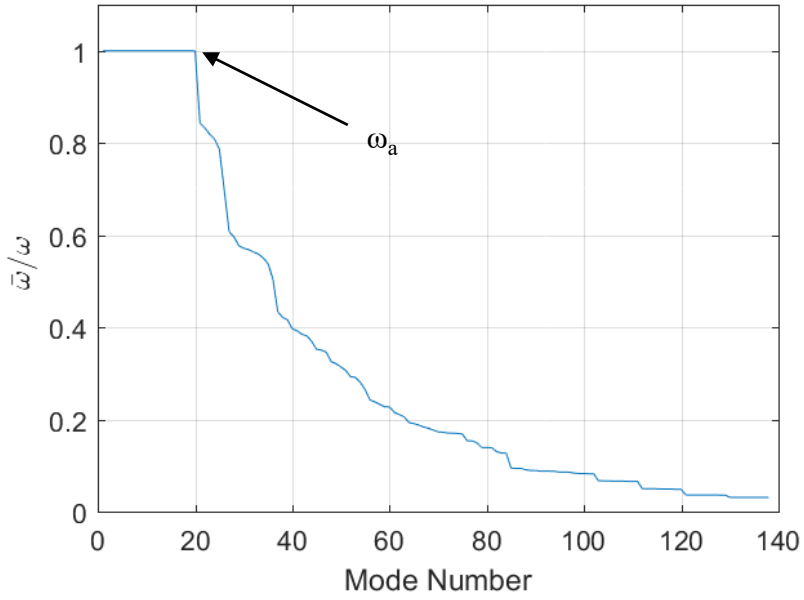

Figure 3.12. Ratio of modified and original angular frequencies of eigenmodes

The explicit time integration suffers from conditional stability. To overcome this problem, selective mass scaling technique which is proposed by Olovsson (2005) and the proposed mass scaling approach are implemented in the developed structural analysis program. Both mass scaling approaches require eigenvalue analysis once before the calculations for the first time step are evaluated.

3.6 Explicit Time Integration

An explicit numerical integration is used to integrate section forces to calculate element end forces. Structural force matrix is constructed from element end forces and by using the mass and damping matrices equation of motion (Equation (3.81)) is solved at each time step by using the following methodology

$$\mathbf{m\ddot{u}+c\dot{u}+f}^{\mathbf{r}} = \mathbf{f}^{\mathbf{ext}} \tag{3.81}$$

where m is the mass matrix, c is the damping matrix, f^r is the restoring force vector, ü, u̇ are the acceleration and velocity vectors, respectively, and f^{ext} is the externally applied force. The equation of motion was solved by the explicit Chung and Lee (1994) time integration. The steps in the integration scheme details were provided in Chung and Lee (1994) are as follows:

Measure the restoring force, f^r, by imposing displacements u_i

Compute the acceleration at time i+1.

$$\ddot{u}_{i+1}=m^{-1}(f_i^{ext}-f_i^r) \tag{3.82}$$

Calculate the displacements at time step i+1.

$$u_{i+1}=u_i+\Delta t\dot{u}_i+\beta_1\ddot{u}_i+\beta_2\ddot{u}_{i+1} \tag{3.83}$$

Calculate the velocities at time step i+1.

$$\dot{u}_{i+1}=\dot{u}_i+\gamma_1\ddot{u}_i+\gamma_2\ddot{u}_{i+1} \tag{3.84}$$

Repeat all steps for the remaining time steps.

Integration constants are given as

$$\beta_1=\Delta t^2(1/2-\beta),\ \ \beta_2=\Delta t^2\beta,\ \ \gamma_1=-1/2\Delta t^2,\ \ \gamma_2=3/2\Delta t^2. \tag{3.85}$$

where β is taken as 1.01.

Equations of motion can be solved for linear or nonlinear systems dynamically. In the pseudo-static case, time integration becomes pseudo time integration since the acceleration and velocity effects on the analysis become significantly smaller.

CHAPTER 4

VERIFICATION STUDIES

4.1 General

In this chapter, verification studies of the developed computer program are presented for a variety of problems. First, the element formulation and the fiber discretization are verified by using a simple analytical constitutive model. Then, the PID algorithm is tested and verified for simple structural elements. Finally, the selective mass scaling approach is used and its efficiency is shown.

4.2 Fiber Discretization

For the verification, a simple statically determinate problem is modelled. Definition of the problem is depicted in Figure 4.1. For this problem, a nonlinear elastic material model is used which it is given in Equation 4.1. For the model; length of the beam was taken as 2 meters, width and height of the cross section were taken as 0.2 m, force is 10000 N.

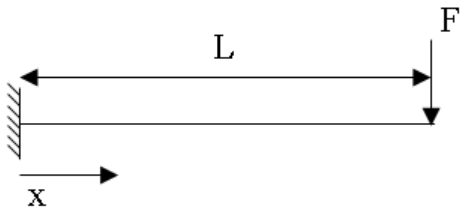

(a) Cantilever beam with loading

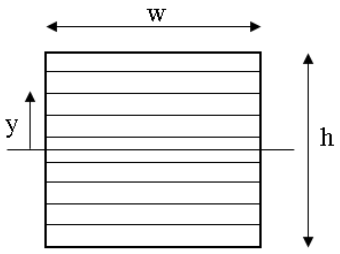

(b) Cross-section with representative fiber discretization

Figure 4.1. Definition of the problem

$$\varepsilon = a\sigma^2 \tag{4.1}$$

where a is a scalar coefficient taken as 10^{-18}.

For validation, the analytical result was first derived and then compared to the numerical result. For the derivation of moment-curvature relationship expression, internal moment equilibrium of the cross section and definition of the curvature is enveloped.

For a cross section, internal moment equilibrium is

$$\int_A \sigma y \, dA = M(x) \tag{4.2}$$

Substitution of the constitutive law (Equation (4.1)) into this equation yields,

$$\int_A \sqrt{\frac{\varepsilon}{a}} y \, dA = M(x) \tag{4.3}$$

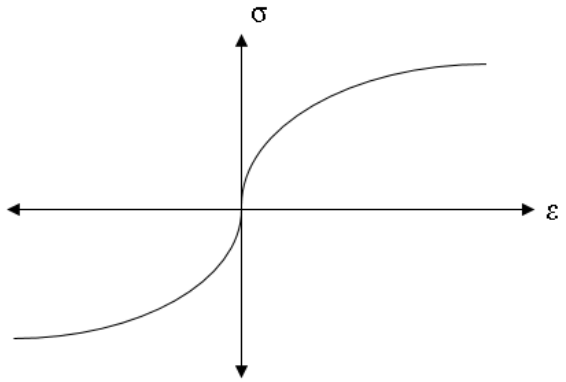

Figure 4.2. Constitutive law used in this problem

Using the curvature-strain relationship, ε=Ky, gives,

$$\int_A \sqrt{\frac{Ky}{a}} y \, dA = M(x) \tag{4.4}$$

Rearranging yields,

$$2\int_0^{h/2} \sqrt{\frac{K}{a}} y^{3/2} w \, dy = M(x) \tag{4.5}$$

Integrating and rearranging the following term is obtained,

$$K(x)=a\left(M(x)\frac{5}{4w}\left(\frac{h}{2}\right)^{-5/2}\right)^2 \tag{4.6}$$

For the derivation of the deflection expression, the following equation is used along with the appropriate boundary conditions i.e. θ(0)=0 and ν(0)=0.

$$\frac{d^2v}{dx^2} = \iint K(x)dx = \iint a\left(M(x)\frac{5}{4w}\left(\frac{h}{2}\right)^{-5/2}\right)^2 dx \tag{4.7}$$

$$\frac{d^2v}{dx^2} = \iint a\left(F(L-x)\frac{5}{4w}\left(\frac{h}{2}\right)^{-5/2}\right)^2 dx \tag{4.8}$$

$$v = \frac{F^2a}{16w^2}\left(\frac{h}{2}\right)^{-5}(x^2)\left(\frac{L^2}{2} - \frac{Lx}{3} + \frac{x^2}{12}\right) \tag{4.9}$$

First, the fiber discretization, element formulation and the time integration are verified as given in this section. For the model, Rayleigh damping is utilized by fixing the first and the second modes' damping ratio as 5%. Mass density of the material was taken as 2500 kg/m^3 and mass was distributed to the nodes by the lumped mass approach. PID algorithm verification is provided in Section 4.3. In this simulation, the loading (given in Figure 4.3(a)) is applied slowly to minimize response velocity and acceleration of the loading point without using the PID algorithm. The tip deflection as a function of time is presented in Figure 4.3(b).

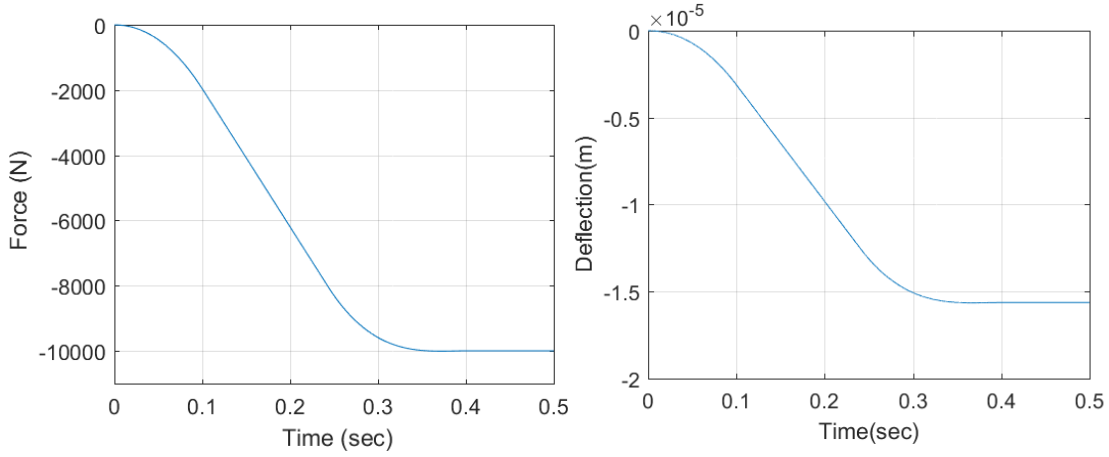

(a) (b)

Figure 4.3. Loading pattern of the system (a) and its response (b)

For verification, the effects of 2 parameters were investigated: the fineness of the fiber discretization and the number of elements used in the model.

Exact solution for the curvature and the tip displacement were 1.5625x10^{-3} 1/m and 1.5625x10^{-3} m, respectively. For the investigation of the effect of the fiber discretization, 4 elements were used in the model. For investigating the effect of the

number of elements, the number of fibers is set to 50 for each cross-section in the element. The numerical results are compared with the analytical solution in Figure 4.4.

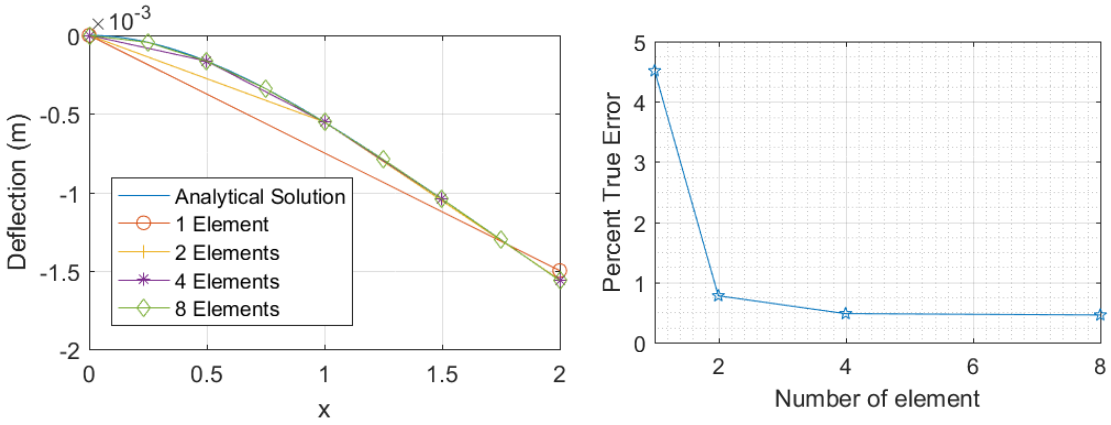

(a) (b)

Figure 4.4. (a) Deflection of the beam with varying number of elements compared to the analytical solution (b) Percent true error in the tip displacement

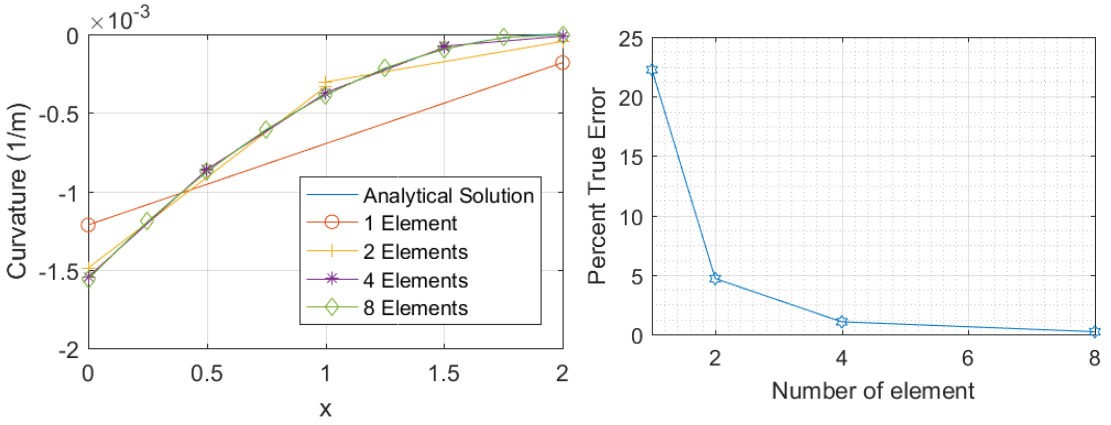

(a) (b)

Figure 4.5. (a) Curvature profile of the beam with varying number of elements compared to the analytical solution (b) Percent true error in curvature values at support

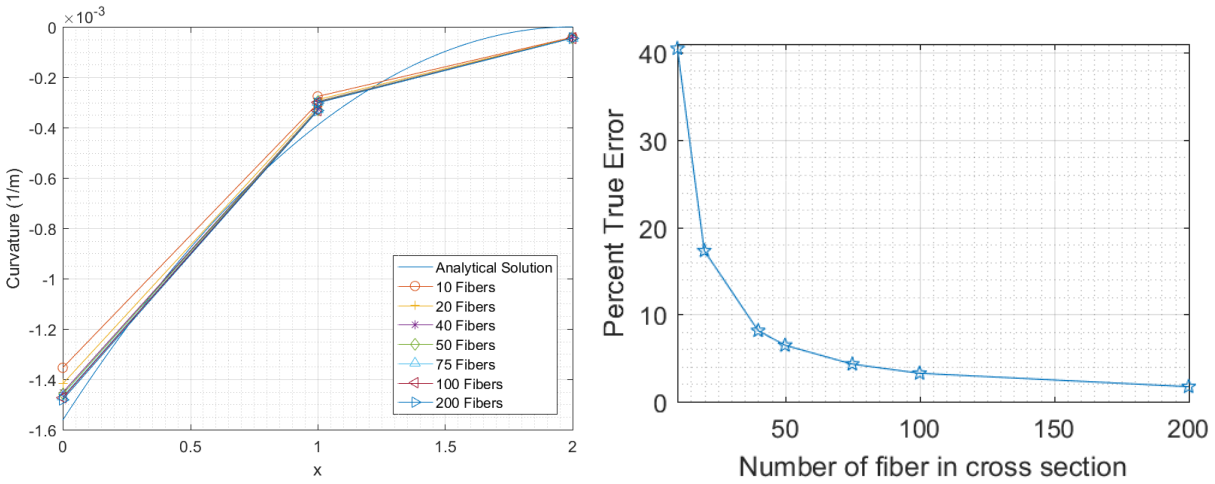

(a) (b)

Figure 4.6. (a) Deflection of the beam with varying cross section discretization compared to the analytical solution (b) Percent true error in the tip displacement

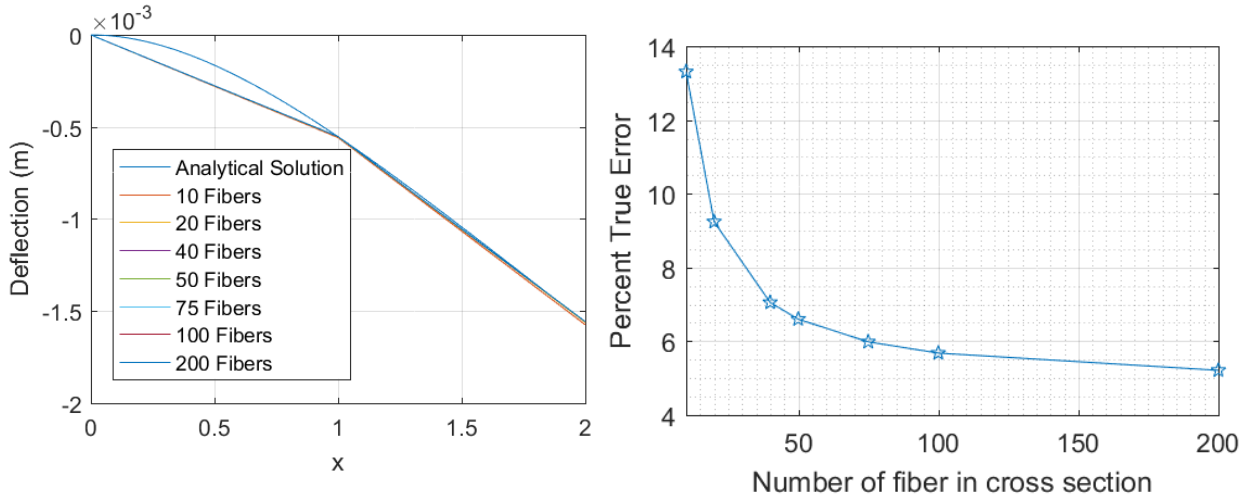

(a) (b)

Figure 4.7. (a) Curvature profile of the beam with varying cross section discretization along with the analytical solution (b) Percent relative true error in curvature values at the support

As can be seen from Figure 4.4 to Figure 4.7, as the number of fibers and the number of elements increase the numerical solution converges quadratically to the exact solution.

4.3 PID Algorithm

In this section, verification studies for the PID algorithm are presented. Unlike the previous verification (Section 4.2), in this and the following verification studies, Mander et al. (1988), Hognestad (1951) and elastoplasticity with kinematic hardening material models were adopted for the confined concrete, unconfined concrete and reinforcing steel, respectively.

4.3.1 Steel Cantilever with PID

The application of a static point load is simulated using explicit time integration and the PID controller in this section. A cantilever beam is modelled using PID controller in the developed program. The beam, 1.5-meter long, is modeled by 0.15x0.15 m^2 cross-section. Three elements were used along the length (Figure 4.8). Each cross section was discretized in to 10 fibers. 3 Gaussian integration points were used for integration within the elements. Damping matrix was obtained using the classical Rayleigh damping method by fixing the first and second mode's damping ratio as 5%. Mass density of the material was taken as 7850 kg/m^3 and mass was distributed to the nodes by the lumped mass approach. As described in Section 2.3.3, the bilinear model with kinematic hardening material model was used as the constitutive model for all fibers. The, modulus of elasticity, kinematic hardening modulus and the yield strength were set as $20x10^4$ MPa, $1.1x10^3$ MPa and 420 MPa, respectively.

Velocity in the vertical direction at the tip of the beam was selected as the control parameter. The PID algorithm implicitly calculated force to be applied to tip while the velocity was being monitored during the simulation. Figure 4.9 shows the prescribed velocity and the response velocity. As can be seen from the figure, response and prescribed velocity values match perfectly.

(a) Cantilever beam with loading

(b) Cross-section with fiber discretization

Figure 4.8. Steel cantilever beam with tip load

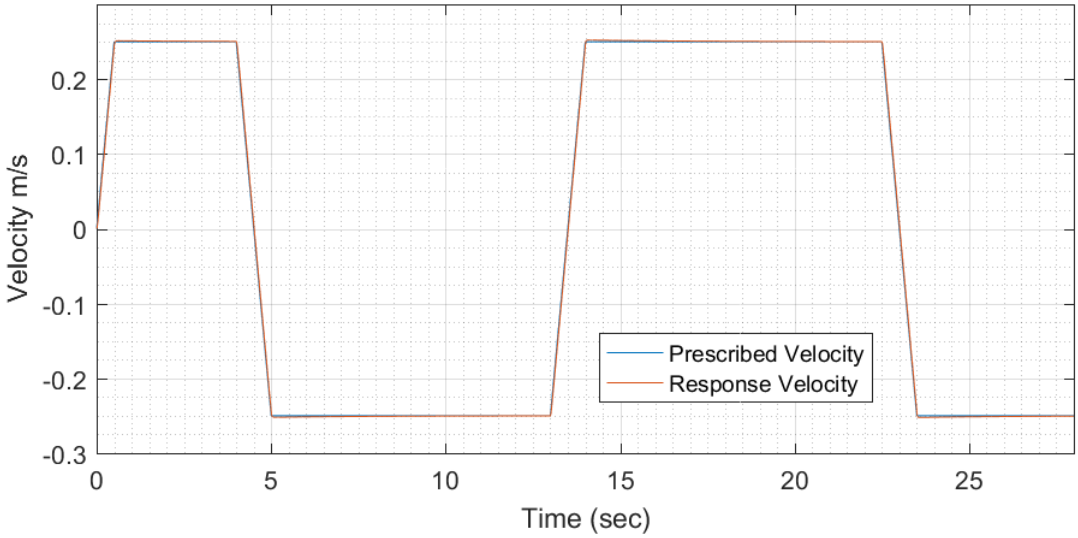

Figure 4.9. Prescribed velocity and the velocity response in the vertical direction at tip of the beam

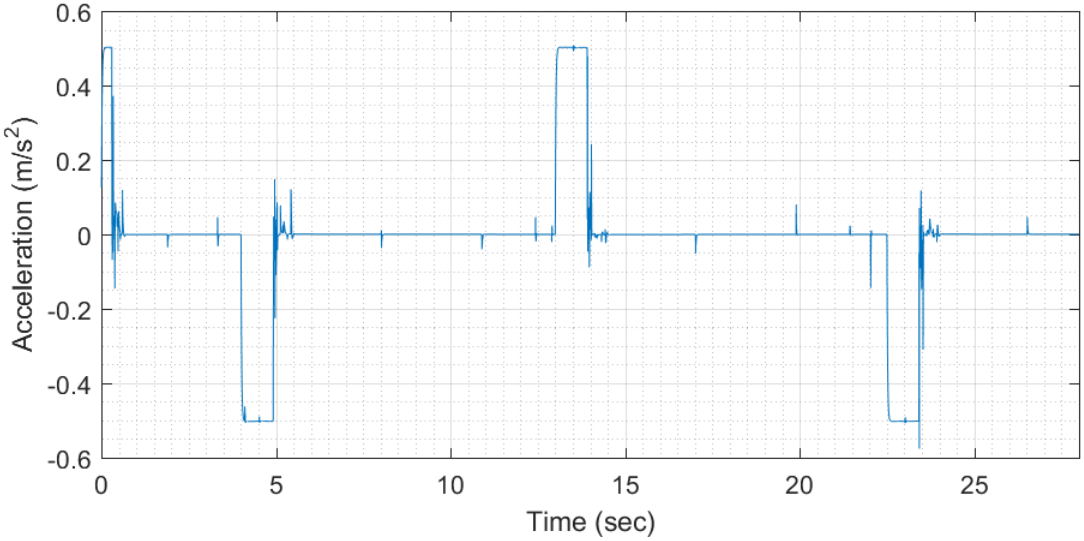

Figure 4.10. Acceleration response in the y-direction at the tip of the beam

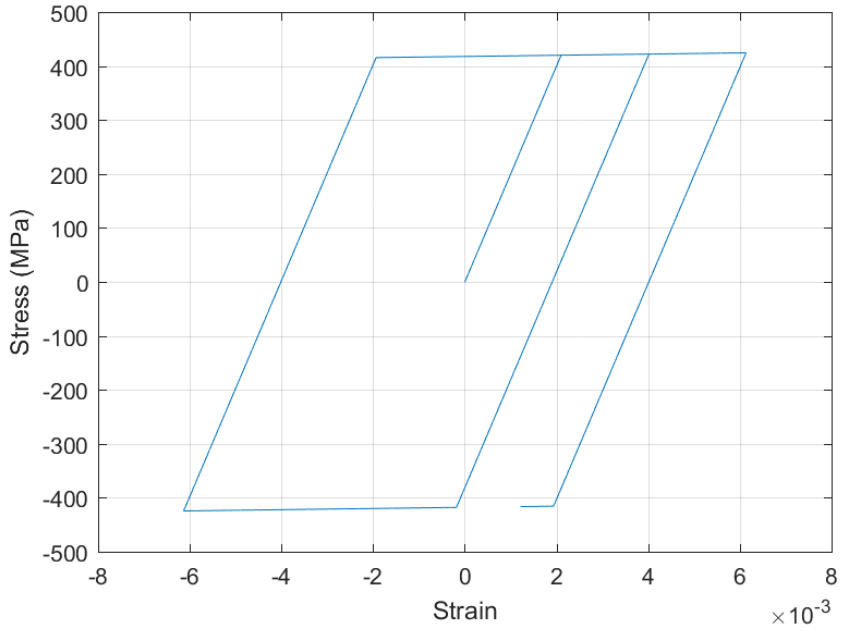

Figure 4.11. Stress-strain history of the steel fiber at the outer most of the cross section at support

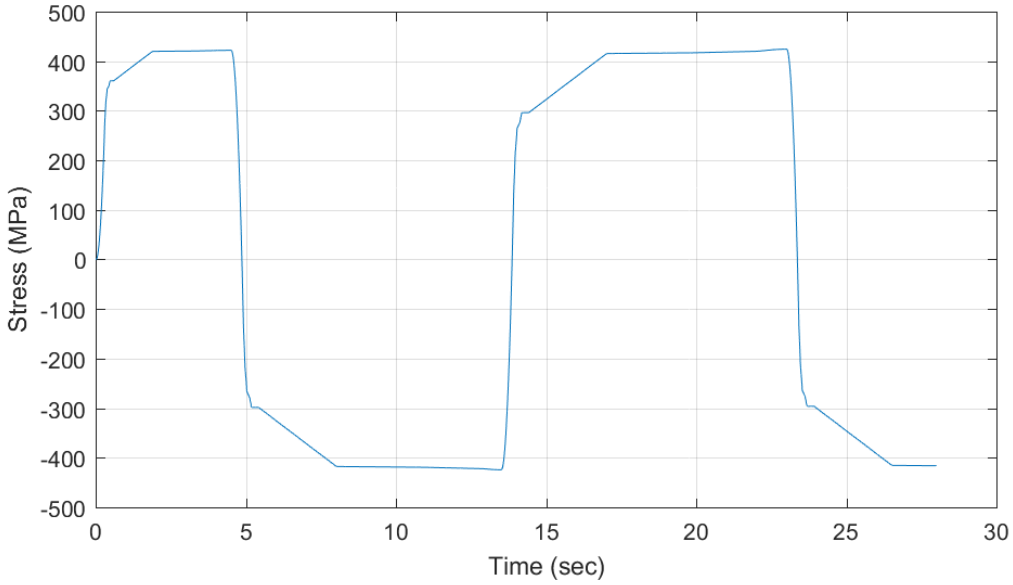

Figure 4.12. Stress history of the steel fiber at the outermost of the cross section at the support

PID coefficients were set as $K_p=3x10^6$ m^{-1}, $K_i=10^6$ $s^{-1}.m^{-1}$ and $K_d=5x10^4$ $s.m^{-1}$. The acceleration response in the y-direction at the tip of the beam can be seen from Figure 4.10. The acceleration values were bounded by [-0.5,0.5] m/s^2. Since the acceleration values are relatively small, and the response and the prescribed velocity values agreed well, the PID controlling algorithm was found to be efficiently controlling the external force.

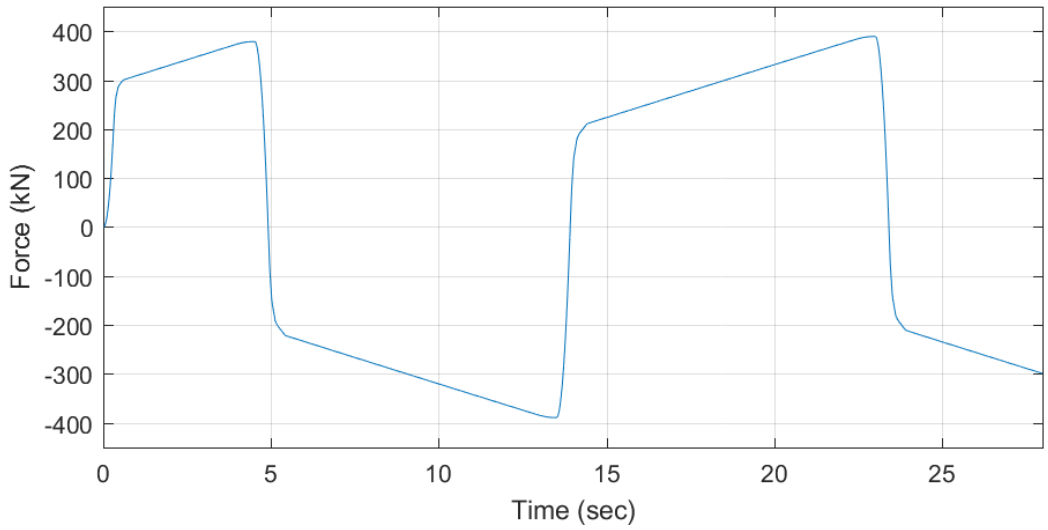

Figure 4.13. External force history calculated by the PID algorithm based on the prescribed velocity time series

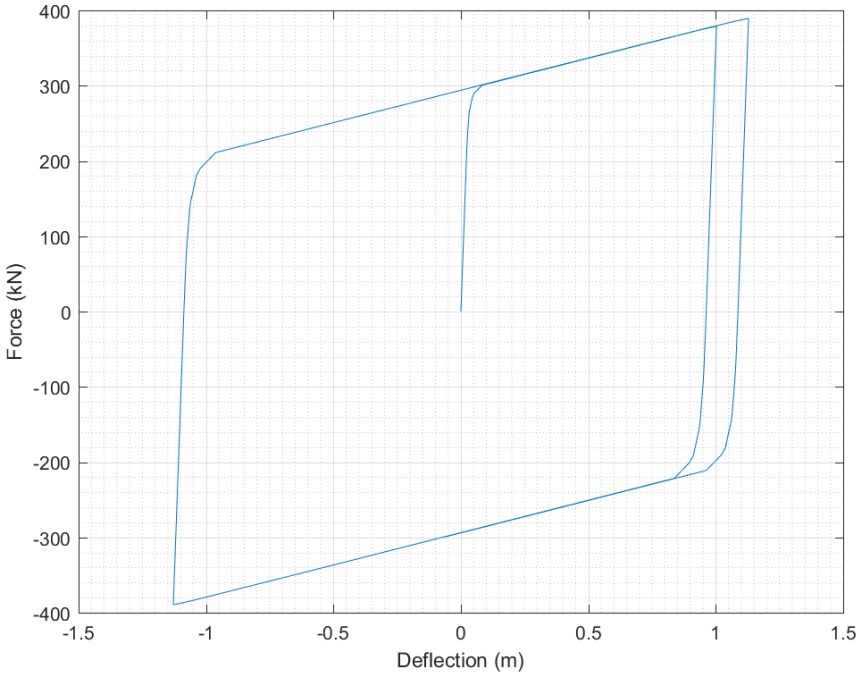

Figure 4.14. Tip deflection vs force

4.3.2 Reinforced Concrete Cantilever Beam with PID

The second validation test for the PID algorithm was a with static tip loading reinforced concrete cantilever beam. The 1.5 m long beam was modelled as 0.15x0.15 m^2 cross section composed of 3 equal elements. The detailed representation of the problem can be seen in Figure 4.15 with the layout of the reinforcing bars. Each cross section was discretized into 10 fibers. The concrete material constitutive law by Mander et al. (1988) was assigned to all fibers in the cross section. Bilinear material with kinematic hardening behavior was assigned to steel bars. Mass densities of the materials were taken as 2500 and 7850 kg/m^3 for the concrete and reinforcing steel bars, respectively. Mass was distributed to the nodes by the lumped mass approach. The peak compressive strength of concrete was set to 60 MPa while the concrete strain at peak compressive stress was chosen as $2x10^{-3}$. Three Gaussian integration points were used within the elements. Damping matrix was obtained using classical Rayleigh damping method by fixing first and second mode's damping ratios to 5%.

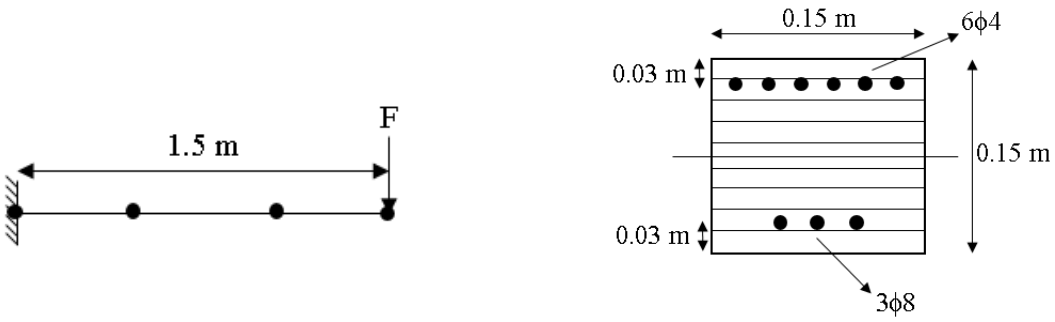

(a) Cantilever beam loaded at the tip

(b) Cross-section with fiber discretization

Figure 4.15. Reinforced concrete cantilever beam with tip load

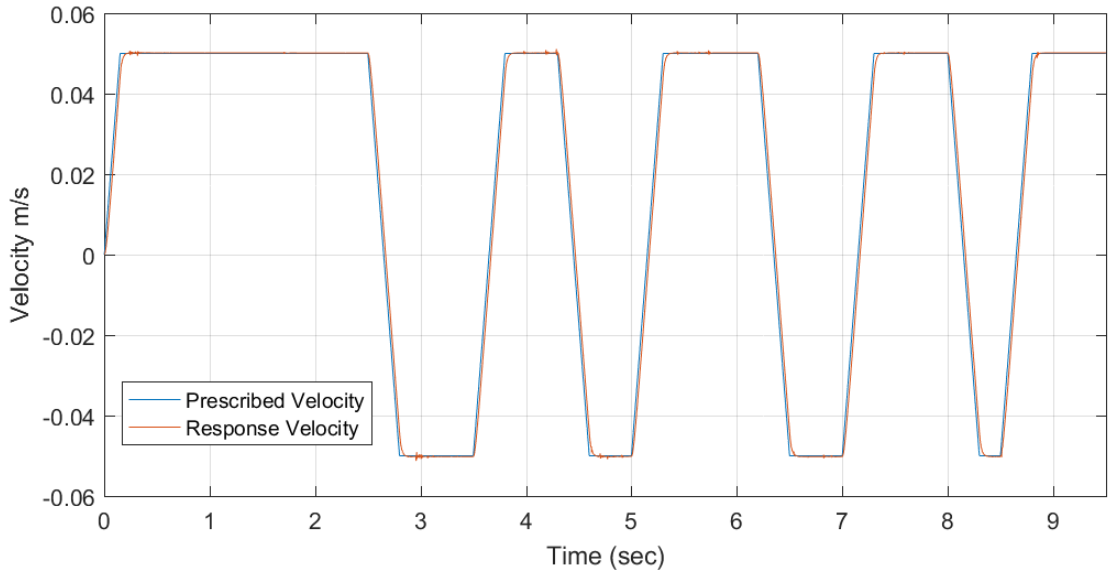

Figure 4.16. Prescribed velocity and the velocity response in the vertical direction at the tip of the beam

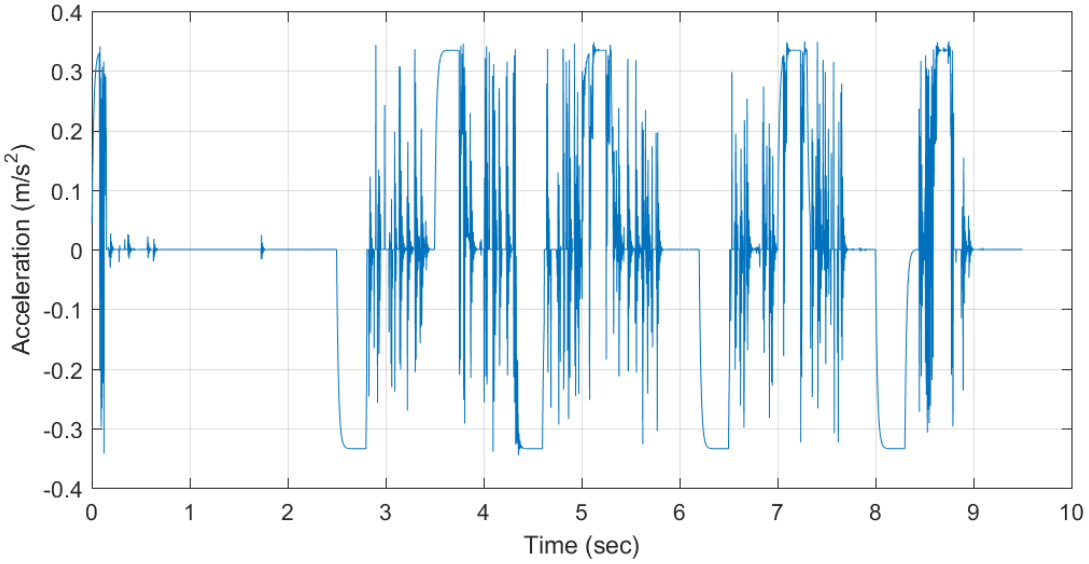

Figure 4.17. Acceleration response in the y-direction at the tip of the beam

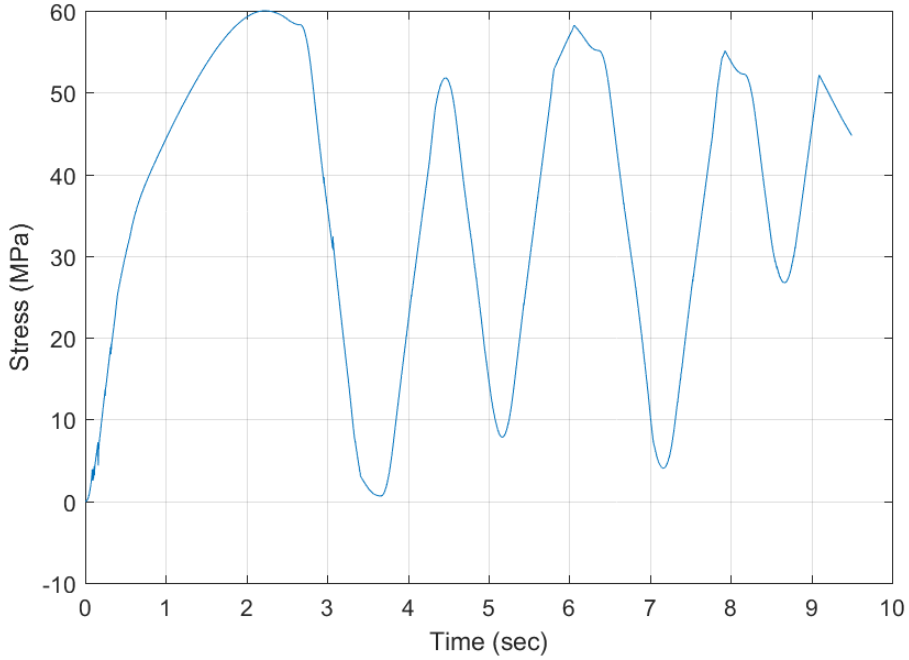

Figure 4.18. Stress history of the fiber located at the most outer of the cross section at the support

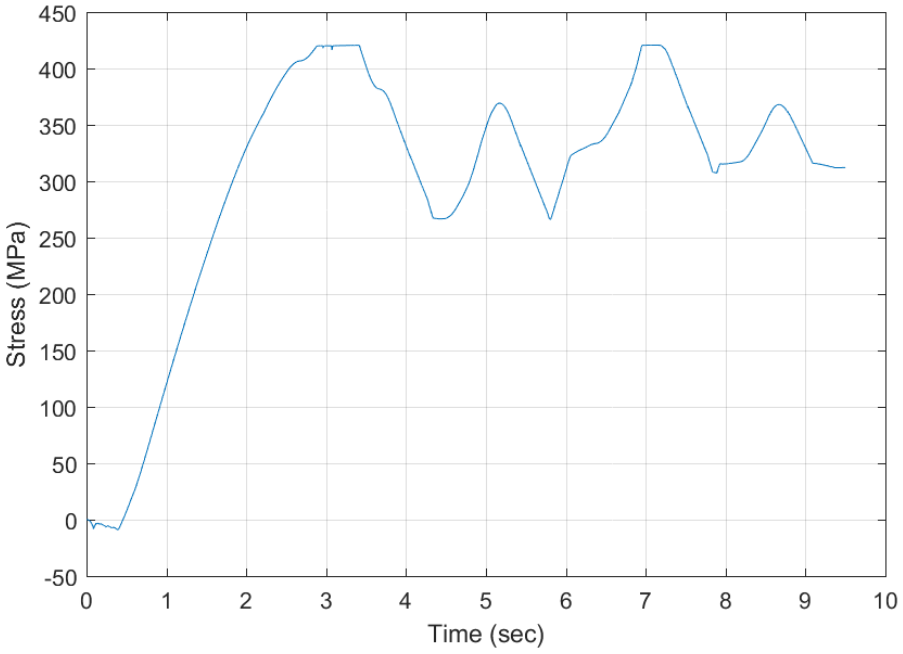

Figure 4.19. Stress history of the steel bar (compression) at the support

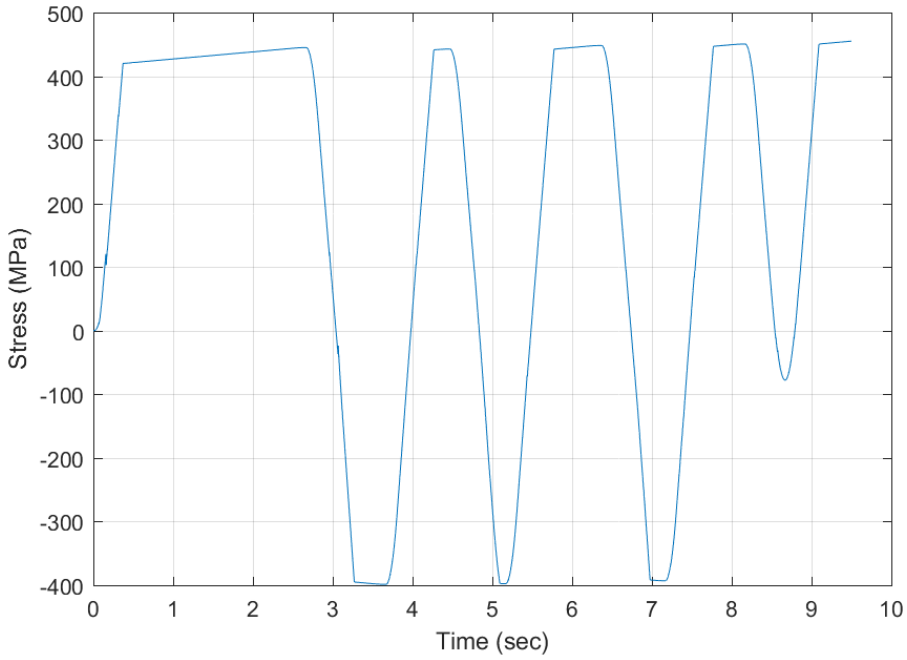

Figure 4.20. Stress history of the steel bar (tension) at the support

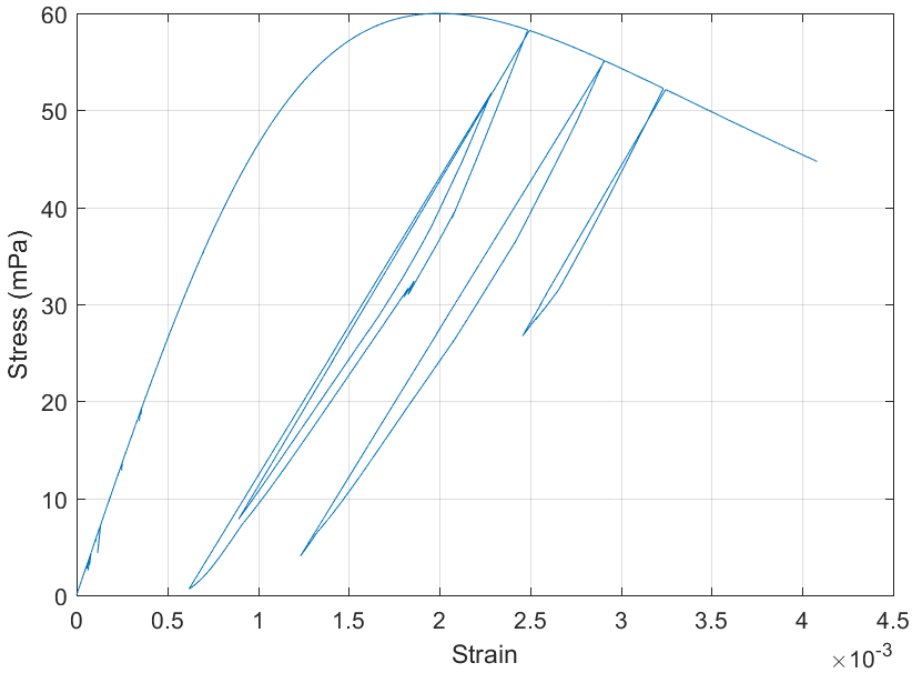

Figure 4.21. Stress-strain history of the concrete fiber at the outermost of the cross section at the fixed end of the beam

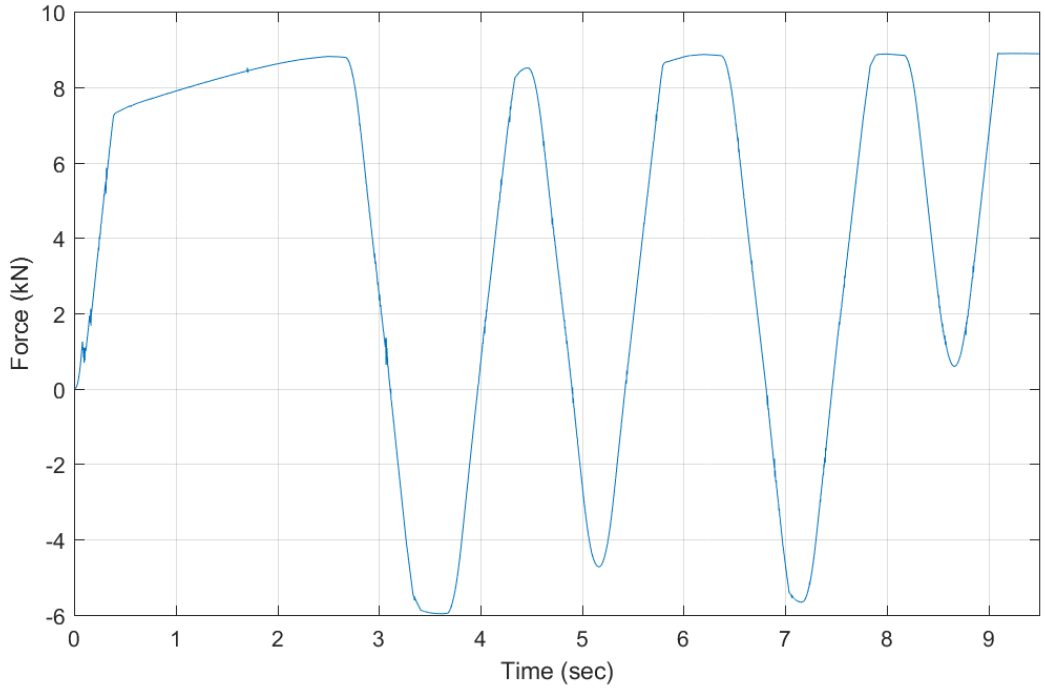

Figure 4.22. Computed external force with the PID algorithm

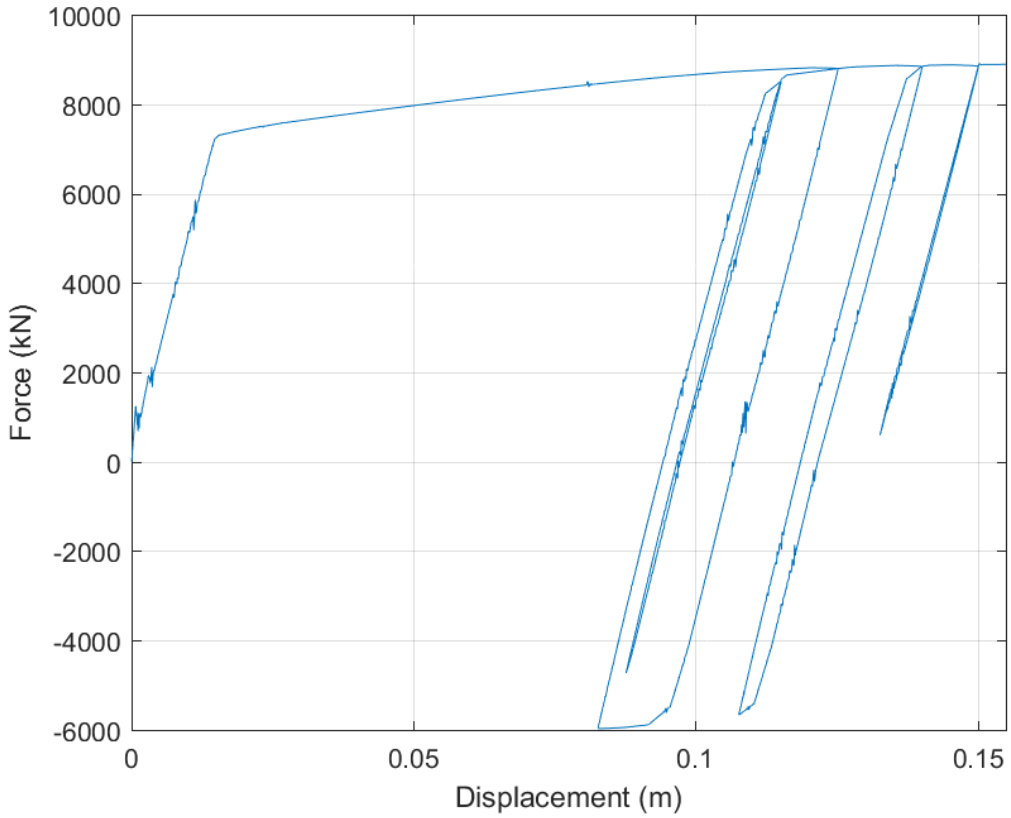

Figure 4.23. Computed external force with PID algorithm versus tip deflection

Velocity in the vertical direction at the tip of the beam was selected as the control parameter and the velocity-time series is prescribed for that point. The PID algorithm calculated the external force to be applied to the tip while the controlling the velocity during the simulation. Figure 4.16 shows the prescribed velocity and the response velocity. As can be seen in the figure, they match very well. Figure 4.17 shows the response acceleration in the vertical direction (which are in between -0.35 m/s^2 and 0.35 m/s^2). For the simulation, the PID coefficients were taken as $K_p=5x10^6$ m^{-1}, $K_i=9x10^5$ $s^{-1}.m^{-1}$, and $K_d=9x10^4$ $s.m^{-1}$. Since the response acceleration values are relatively small and response velocity values agree well with prescribed values, the PID controlling algorithm was found to be efficiently working.

4.4 Mass Scaling and Comparison with Experiment Data

In this section, simulations using mass scaling approaches are investigated and verified using the results from the experiments performed at the Middle East Technical University in 2012 as benchmark.

4.4.1 Description of Experimental Setup and Its Model

A testing program was executed to do develop the basis of revisions for performance-based evaluation procedures and strengthening methods of the Turkish Earthquake Code (2007) at the Structural and Earthquake Laboratory of Middle East Technical University in February 2010. In the scope of the testing program, prototype RC frame building was designed according to the regulations of TEC (2007). 3-bay, 3-story half-scaled RC frame specimen was built representing the interior frame of the prototype building (Figure 4.24). A continuous pseudo-dynamic (PsD) test was carried out using synthetic ground motions compatible with the site-specific earthquake spectra developed for the city center of Duzce (Turkey). In order to test the ability of the computational model to estimate the lateral deformation capacity and ductility, the envelope of the measured response of the structure to the applied ground motions was used along with the local maximum column end rotations.

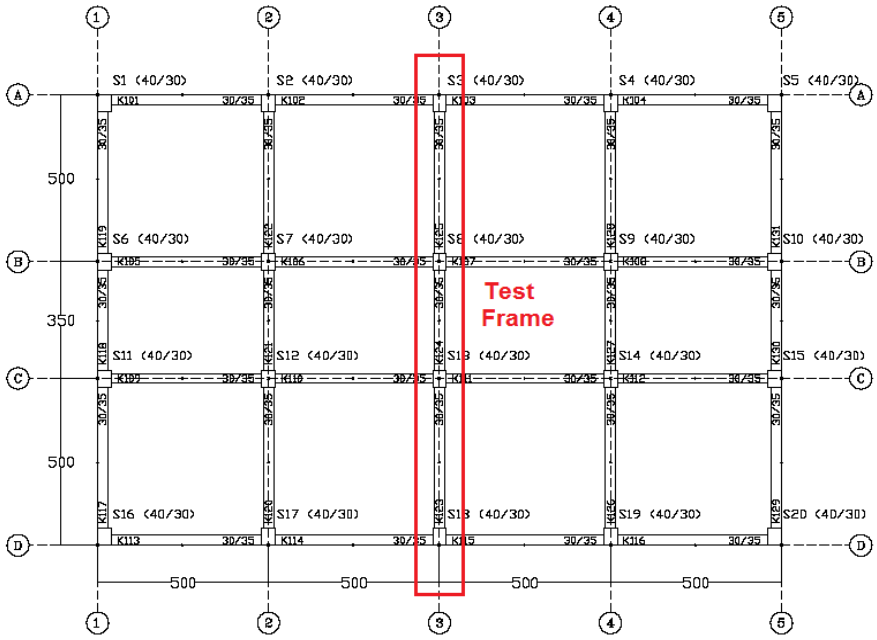

Figure 4.24. Plan view of the prototype building and the selected two-dimensional frame

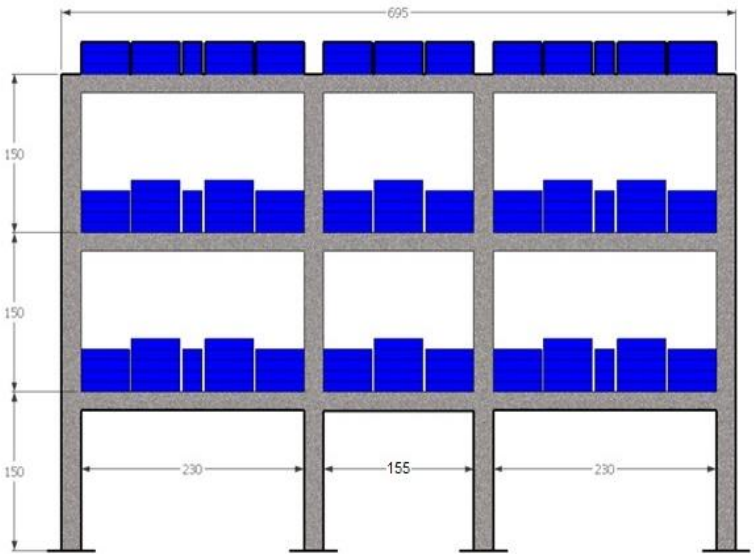

Figure 4.25. Front view of the frame

Section properties of the test specimen are given in Figure 4.26. Column longitudinal reinforcement ratio was about 2%. Average uniaxial compressive strength of concrete used for the specimen was 33.7 MPa. Deformed bars, used as longitudinal reinforcement, had a yield strength of 480 MPa and plain bars, used as transverse reinforcement, had a yield strength of 240 MPa (reported laboratory measurements). The details of the test setup and the measurement system are shown in Figure 4.27.

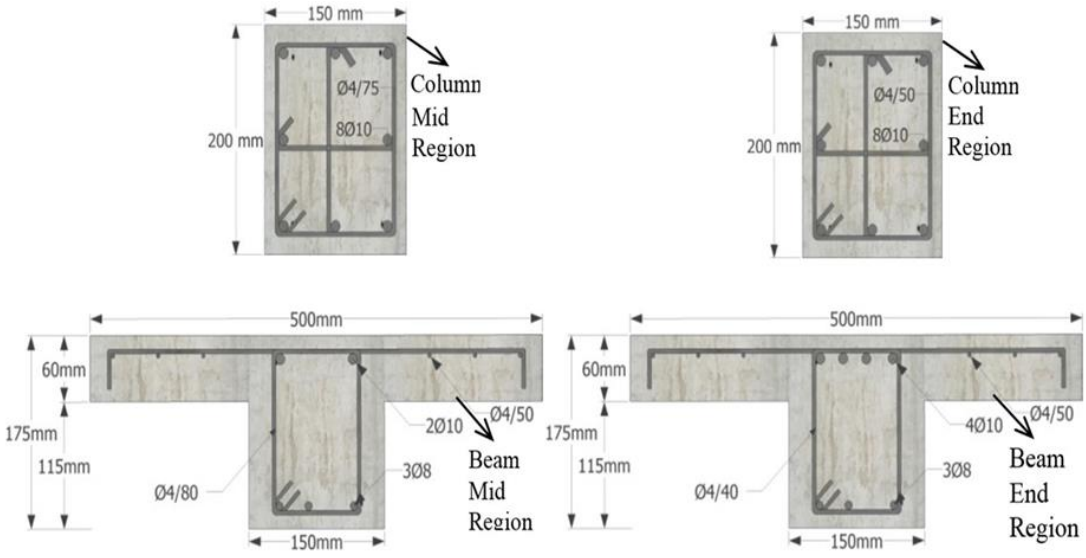

Figure 4.26. Section details of test frame (Mutlu 2012)

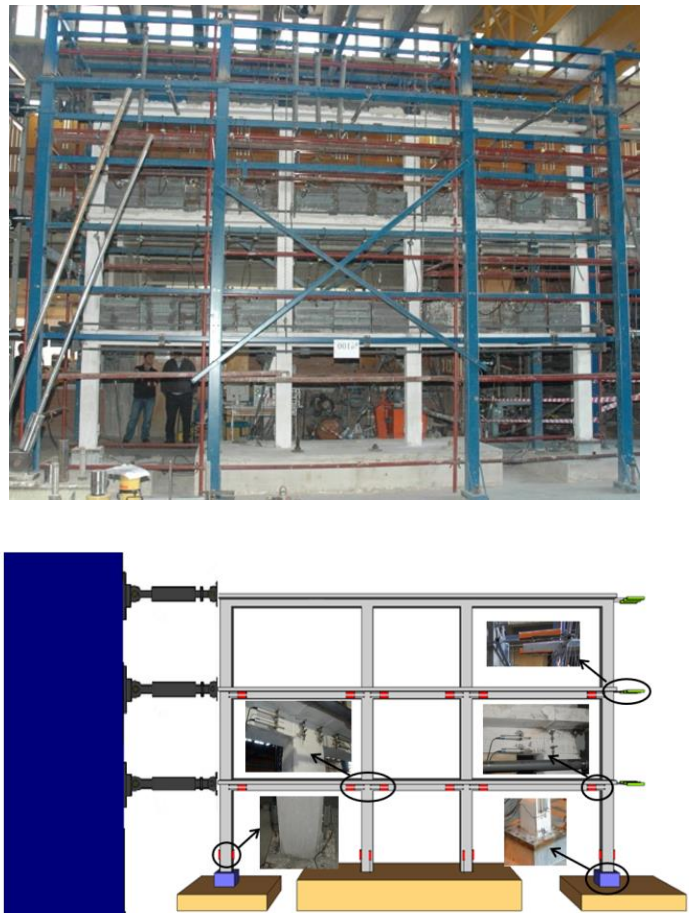

Figure 4.27. Test setup and locations of measurement instruments (Mutlu 2012)

A numerical model for the test frame was prepared by using the developed computational platform. Plastic hinge lengths were calculated using formulation proposed by Paulay and Priestly (1992). Plastic hinges were modelled with a single element having 3 fiber sections. Beam and column regions expected to remain below yielding but to exceed cracking stage were modelled with one element having 5 fiber sections. Mass densities of the materials were taken as 2500 and 7850 kg/m^3 for the concrete and reinforcing steel bars, respectively. Mass of the system was idealized with the lumped mass approximation and damping was calculated by using the classical Rayleigh damping method whose coefficients were calculated by fixing first and second mode's damping ratios as 2%.

In the test setup, the gravity load was applied by placing steel blocks on the beams and self-weight of the structure. Therefore, in the simulation before the application of the lateral force, gravity load was considered first. For this purpose, the PID algorithm was

employed for the gravity load. The PID coefficients were determined as K_i=0 m^{-1}, K_p=5x10^2 $s^{-1}.m^{-1}$, and K_d=0 $s.m^{-1}$ by a simple trial and error procedure. Velocity in the y-direction was prescribed at the top midpoint of the structure, and during the simulation, PID algorithm calculated the scale factor of the gravity load pattern. In Figure 4.28, it is shown that the prescribed velocity and the response velocity are in a good agreement upon the application of the control algorithm. As shown in the same figure, acceleration values were kept sufficiently small so that gravity loading did not result in excessive damage.

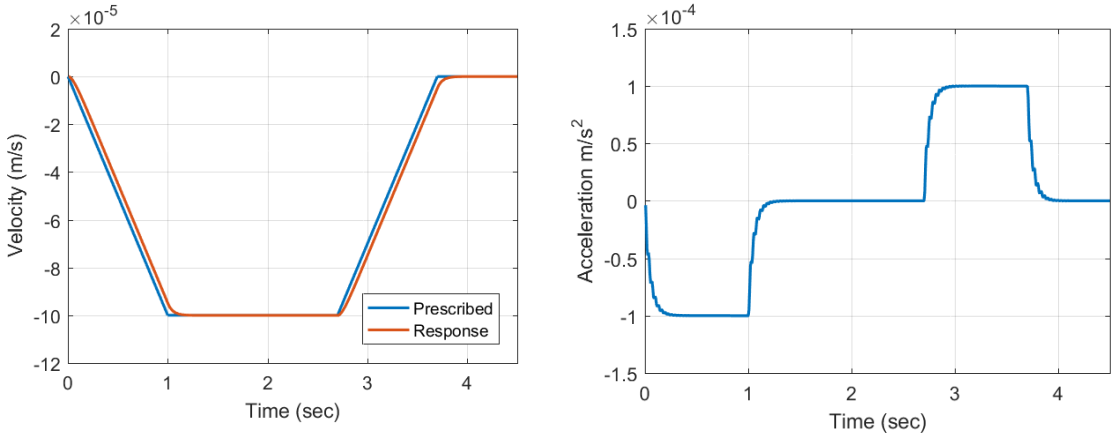

(a) (b)

Figure 4.28. Velocity and acceleration at the control point
(a) prescribed and response velocity, (b) response acceleration

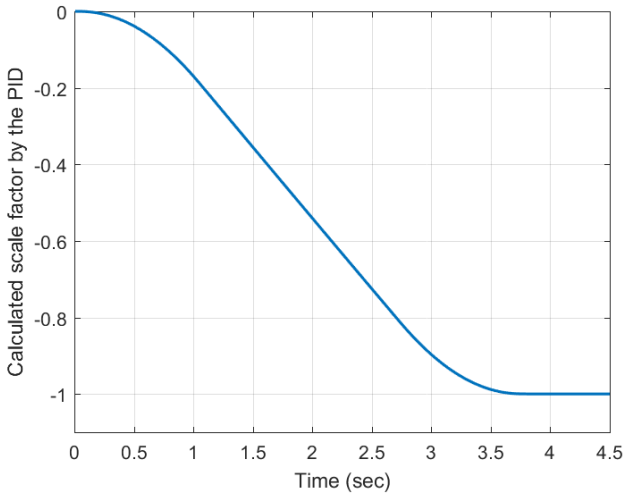

Figure 4.29. Gravity load scale factor calculated by the PID

K_p, K_i, K_d values were critical for the controller and their estimation was challenging to calculate explicitly for this type of complex structures. For vibration problems, whole model can be reduced to a simple model by ignoring the vibrational modes which do not contribute response of the structure (Khot and Yelve 2011). Since the structure was laterally loaded, the response mainly consisted of the first mode. Therefore, the full model can be simplified to a first mode in order to calculate the PID coefficients. This approach is consistent with the general idea of pushover analysis as well. Ziegler and Nichols (1942) method was employed to determine K_p, K_i, K_d values after the calculation of the first mode's modal mass, stiffness and damping terms with the eigenvalue analysis. Their values are tabulated in Table 4.1. In Figure 4.30, it is shown that the prescribed velocity and the response velocity are in a good agreement upon the application of our control algorithm. As shown in the same figure, acceleration values were kept sufficiently small. Hence, it can be said that during the analysis with the explicit time integration, inertial forces do not affect the overall response, validating the application of the procedure. Strain and time derivation of strain response of reinforcing steel at the base element are shown in Figure 4.31.

Table 4.1. Parameters of the PID controller for the model

K_p	K_i	K_d
$8x10^8$ m^{-1}	$5x10^9 s^{-1}.m^{-1}$	$5x10^6$ $s.m^{-1}$

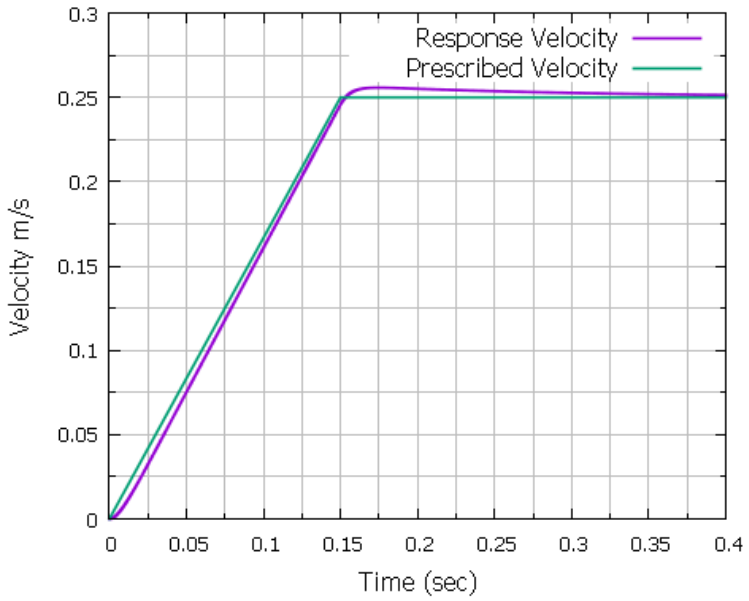

(a)

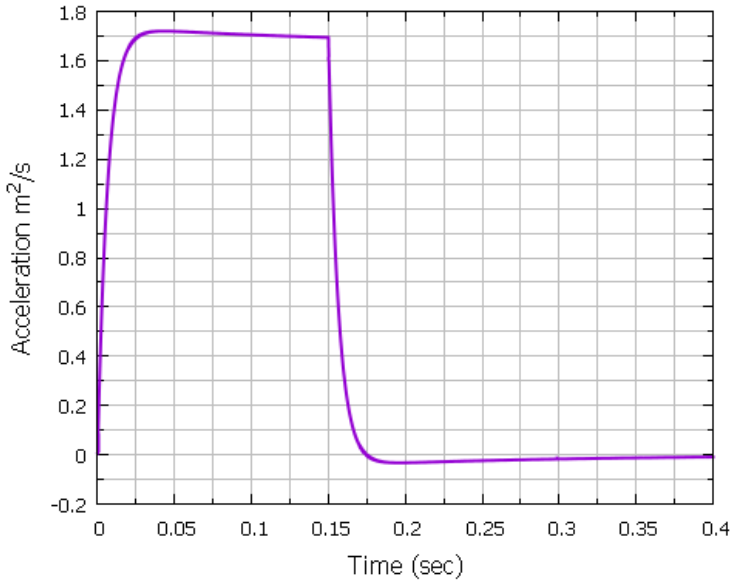

(b)

Figure 4.30. Velocity and acceleration at load applied node
(a) prescribed velocity and the velocity response, (b) acceleration response

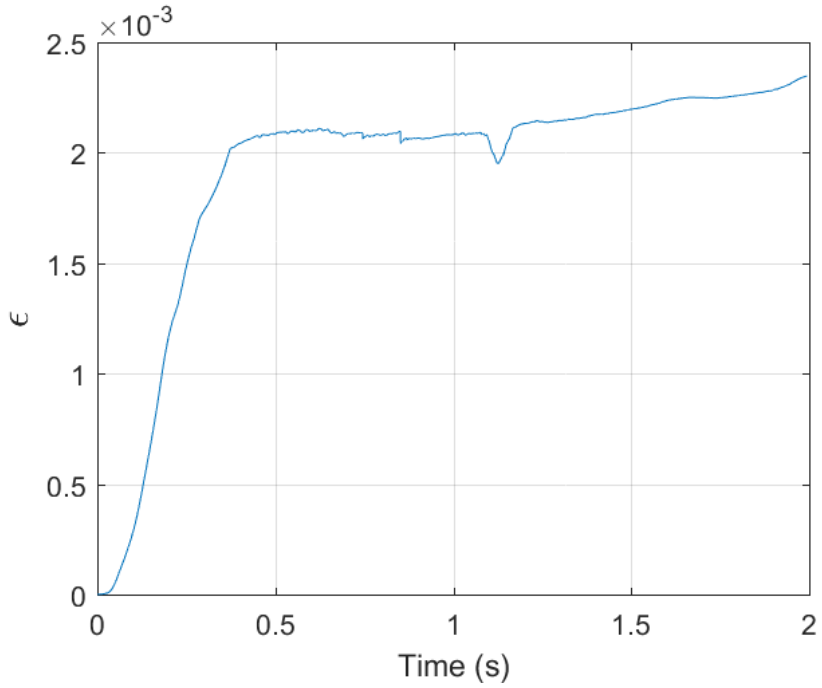

(a)

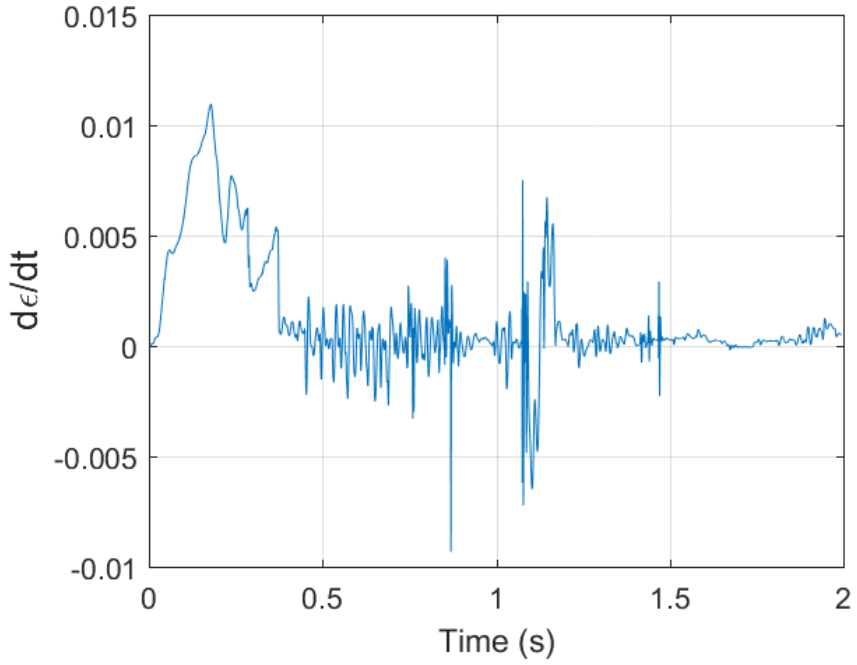

(b)

Figure 4.31. Strain response of reinforcing steel at the base
(a) strain-time series, (b) rate of strain – time series

4.4.2 Comparison with The Experiment Results

First, only the gravity load was applied to the structure with the appropriate PID coefficients. Thereafter, in addition to the gravity load, the lateral load was applied to the structure. Roof displacement-base shear force relationship from the test and simulation are shown in Figure 4.32. It should be noted that the test was conducted pseudo dynamically and only the envelope curve is presented in the Figure 4.32. For the simulation, the PID control scheme was applied to obtain the envelope pushover curve. The two results seem to agree in a reasonable manner while the ultimate capacity in the positive direction was slightly overestimated. The hinging pattern obtained from the simulation is presented in Figure 4.33 whereas the estimated damage states of the test frame reported by Mutlu (2012) are shown in Figure 4.34. In Figure 4.32, asterisk shows the element in which reinforcing steel strain reached the ultimate strain. The measured maximum column base rotations are compared with those obtained from simulations in Table 4.2. Numerical base rotations were obtained at the maximum roof displacement demand measured during the test. The base rotation demands from the experimental and simulation results agreed well. These results increase the level of confidence in the developed methodology.

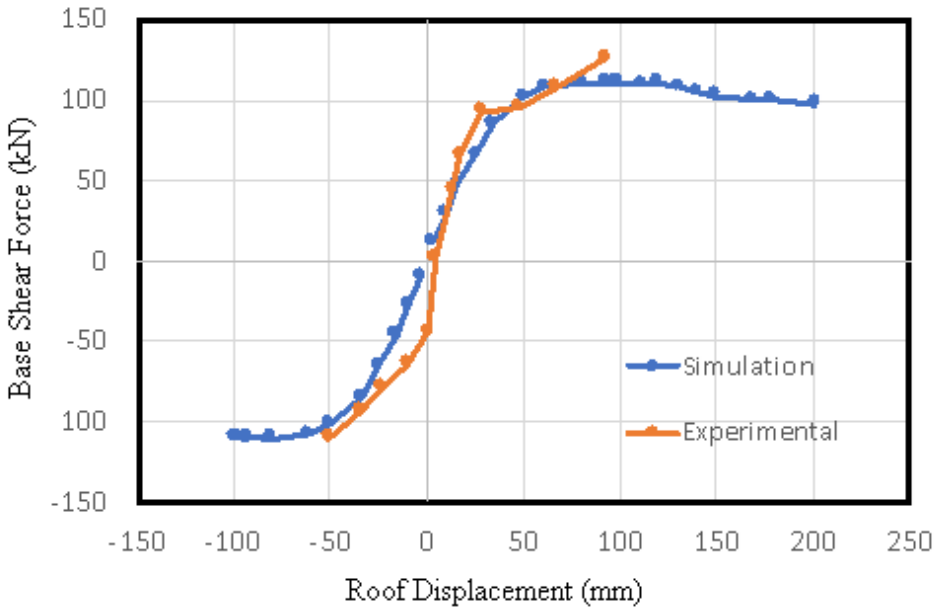

Figure 4.32. Base shear – roof displacement curves

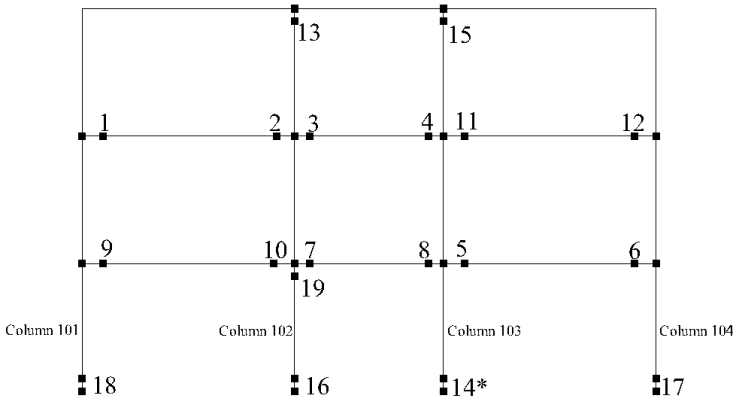

Figure 4.33. Plastic hinge formation sequence predicted by the numerical simulation

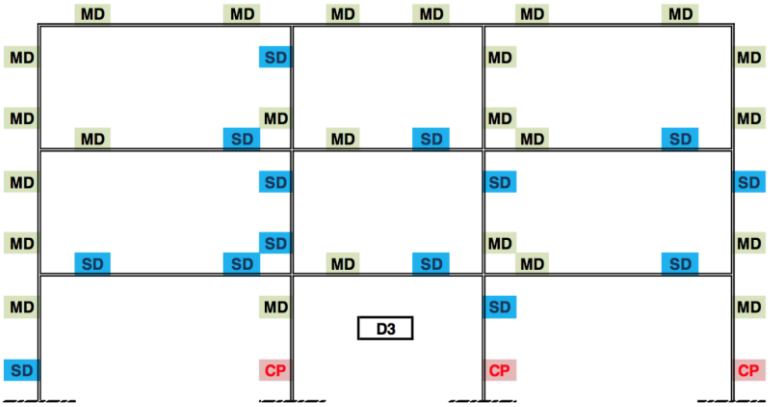

Figure 4.34. Damage assessment result from Mutlu (2012)
CP: Collapse, SD: Significant Damage, MD: Minimum Damage according to TEC (2007)

Table 4.2. Comparison of bottom end rotations of 1st story columns

	Column 101	Column 102	Column 103	Column 104
Experiment	-0.025	-0.032	-0.031	-0.029
Simulation	-0.019	-0.024	-0.026	-0.025

4.4.3 Mass Scaling

Olovsson's stiffness proportional mass scaling approach was applied to the model and applicable time step and runtime values with varying α values are provided in Table 4.3. Stable time step values were found by a trial and error procedure. Time-elapsed

during the analysis were found by using a computer that has Intel i7-3610QM CPU with a frequency of 2.30 GHz and random access memory capacity of 4x2 GB with a frequency of 800 MHz. The model has 162 degree of freedom.

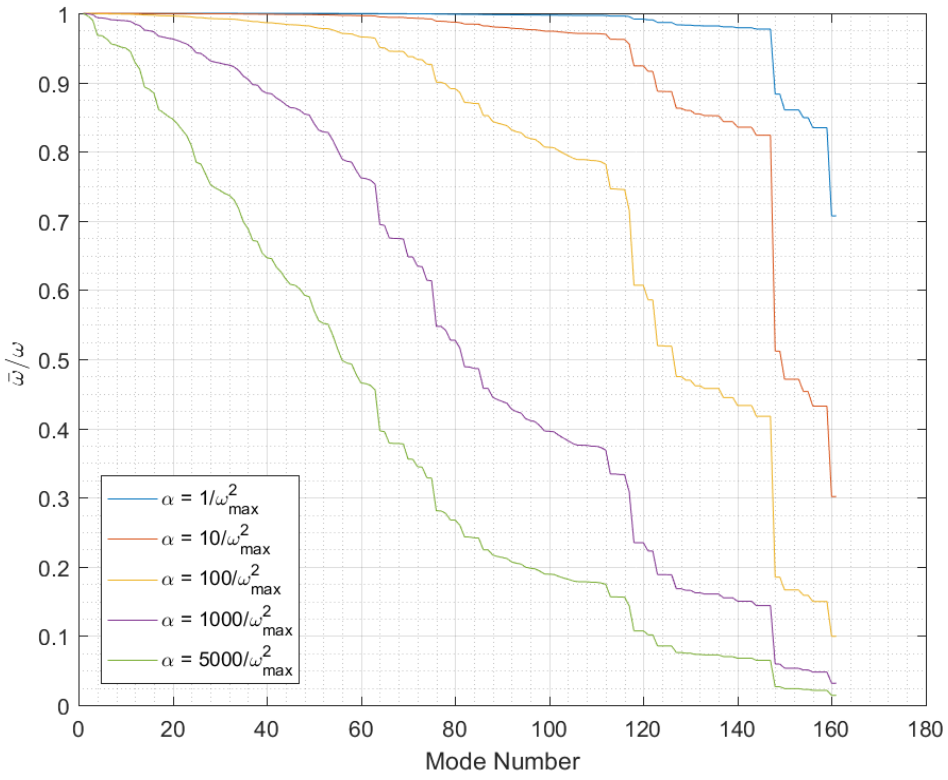

Figure 4.35. Ratio of modified and original angular frequencies of system with varying α

Table 4.3. Stable time step and runtime values for varying α cases.

α	α	Δt	Runtime
0	$0/w^2_{max}$	$2.5x10^{-7}$	11hr 14min 31s
$5.5898x10^{-12}$	$1/w^2_{max}$	$2.7x10^{-7}$	10hr 23min 41s
$5.5898x10^{-11}$	$10/w^2_{max}$	$5x10^{-7}$	5hr 41min 52s
$5.5898x10^{-10}$	$100/w^2_{max}$	$2.5x10^{-6}$	1hr 8min 25s
$5.5898x10^{-9}$	$1000/w^2_{max}$	$2x10^{-5}$	8min 24s
$2.7949x10^{-8}$	$5000/w^2_{max}$	$4x10^{-5}$	4min 13s

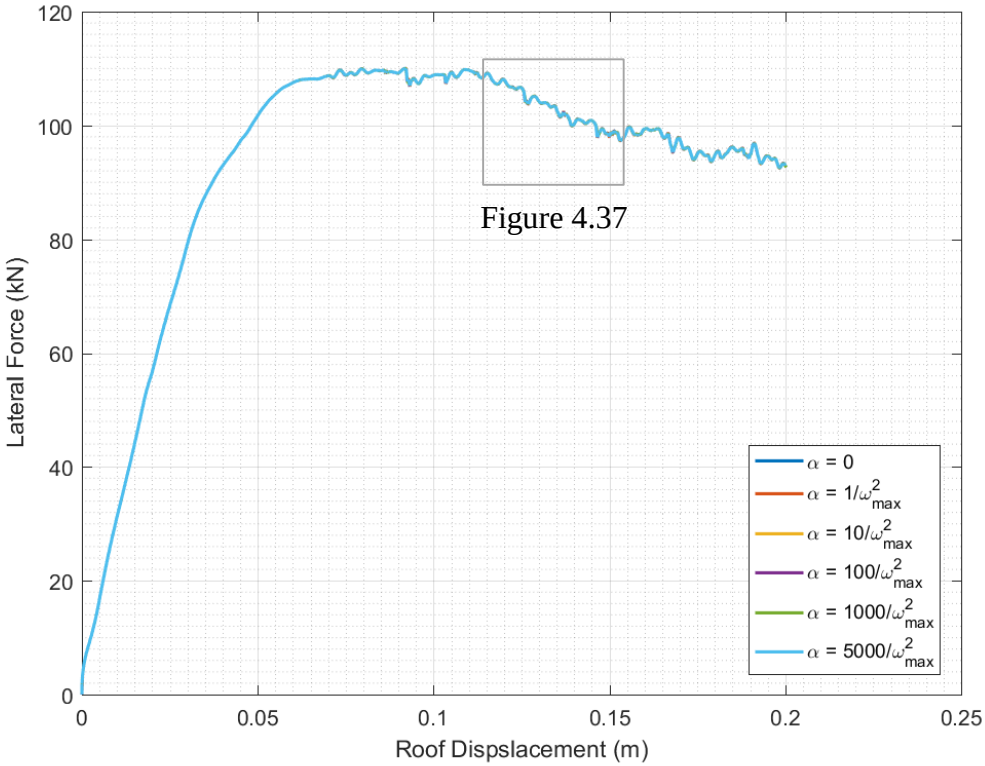

Figure 4.36. Effect of α on the numerical results

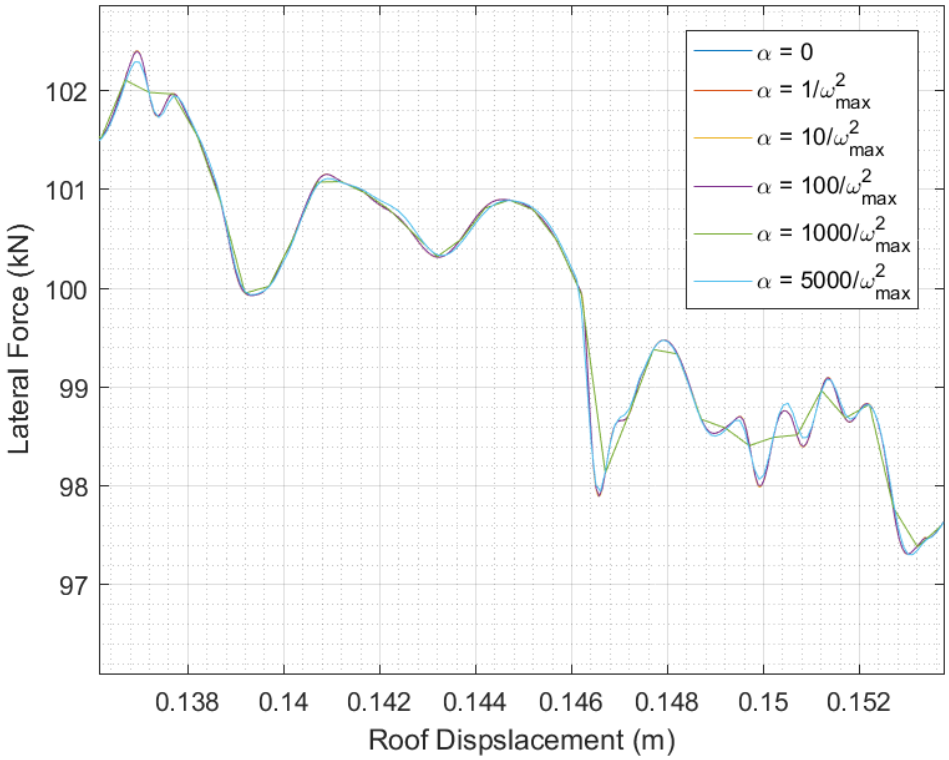

Figure 4.37. Effect of α on the numerical results (zoomed)

As seen from Figure 4.36 and Figure 4.37, response of the all analysis with varying mass scaling coefficients agree very well. The difference comes from the Δt value used in the analysis. It should be noted that used PID coefficients were not modified with respect to the mass scaling effect, i.e., for all parametric mass scaling simulations, same PID coefficients are used. Even though the same PID coefficients were used for different mass scaling levels including no mass scaling case, the velocity response and acceleration response did not depend on mass scaling, i.e., they were exactly same with the no mass scaling case (Figure 4.30).

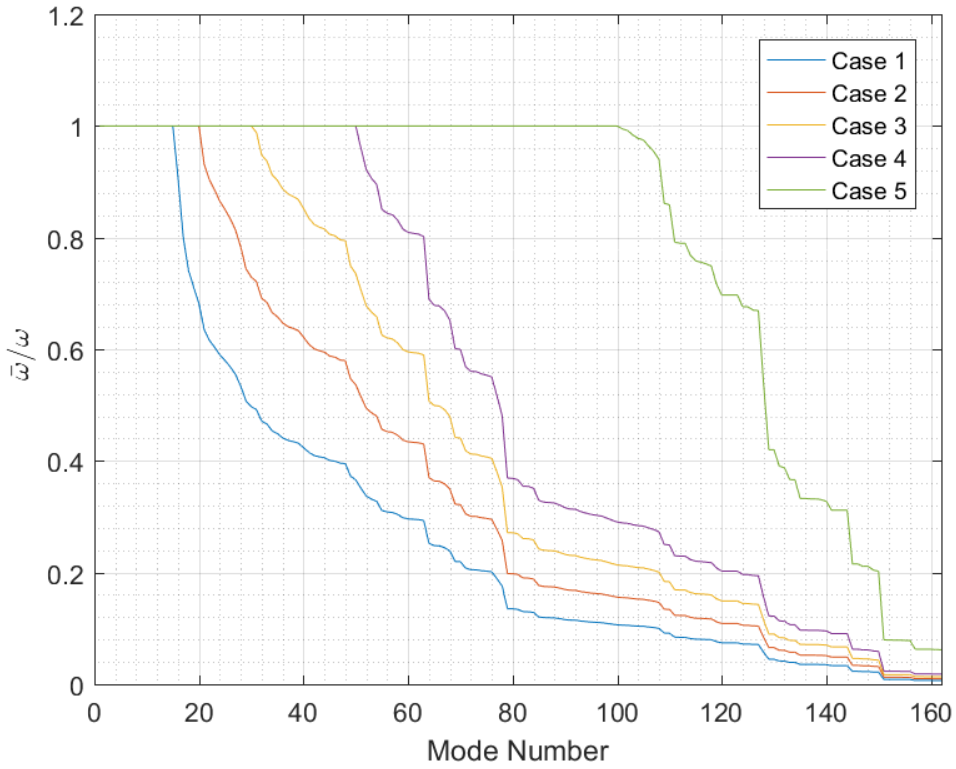

Figure 4.38. Ratio of modified and original angular frequencies of the system with varying selected corner modes

The proposed mass scaling method (Section 5.5) was also implemented in the developed computer program. In this mass scaling method, a corner frequency must be chosen and once mode number is chosen, modes having greater frequencies are fixed to the corner mode's frequency. For this parametric work, corner modes are chosen as 15^{th}, 20^{th}, 30^{th},50^{th} and 100^{th} modes. Trial and error simulations showed that if the corner mode is selected smaller than the 15^{th} mode, the results are not acceptable.

Table 4.4. Stable time step and runtime values for proposed mass scaling technique cases

Case	Selected Corner Mode	Δt	Runtime
1	15	$1.8x10^{-4}$	1 min 1s
2	20	$1.25x10^{-4}$	1 min 31s
3	30	$1x10^{-4}$	1 min 51s
4	50	$7.5x10^{-5}$	2 min 26s
5	100	$2.5x10^{-5}$	6 min 44s

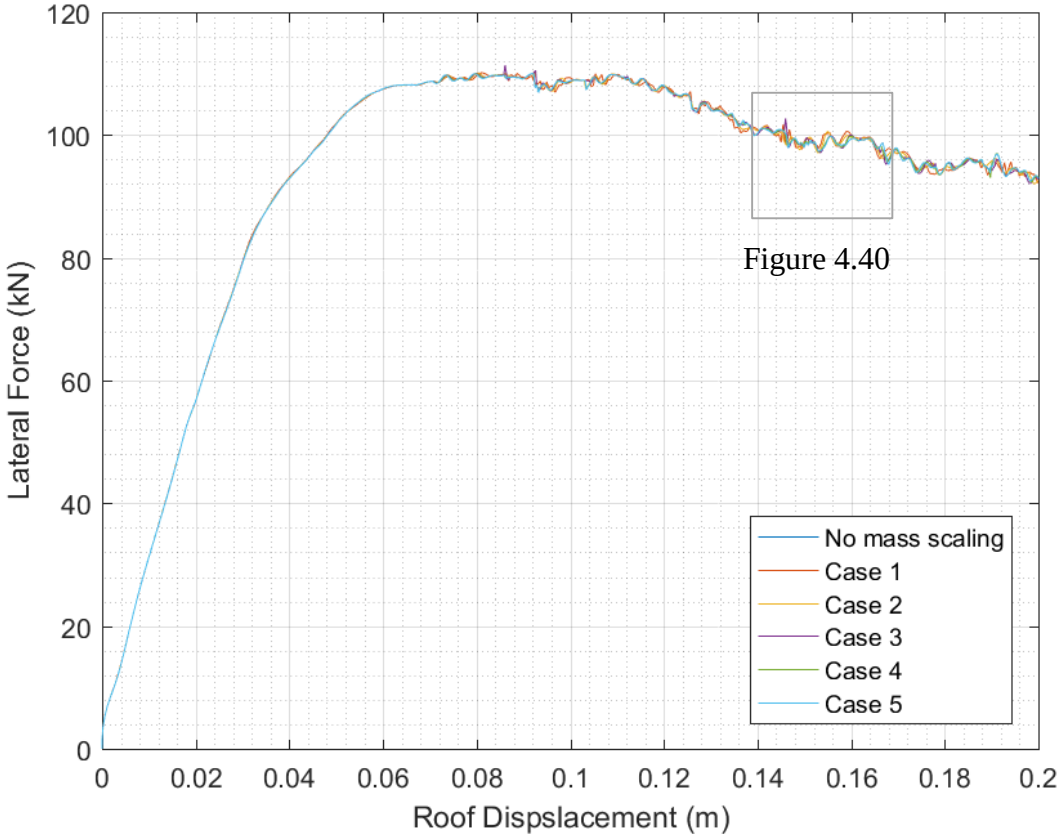

Figure 4.39. Sensitivity of the results on mass scaling.

Proposed mass scaling technique was applied on the same model which was described in Section 3.4.2. For each mass scaling case; selected corner mode, stable time step and runtime values are given in Table 4.4. Stable time step values were found by a trial and error procedure. PID coefficients used in the analyses were identical with the no mass scaling case. Results for this parametric investigation are given in the Figure 4.39

and Figure 4.40. As can be seen from the figures, the response of the system does not change significantly for different levels of mass scaling. Although the same PID coefficients were used for different mass scaling levels including no mass scaling case, response velocity and response acceleration did not depend on mass scaling, i.e., they were exactly same with the no mass scaling case (Figure 4.30).

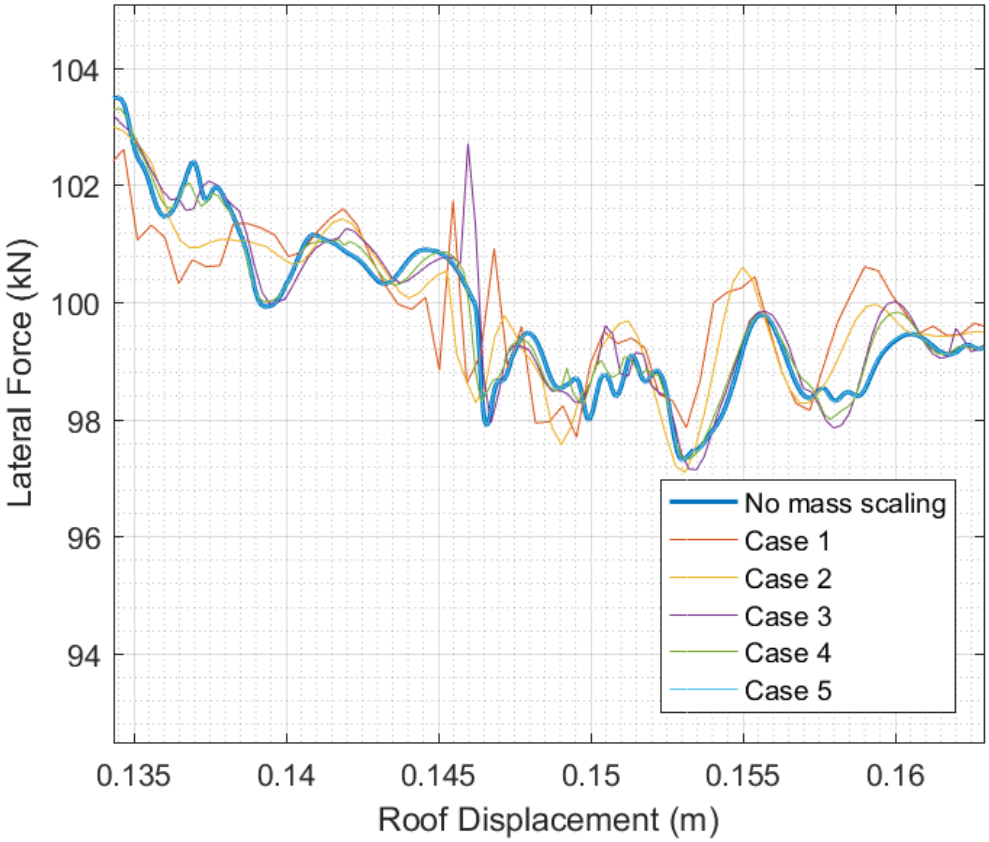

Figure 4.40. Sensitivity of the results on mass scaling (zoomed).

Both Olovsson's stiffness proportional selective mass scaling and proposed mass scaling techniques effectively increase the stable time step without losing significant accuracy. Both methods require eigenvalue analysis prior to the simulation. Since, with the PID controller, velocity is controlled (and implicitly acceleration is also controlled) changing mass matrix with the mass scaling technique did not significantly affect the damping and inertial forces. Results show that application of mass scaling with the PID controller gives rational results.

4.5 Ground Motion Simulation and Comparison with Experimental Data

Three ground motions were sequentially exerted on the structure with pseudo-dynamic testing technique (Mutlu 2012). Ground motions were synthetic time-acceleration series prepared for the Duzce province. The acceleration time series used in the tests were named as D1, D2 and D3, compatible with the site-specific earthquake spectra for different probabilities of being exceeded on different soil classes as shown in Table 4.5. The acceleration time series, in the sequence of application, is shown in Figure 4.41.

Table 4.5 Ground motion properties

Earthquake	Probability of Being Exceeded in 50 years	Soil Class/Type	PGA (g)
D1	50 %	Z1 / Rock	0.254
D2	10 %	Z1 / Rock	0.545
D3	10 %	Z3 / Soft	0.604

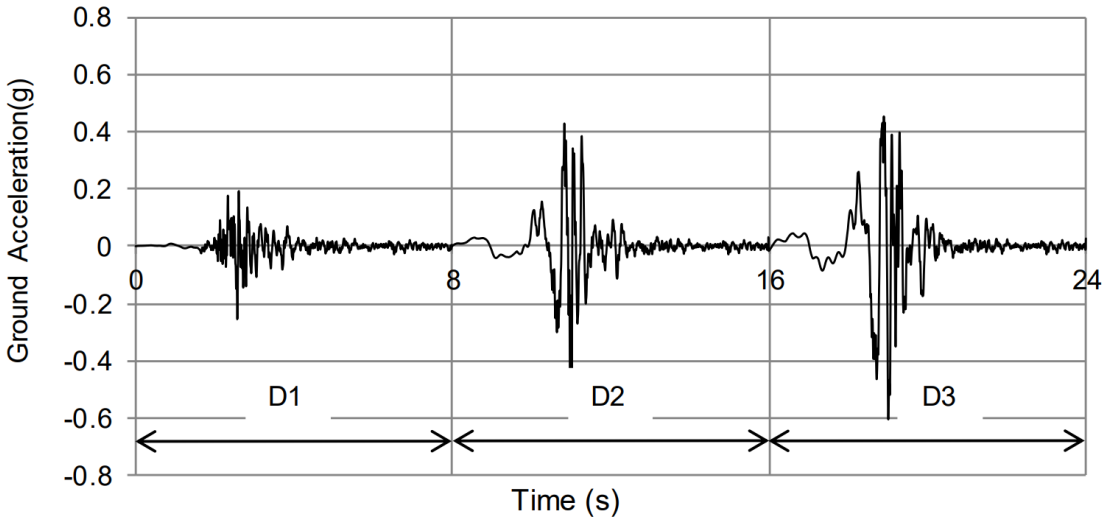

Figure 4.41. Synthetic Ground motions

The same numerical model described in the Section 3.4.1 was used except for mass scaling. After the application of the gravity load, ground motion was applied to the structure. Besides the results of pseudo-dynamic experiment, the results of the numerical models which were used by Mutlu (2012) are presented along with the results of the developed computer program. Two models were prepared by Mutlu (2012) for simulation of the experiment results, Model A and Model B. In Model A, a

continuum approach was followed to model the test frames, i.e. two-dimensional nonlinear plane stress elements with embedded reinforcements were employed and TNO DIANA Release 9.3 (2008) was used. In Model B, force-based frame elements defined with nonlinear fiber sections at integration points were used for the simulations in the OpenSees Simulation Platform (Mazzoni et al. 2010).

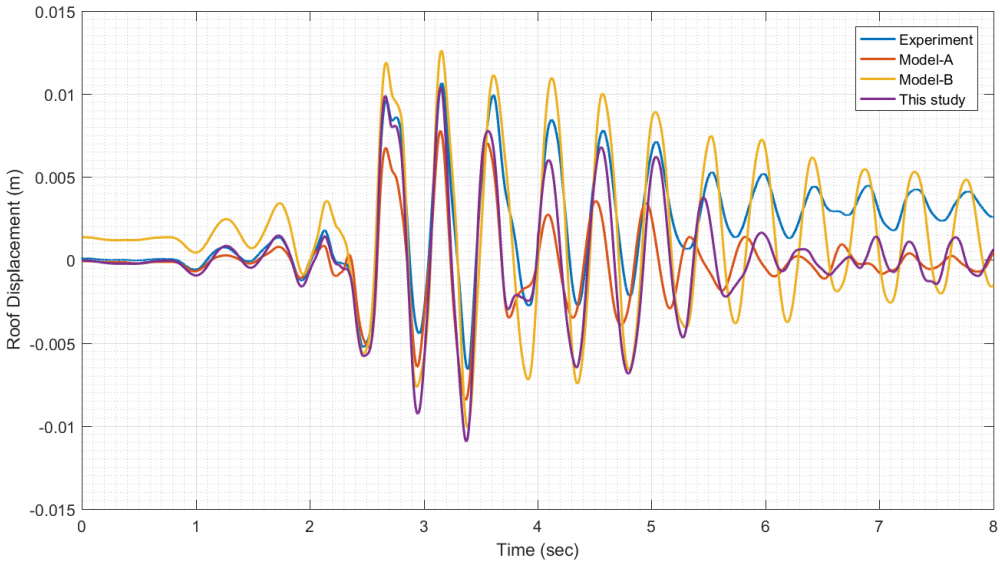

Figure 4.42. Comparison of results for the D1 earthquake

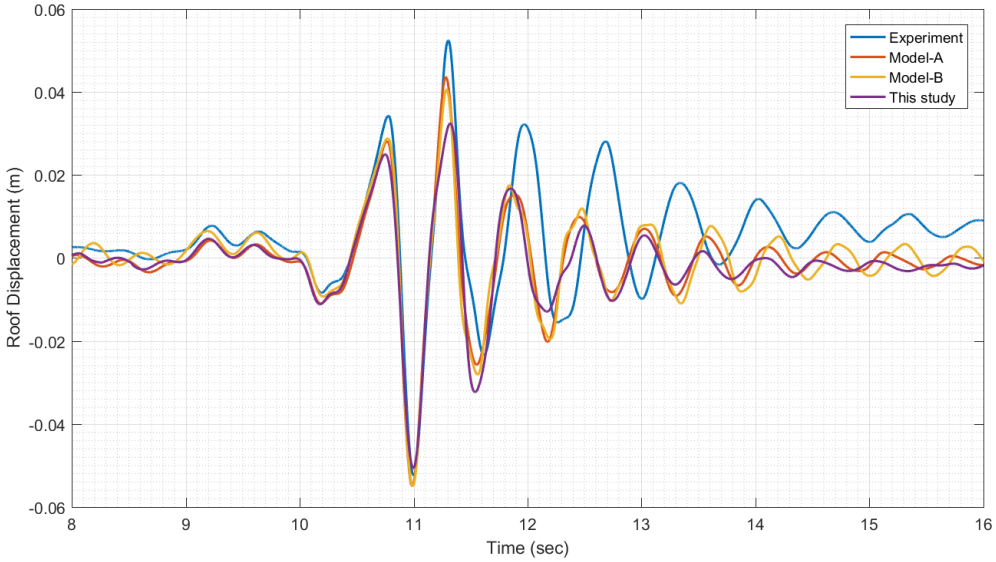

Figure 4.43. Comparison of results for the D2 earthquake (Continuation of D1)

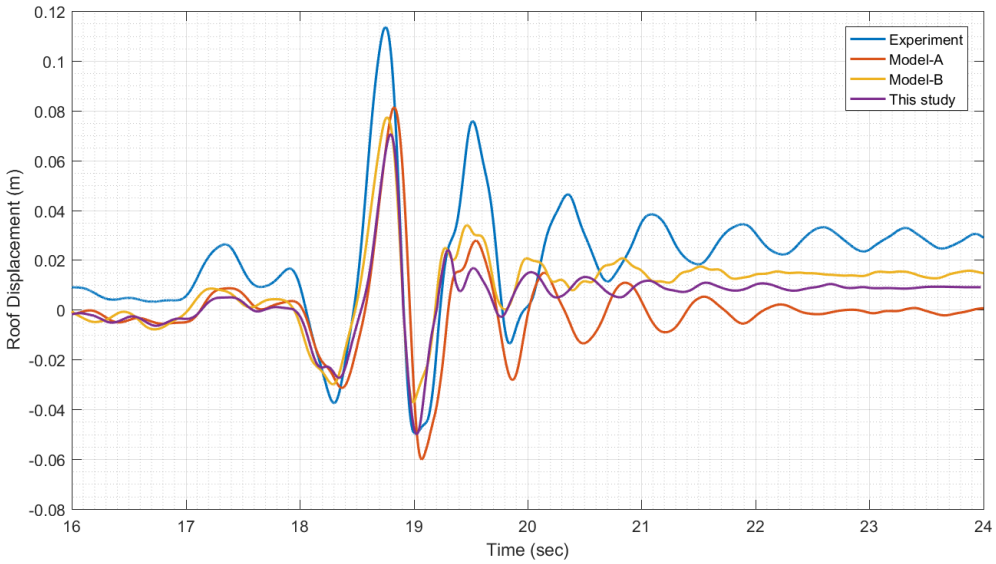

Figure 4.44. Comparison of results for the D3 earthquake (Continuation of D2)

As can be seen from Figures 3.41 to 3.43, the result agreed well with the result from Model A and B, but, plastic damage was underestimated in comparison to the experiment. Plastic damage was found slightly lower than the Model B and higher than the Model A. It should be noted that, for earthquakes D2 and D3, all of the numerical models estimated the plastic damage lower than the experimental measurement. Furthermore, for earthquake D3, peak roof displacement was determined to be lower than the experimental measurements. On the other hand, the frequency of the structure is matched well for earthquake D1, but, there was a slight variation in period in comparison with experiment for earthquakes D2 and D3.

CHAPTER 5

CONCLUSIONS

A computer program was developed to simulate the quasi-static behavior reinforced concrete structures. The program was based on the displacement-based finite elements with the fiber discretization approach and explicit type time integration. Several tools such as the PID controlling algorithm and mass scaling were implemented in order to meet the needs of modern day structural analysis requirements. Numerical simulations verified the capability of the developed program in estimation of the behavior of reinforced concrete members and structures. Following key conclusions can be drawn based on the performed test simulations:

- PID control algorithm was implemented to extend the capability of explicit dynamic analysis methodology to quasi-static analysis of structures. It was shown that PID control allows the simulation of displacement controlled experiment for which load levels are expected to decrease as a result of damage.
- Explicit time integration methods are conditionally stable. Their stability depends on the largest eigenvalue of the system. Applying selective mass scaling decreased the largest eigenvalues of the model without causing accuracy problems.
- A new mass scaling approach was proposed in this thesis work. In this method a corner eigenmode is selected before the simulation. Once the corner eigenmode is selected, frequencies of modes that have higher eigenvalues than the corner mode are set to the frequency of selected corner mode. Numerical results showed that the proposed method is more effective than the selective mass scaling method in increasing the stable time step used in simulations without noticeable accuracy issues.
- When PID control and mass scaling technique are used in the same analysis, runtime decreases significantly and sufficiently accurate results are obtained.

REFERENCES

Anagnostopoulos, S. A. (1981). “Inelastic Beams for Seismic Analyses of Structures.” *Journal of Structural Division, ASCE*, 107(ST7, July).

Argyris, J. H. (1954). “Energy Theorems and Structural Analysis: A Generalized Discourse with Applications on Energy Principles of Structural Analysis Including the Effects of Temperature and Non-Linear Stress-Strain Relations.” *Aircraft Engineering and Aerospace Technology*, 26(10), 347–356.

Argyris, J., and Kelsey, S. (1957). “The matrix force method of structural analysis and some new applications.” *Report of Aeronautical Research Council*, 3034(3034), 1–41.

Bae, S., and Bayrak, O. (2008). “Plastic hinge length of reinforced concrete columns.” *ACI Structural Journal*, American Concrete Institute, 105(3), 290–300.

Baker, A. L. L., and Amarakone, A. M. N. (1965). “Inelastic hyperstatic frames analysis.” *Special Publication*, 12, 85–142.

Bathe, K. J. (1982). *Finite element procedures in engineering analysis*. Prentice Hall, Pearson Education, Inc., New York.

Bažant, Z. P., and Oh, B. H. (1983). “Crack band theory for fracture of concrete.” *Matériaux et Constructions*, Kluwer Academic Publishers, 16(3), 155–177.

Belytschko, T., Liu, W., and Moran, B. (2000). *Nonlinear Finite Elements for Continua and Structures*. Wiley, New York.

Berry, M. P., Lehman, D. E., and Lowes, L. N. (2008). “Lumped-plasticity models for performance simulation of bridge columns.” *ACI Structural Journal*, American Concrete Institute, 105(3), 270.

Bertero, V., Aktan, A. E., Charney, F., and Sause, R. (1984). “Earthquake simulator tests and associated experimental, analytical, and correlation studies of one-fifth scale model.” *Special Publication*, 84, 375–424.

Charney, F. A., and Bertero, V. V. (1982). “An evaluation of the design and analytical seismic response of a seven-story reinforced concrete frame-wall structure.” *NASA STI/Recon Technical Report N*, 83.

Chung, J., and Hulbert, G. M. (1993). “A Time Integration Algorithm for Structural

Dynamics With Improved Numerical Dissipation: The Generalized-α Method." *Journal of Applied Mechanics*, 60(2), 371.

Chung, J., and Lee, J. M. (1994). "A new family of explicit time integration methods for linear and non-linear structural dynamics." *International Journal for Numerical Methods in Engineering*, 37(23), 3961–3976.

Ciampi, V., and Carlesimo, L. (1986). "A nonlinear beam element for seismic analysis of structures." *8th European Conference on Earthquake Engineering*, 3–6.

Clough, R., and Johnston, S. (1966). "Effect of stiffness degradation on earthquake ductility requirements." *Trans. Japan Earthg. Engrg Symposium*, Tokyo, 195–198.

Clough, R. W. (1960). "The finite element method in plane stress analysis." *Proceedings of the 2nd Conference on Electronic Computation of American Society of Civil Engineers*, 345–378.

Cocchetti, G., Pagani, M., and Perego, U. (2013). "Selective mass scaling and critical time-step estimate for explicit dynamics analyses with solid-shell elements." *Computers & Structures*, Pergamon, 127, 39–52.

Code, T. E. (2007). "Specification for structures to be built in disaster areas." *Ministry of Public Works and Settlement Government of Republic of Turkey*.

Coleman, J., and Spacone, E. (2001). "Localization Issues in Force-Based Frame Elements." *Journal of Structural Engineering*, 127(11), 1257–1265.

Cook, R. D. (1981). *Analysis, Concepts and Application of Finite Element*. John Wiley & Sons, New York.

Corley, W. (1966). "Rotational capacity of reinforced concrete beams." *Journal of the Structural Division*, ASCE, 92(5), 121–146.

Filippou, F. C., and Issa, A. (1988). "Nonlinear analysis of reinforced concrete frames under cyclic load reversal." *Earthquake Engineering Research Center College of Engineering*, (1–3), 223–227.

Giberson, M. F. (1967). "The Response of Nonlinear Multi-story Structures Subjected to Earthquake Excitation." *California Institute of Technology, Pasadena, CA*.

Green, A. E., and Naghdi, P. M. (1977). "On thermodynamics and the nature of the second law." *Proc. R. Soc. Lond. A*, The Royal Society, 357(1690), 253–270.

Hahn, G. D. (1991). "A modified Euler method for dynamic analyses." *International Journal for Numerical Methods in Engineering*, Wiley Online Library, 32(5),

943–955.

Hang, C. C., Åström, K. J., and Ho, W. K. (1991). “Refinements of the Ziegler--Nichols tuning formula.” *IEE Proceedings D (Control Theory and Applications)*, 111–118.

Hilber, H. M., Hughes, T. J. R., and Taylor, R. L. (1977). “Improved numerical dissipation for time integration algorithms in structural dynamics.” *Earthquake Engineering & Structural Dynamics*, Wiley Online Library, 5(3), 283–292.

Hildebrand, F. B. (1974). “Introduction to Numerical Analysis, International Series in Pure and Applied Mathematics.” McGraw-Hill, New York.

Hognestad, E. (1951). *Study of combined bending and axial load in reinforced concrete members*.

Khot, S., and Yelve, N. P. (2011). “Modeling and response analysis of dynamic systems by using ANSYS© and MATLAB©.” *Journal of Vibration and Control*, SAGE PublicationsSage UK: London, England, 17(6), 953–958.

Krieg, R. D. (1973). “Unconditional Stabilty in Numerical Time Integration Methods.” *Journal of Applied Mechanics*, 40(2), 417–421.

Lai, B. S., Will, G. T., and Otani, S. (1984). “Model for Inleastic Biaxial Bending of Concrete Members.” *Journal of Structural Division, ASCE*, 110(11), 2563–2584.

Lee, T. H., and Mosalam, K. M. (2006). “Probabilistic seismic evaluation of reinforced concrete structural components and systems. Report 2006/04, Pacific Earthquake Engineering Research Center.” *University of California, Berkeley, USA Google Scholar*.

Lehman, D., Moehle, J., Mahin, S., Calderone, A., and Henry, L. (2004). “Experimental evaluation of the seismic performance of reinforced concrete bridge columns.” *Journal of Structural Engineering*, American Society of Civil Engineers, 130(6), 869–879.

Mander, J. B., Priestley, M. J. N., and Park, R. (1988a). “Theoretical Stress-Strain Model for Confined Concrete.” *Journal of Structural Engineering*, 114(8), 1804–1826.

Mander, J. B., Priestley, M. J. N., and Park, R. (1988b). “Observed Stress-Strain Behavior of Confined Concrete.” *Journal of Structural Engineering*, 114(8), 1827–1849.

Mazzoni, S., McKenna, H., Scott, M. H., and Fenves, G. L. (2010). “OpenSees

Manual.” *Pacific Earthquake Engineering Research Center*.

Morita, S., and Kaku, T. (1975). “Cracking and deformation of reinforced concrete beams subjected to tension.” *Liege colloquium inter-association*.

Mutlu, M. B. (2012). “Numerical Simulations Of Reinforced Concrete Frames Tested Using Pseudo-Dynamic Method.” Middle East Technical University.

Olovsson, L., and Simonsson, K. (2006). “Iterative solution technique in selective mass scaling.” *International Journal for Numerical Methods in Biomedical Engineering*, Wiley Online Library, 22(1), 77–82.

Olovsson, L., Simonsson, K., and Unosson, M. (2005). “Selective mass scaling for explicit finite element analyses.” *International Journal for Numerical Methods in Engineering*, 63(10), 1436–1445.

Otani, S. (1974). “Inelastic analysis of R/C frame structures.” *Journal of the Structural Division*, 100(Proc. Paper 10686).

Otani, S. (1980). “Nonlinear Dynamic Analysis of Reinforced Concrete Building Structures.” *Canadian Journal of Civil Engineering*, 7(2), 333–344.

Park, R., and Paulay, T. (1975). *Reinforced concrete structures*. John Wiley & Sons, New York.

Park, R., Priestley, M. J., and Gill, W. D. (1982). “Ductility of square-confined concrete columns.” *Journal of the structural division*, ASCE, 108(4), 929–950.

Paulay, T., and Priestley, M. J. N. (1992). *Seismic design of reinforced concrete and masonry buildings*. Wiley.

Paulay, T., and Priestly, M. J. N. (1992). *Seismic Design of Reinforced Concrete and Masonry Buildings*. John Wiley & Sons, Inc., Hoboken, NJ, USA.

PEER. (2011). “PEER Structural Performance Database.” <https://nisee.berkeley.edu/spd/>.

Priestley, M. J. N., and Park, R. (1987). “Strength and ductility of concrete bridge columns under seismic loading.” *Structural Journal*, 84(1), 61–76.

Przemieniecki, J. S. (1967). *Theory of Matrix Structural Analysis*. McGraw-Hill, New York.

Scott, M. H., and Fenves, G. L. (2006). “Plastic Hinge Integration Methods for Force-Based Beam–Column Elements.” *Journal of Structural Engineering*, 132(2), 244–252.

Spacone, E. (1994). “Flexibility-based finite element models for the nonlinear static

and dynamic analysis of concrete frame structures." University of California at Berkeley.

Spacone, E., Ciampi, V., and Filippou, F. C. (1996a). "Mixed formulation of nonlinear beam finite element." *Computers and Structures*, 58(1), 71–83.

Spacone, E., Filippou, F. C., and Taucer, F. F. (1996b). "Fibre Beam-Column Model for Non-linear Analysis of R/C Frames: Part 1. Formulation." *Earthquake Engineering & Structural Dynamics*, 25(7), 711–725.

Spencer, B., Heinstein, M., Hales, J., and Pierson, K. (2008). "Multi-length scale algorithms for failure modeling in solid mechanics." *Technical Report SAND2008-6499*, Albuquerque, New Mexico.

Steffensen, J. F. (1950). "Interpolation." *Chelsea, New York*.

Takayanagi, T., and Schnobrich, W. C. (1979). "Non-linear analysis of coupled wall systems." *Earthquake Engineering & Structural Dynamics*, Wiley Online Library, 7(1), 1–22.

Takizawa, H. (1976). "Notes on Some Basic Problems in Inelastic Analysis of Planar RC Structures." Part I: Feb 51-62; Part II:March 65-67.

Tamma, K. K., and Namburu, R. R. (1990). "A robust self-starting explicit computational methodology for structural dynamic applications: Architecture and representations." *International Journal for Numerical Methods in Engineering*, 29(7), 1441–1454.

Taucer, F. F., Spacone, E., and Filippou, F. C. (1991). *A Fiber Beam-Column Element for Seismic Response Analysis of Reinforced Concrete Structures*. *Ucb/Eerc-91/17*.

Tehrani, K. A., and Mpanda, A. (2012). "PID control theory." *Introduction to PID Controllers-Theory, Tuning and Application to Frontier Areas*, InTech.

Turner, M. J., R. W., C., H. C., M., and Top, J. (1956). "Stiffness and Deflection Analysis of Complex Structures." *Journal of the Aeronautical Sciences*, 23(9), 805–823.

Ueberhuber, C. W. (1997). *Numerical Computation 2: Methods, Software, and Analysis*. Springer-Verlag.

Warburton, G. B. (1985). "Some recent advances in structural vibration." *Vibrations of engineering structures*, Springer, 215–224.

Wood, W. L., Bossak, M., and Zienkiewicz, O. C. (1980). "An alpha modification of

Newmark's method." *International Journal for Numerical Methods in Engineering*, Wiley Online Library, 15(10), 1562–1566.

Ziegler, J. G., and Nichols, N. B. (1942). "Optimum settings for automatic controllers." *trans. ASME*, 64(11).

Zienkiewicz, O. C. (1996). "Origins, milestones and directions of the finite element method-A personal view." *Handbook of Numerical Analysis*, 4(Part 2), 3–67.

Zienkiewicz, O. C., and Taylor, R. L. (1989). *The finite element method*. McGraw-hill., London.